UNIVERSITÀ DI SIENA 1240

Dipartimento di Medicina Molecolare e dello Sviluppo

Dottorato in Medicina Molecolare

XXXV° Ciclo

Coordinatore: Prof. Vincenzo Sorrentino

Extracellular Vesicles as a platform with potential clinical and industrial applications: from cancer diagnosis to cell-free therapy.

Settore scientifico disciplinare: BIO/09 Fisiologia

Candidato/a
Marta Venturella
Siena

Firma digitale del/della candidato/a

Marta Venturella

08/05/2024 09:06:06
MARTA VENTURELLA

Supervisore
Prof.ssa Antonella Naldini
Università di Siena

Co-supervisore/i
Dr. Davide Zocco
Lonza CGT

Anno accademico di conseguimento del titolo di Dottore di ricerca
2022/23

Università degli Studi di Siena
Dottorato in Medicina Molecolare
XXXV° Ciclo

Data dell'esame finale
30/05/2024

Commissione giudicatrice
Prof.ssa Daniela Rossi
Dr.ssa Marianna Vitiello
Dr.ssa Elena Sticchi

Supplenti
Dr. Rosario Amato

Index.

Abbreviations.

EVs: Extracellular vesicles

sEVs: small Extracellular Vesicles

MVs: Microvesicles

lEVs: large Extracellular Vesicles

MVBs: Multivesicular Bodies

ISEV: International Society for Extracellular Vesicles

MISEV: Minimal Information for Studies of Extracellular Vesicles

CCM: Cell Conditioned Media

SEC: Size-Exclusion Chromatography

TFF: Tangential Flow Filtration

FFF: Field-Flow Fractionation

UC: Ultracentrifugation

DG: Density Gradient

DNA: Deoxyribonucleic Acid

RNA: Ribonucleic Acid

CTCs: Circulating Tumor Cells

GMPs: Good Manufacturing Practices

UP: Upstream Processing

DP: Downstream Processing

CAFs: Cancer Associated Fibroblasts

EMT: Epithelial-to-Mesenchymal Transition

HIFs: Hypoxia-Inducible Factors

HRE: Hypoxia Response Element

PHDs: Prolyl Hydroxylases

VHL: Von Hippel Lindau protein

FIH: Factor Inhibiting HIF

WHO: World Health Organization

CSD: Cumulative Sun Damage

CA-IX: Carbonic Anhydrase IX

FBS: Fetal Bovine Serum

RT: Room Temperature

SPR: Surface plasmon resonance

ddPCR: droplet digital PCR

Ct: threshold cycle

hbm MSCs: human bone marrow Mesenchymal Stem Cells

TEM: Transmission Electron Microscopy

CFSE: Carboxyfluorescein Succinimidyl Ester

GO: Gene Ontology

CC: Cellular Component

WTA: Whole Transcriptome Assay

NGS: Next-generation Sequencing

HUVECs: Human Umbilical Vein Endothelial Cells

VEGF: Vascular Endothelial Growth Factor

1. Introduction.

1.1 Extracellular Vesicles.

Extracellular Vesicles (EVs) is a generic term referred to a heterogeneous group of cell-derived membrane-limited vesicles, with different sizes and origins, not capable of replicating and without a functional nucleus [1]. All cell types are able to secrete EVs into the extracellular space and this process is a conserved mechanism throughout evolution, present both in unicellular and multicellular organisms [2–4]. EV release was initially supposed to be a mechanism to discard unneeded compounds from the cells. Further research in the past decades demonstrated that EVs are a complex mechanism of cell-to-cell communication. In particular, they can transfer functional cargos influencing several processes, in both physiological and pathological conditions [5]. This is the reason why the field of EVs continues to grow esponentially.

1.2 Discovery of the EVs.

The first study describing EVs can be considered the article published by Chargaff in 1945 on blood coagulation. He described a particulate fraction isolated from blood with high clotting potential [6]. After 17 years, Wolf published electron microscope pictures of a particulate sedimented from platelets, that he called «platelet dust» [7].

In the 70s, several studies reported cell-derived vesicles found in other organisms (algae, yeasts, bacteria) [8,9].

Nunez et al. described for the first time in 1974 the presence of multivesicular bodies (MVBs) near the apical plasma membrane of the cell, hypothesizing the fusion with the cell membrane and the release of vesicles into the luminal space [10].

In the 80s, Johnstone and Stahl, studying the reticulocyte maturation, discovered the exosome secretion pathway and called these vesicles «exosomes». Johnstone postulated that EVs are a mechanism of waste disposal and this opinion stood in the mind of researchers for the following decade [11,12].

During the 90s, several papers were published about the implication of EVs in other biological processes. Raposo showed that EVs from immune cells are capable of presenting antigens

[13]. The idea that EVs could be used as biomarkers, and that they could have therapeutic applications, started to arise.

Since 2000, the increasing number of published papers, patent applications and grant funding proved the exponential growth of the field. Researchers started to publish the first reviews and to investigate in more depth the proteome and lipidome composition of EVs [14,15]. Moreover, the first studies demonstrated the EV functionality throught the transfer of specific cargo to recipient cells [16,17].

The first international researchers meetings started to be organized, in order to share ideas and results. The International Society for Extracellular Vesicles (ISEV) was formed in 2011 and numerous National Societies had been established.

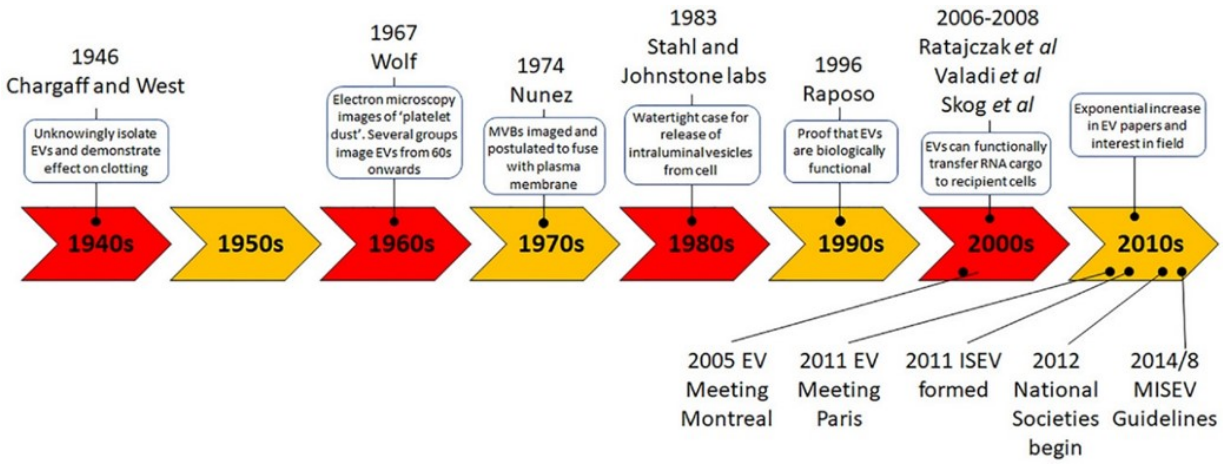

Figure 1. Timeline representing some key milestones in the history of EVs [18].

1.3 Classification of EVs.

Traditionally, lack of standardised nomenclature and classification has been one of the major gaps in the field of EV research. In early reports, researchers used different terms reflecting EV functions (such as «prostasomes» for vesicles released from prostate epithelium) [19]. Despite the efforts of ISEV, the adoption of standardised terms to classify EVs has been disomogenous among researchers, as ISEV's recommendations have not been fully embraced by the research community [18].

According to the MISEV (Minimal Information for Studies of Extracellular Vesicles) guidelines, EVs should be classified into two main categories, based on their size and biogenesis. Based on size, two EV types can be identified: small EVs, formerly called exosomes, with a diameter ranging between 30 nm to 120 nm and large EVs with diameter >120 nm. Large EVs comprise microvesicles (MVs), called also microparticles or ectosomes (120-1000 nm), oncosomes and apoptotic bodies (1-10 µm) [2,20,21].

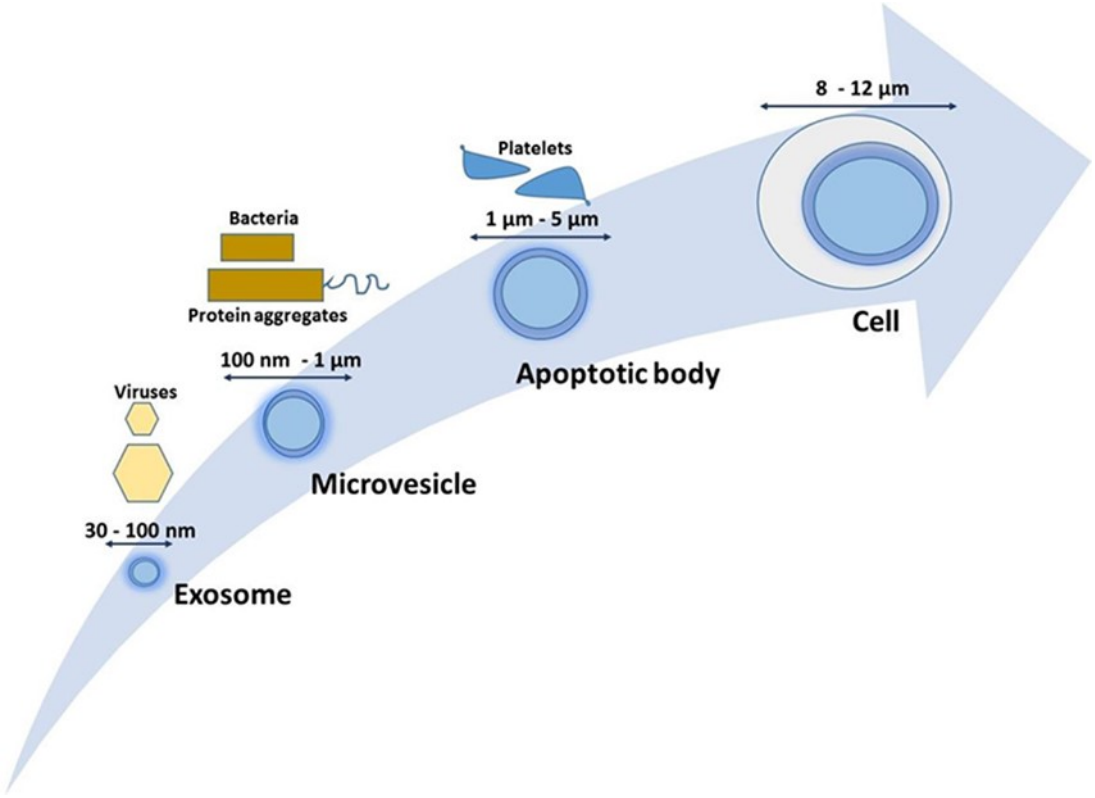

Figure 2. Size ranges of different types of EVs [22].

In 2018, nanoparticles smaller than 50 nm in diameter, the exomeres, were discovered in small EVs preparations. Molecular analyses showed that exomeres are not membrane-bound and carry distinct molecular signatures [23]. A specific ultracentrifugation protocol was developed to separate exomeres from small EVs [24]. More recently, another smaller class of nanoparticles was identified from the supernatant of the exomeres, the supermeres [25].

EVs can be distinguished according to their biogenesis and release pathway. Exosomes are produced after the inward budding of the endosomal membrane and the formation of

multivesicular bodies (MVBs). MVBs fuse with the cell plasma membrane and release their content, the exosomes, in the extracellular environment [26].

MVs, instead, are generated following the rearrangement of the cell cytoskeleton and budding of plasma membrane. When plasma membrane-budding occurs in the context of apoptosis, these large EVs are referred to as apoptotic bodies. Apoptotic EVs have a distinct cargo including whole (or fragmenting) organelles and larger amounts of fragmented genetic material.

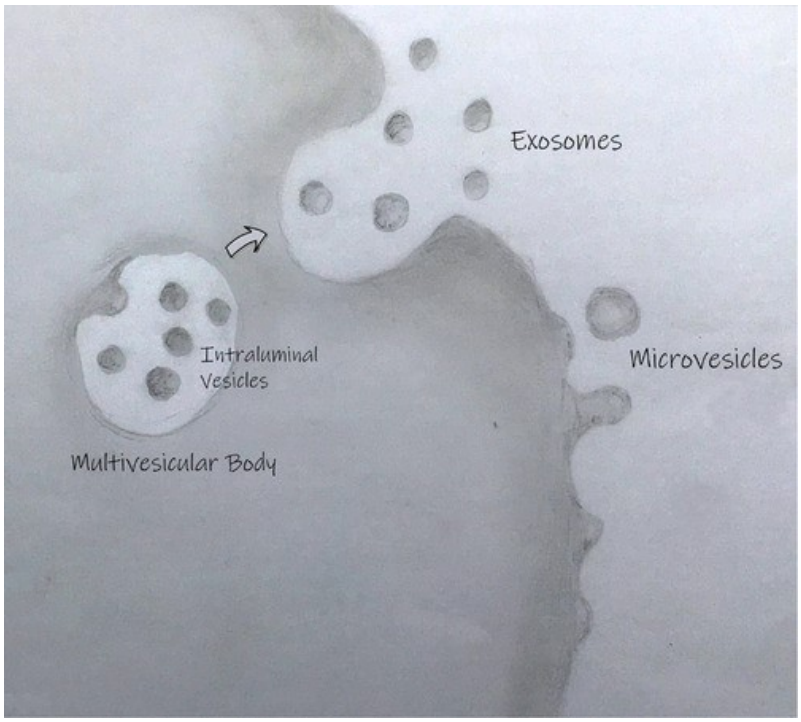

Figure 3. Biogenesis of exosomes and microvesicles [18].

1.4 The need for standardization of EV-based studies.

EVs can be isolated from biofluids or from cell culture supernatants. The sample collecting phase and the biobanking activities have an impact on the final EV preparation and they can be sources of artifacts [27–32]. For example, in case of blood sampling, platelets become easily activated during sample collection and handling, and, as a consequence, they release confounding EVs that interfere with the isolation of EVs of interest [33].

Instead, before isolating EVs from cell conditioned media (CCM), it is recommended to use either serum-free medium, or EV-free serum as growth supplement in cell culture medium [34].

Reporting a complete list of pre-analytical parameters is important to improve data interpretation and reproducibility. The EV-TRACK knowledgebase has been developed by an international consortium of researchers to record experimental parameters of EV-related studies, in order to facilitate standardization of EV research [35]. Other two examples of databases for EV-related studies are ExoCarta and Vesiclepedia [36,37].

The current available technologies do not allow to efficiently separate a specific subtype of EV or to avoid contamination with non-vesicular moieties [38]. The final EV preparation often contains different EV subtypes which overlap in size, composition and density.

Moreover, methods for the preparation of EV samples are affected by intra- and inter-laboratory variability. For example, in the case of centrifugation-based experiments, it is essential to report all the variables of the centrifugation procedure: speed, time, rotor type (if fixed angle or swinging bucket), pelleting efficiency (rotor k-factor), sample viscosity and gradient characteristics used. All these parameters will affect the final EV preparation [39].

Thus, it is difficult to assign a specific function to a particular EV subtype. EV isolation method should be chosen based on the desired degree of recovery versus the degree of specificity, and the intended application of the EVs [39,40]. If the purpose is the detection of established EV biomarkers, a high-throughput isolation method with high yields but low purity might be suitable. On the other hand, in case of novel biomarker studies, a method resulting in high EV purity but low yields is recommended [41].

In conclusion, since the choice of separation method influences the identification of EV cargo and downstream applications, it is important to report experimental details to support data reproducibility [42].

Table 1 and Figure 4 report the commonly used EV purification methods, exploiting different physical/chemical principles: centrifugation-based methods, size-based isolation, affinity-based isolation, precipitation, and, recently developed, microfluidic techniques [43–46]. Novel approaches combine different isolation methods to improve EV purity [47,48].

Isolation method	Principle	Advantages	Disadvantages
Differential centrifugations, followed by ultracentrifugation	Size, density	Most studied and most commonly used; easy to do; high EV yield	Time-consuming; possible EV damage or EV aggregation; low EV purity; low-throughput
Iodixanol or sucrose density gradient ultracentrifugation	Size, density	High EV purity; less EV damage compared to normal ultracentrifugation	Time-consuming and laborious; different subtypes of EVs can be co-purified; low-throughput
Size-Exclusion Chromatography (SEC)	Size (hydrodynamic volume)	Fast; no special equipment needed; gentle method resulting in structurally intact and functional EVs; high EV purity	Dilution of final EV sample, thus need to proceed with other methods; lEVs and sEVs are often co-purified
Ultrafiltration	Size	Fast; no special equipment required; easy to do	Low EV integrity; change in EV morphology; low EV purity; EVs may adhere to the filter (possible loss of EV subpopulations)
Tangential Flow Filtration (TFF)	Size	High EV yield and preserved EV integrity compared to ultrafiltration; scalability	Expensive (need of specialized equipment); in bioprocess it requires the control of multi-parameters
Field-Flow Fractionation (FFF)	Diffusion coefficient	Separates complex molecules better than SEC; more gentle compared to SEC	Expensive (need of specialized equipment); in bioprocess it requires the control of multi-parameters
Polymer Precipitation	Solubility	Low sample input volume; easy to use; no special equipment required; fast; high EV yield	Poor EV purity; polymer is difficult to be removed
Immunocapture	Specific interactions between proteins on the EV membrane and the corresponding receptors	Easy to perform; high EV purity	Low EV yield; expensive; not feasible with internal EV antigens; not scalable
Microfluidic technology	Size or affinity with surface markers	Fast; high-throughput; low sample input volume; high EV integrity	Skilled technique in microfluidic experiments is required; lack of standardization

Table 1. Overview of EV isolation methods and their main advantages and disadvantages.

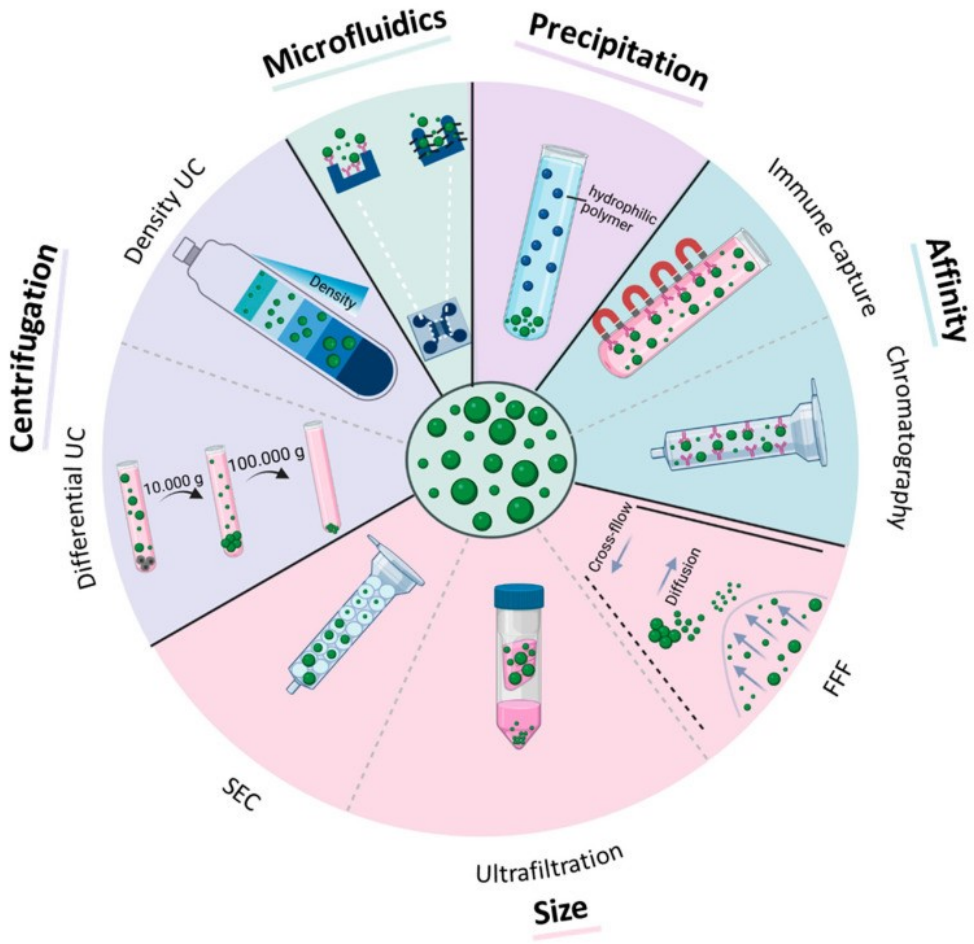

Figure 4. EV isolation methods exploit different physical/chemical principles [49].

2. Clinical and industrial applications of EVs.

2.1 Diagnostic value of EVs in liquid biopsy.

Tissue biopsies are invasive and non-feasible for longitudinal monitoring of patients; moreover, they do not capture the heterogeneity of the tissue. On the contrary, liquid biopsies are non-invasive and enable a real time snapshot of the tissue homeostasis or alterations by detection of relevant biomarkers. There are several biological specimens that can be assessed by liquid biopsy: circulating cell-free DNA (cfDNA) and RNA (cfRNA), released by dying cells, and circulating tumor cells (CTCs). In oncology, the most important cfDNA is circulating tumor DNA (ctDNA), which comes from cancerous cells. CTCs are intact, viable cells with malignant features, that are released from a primary tumor [50].

In recent years, also EVs have emerged as diagnostic tools in liquid biopsy. EVs are produced by most cell types and are present in body fluids (e.g., blood, saliva, urine, cerebrospinal fluid, and milk) [51]. EVs carry and protect from the extracellular environment many molecules, originating from the host cells, including proteins, lipids, carbohydrates, cytokines, DNA and many species of RNA, such as messenger RNAs (mRNAs), microRNAs (miRNAs), transfer RNAs (tRNAs), ribosomal RNAs (rRNAs), and other non-coding (nc) RNAs (long non-coding RNAs (lncRNAs), small interfering RNAs (siRNAs), small nuclear RNAs (snRNAs), small nucleolar RNAs (snoRNAs), piwi-interacting RNAs (piRNAs), circular RNAs (circRNAs), and Y-RNAs) [52–54]. The EV content is not only determined by the cellular source, but also by the cellular status and some environmental conditions like hypoxia, acidic pH, and oxidative stress [55].

Thus, they present several advantages compared to CTCs and cfDNA: like CTCs, they allow the detection and quantification of different kinds of cancer-related molecules, and, as opposed to CTCs, EVs are highly abundant in all human body fluids. In addition, EV cargo is more protected and more stable than cfDNA and soluble proteins in body fluids [41].

Since EVs are released at an early stage of pathogenesis, they are suitable for early detection and monitoring of cancer or other diseases [54,56].

The major challenge in using EV-based liquid biopsy is the tremendous complexity of biofluid samples, heterogeneity of extracellular vesicles and the low abundance of specific disease markers [49].

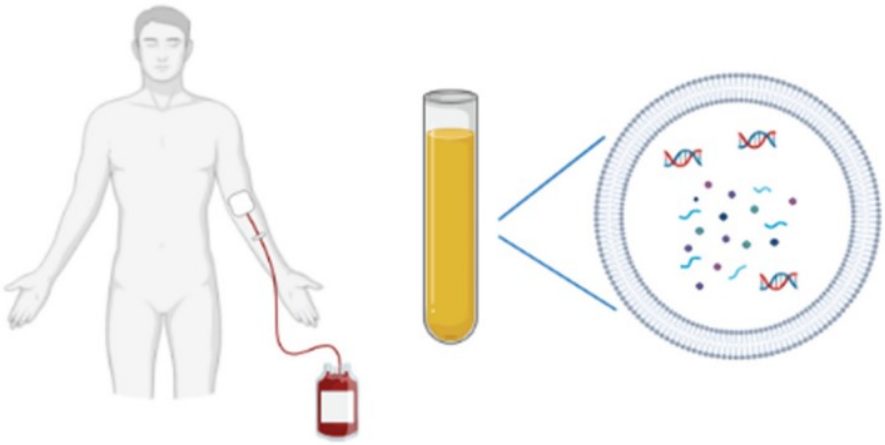

Figure 5. The liquid biopsy approach: a simple blood sampling allows the EV isolation from plasma, for biomarker discovery studies [56].

2.2 Therapeutic potential of EVs.

EVs by themselves (like EVs from mesenchymal stem cells) or as vehicles for the delivery of drug payload(s) have been investigated as therapeutic agents for many diseases, including neurodegenerative conditions and cancer [57].

EVs can be engineered to deliver diverse therapeutic molecules, including short interfering RNAs, antisense oligonucleotides, chemotherapeutic agents and immune modulators, with an ability to bind specifically the target cells [58,59].

EVs present several advantages compared to artificial vesicles, like liposomes. In fact, EVs are well tolerated, do not induce toxicity when repeatedly injected, are efficient at entering other cells and, having a superior systemic retention, can deliver a functional cargo at distant sites [60,61]. Moreover, EV intrinsic or engineered cargo is protected from degradation by blood-derived ribonucleases [62].

The natural function of EVs in the intercellular communication between cells can be exploited in the field of immunotherapy, where exosomes have been shown to have a therapeutic potential [63,64]. EVs containing antigens of specific tumors can induce an immune response against cancer cells containing their antigen spectrum, leading to the apoptosis of tumor cells. EV-based vaccines to target tumor or inflamed cells are the subject of several ongoing preclinical studies [65–67].

2.2.1 Industrial manufacturing of EVs.

Increasing evidence suggests that EVs produced in 3D bioreactors have superior therapeutic effects compared to 2D-derived EVs [68–70].

In spite of substantial progress in the field, the industrial production of EVs for therapeutic applications has some limitations, that need to be addressed in order to assure the development of safe, efficacious, and cost-effective cell-free therapies.

The first challenge is to meet the demand of EVs for pre-clinical and clinical studies. MSC-EV-based therapies require significant amounts of EVs per treatment [43]. For example, recent studies report that a single patient needs approximately 100 μg/kg of exosomes per treatment or 0.5 –1.4 × 10^{11} total EVs per treatment [71–73]. Moreover, unlike immortal cell lines, the expansion of MSCs is limited in culture and, according to most studies, only cells within passage six can be used [43]. Thus, a robust and scalable biomanufacturing process to produce sufficient MSC-EVs remains a major challenge [68,71].

Compared with conventional 2D culture, the 3D culture systems increase total EV production [74,75]. 3D-sEVs were reported to be more concentrated in the harvested supernatants (15.5-fold) than 2D-sEVs, which led to a higher sEVs collection efficiency of 3D culture system [76,77]. Conventional 2D culture would require several operating hours to harvest an equivalent quantity of EVs.

A strategy commonly used for large-scale production is microcarrier-based 3D culture, where cell density reaches 40000 cells/cm^2, double the density obtained in 2D cultures [68]. These bioreactors use an agitation system to maintain microcarriers in suspension and allowing medium homogenization.

There are other important aspects that need to be taken into consideration for the industrial production of EVs. Large-scale manufacturing process should be GMP-compatible and have integrated analytics to monitor and control culture parameters [43,78]. Also the choice of an appropriate serum-free cell culture medium is challenging [79].

The manufacturing process consists of sequential operations: tissue collection, cell isolation, cell culture and expansion in a 3D system (USP: Upstream Processing), CCM harvest and EV purification (DSP: Downstream Processing), and, finally, product formulation and storage. Limitations described above concern not only USP, but also DSP. In fact, EV isolation method is required to be easily scalable and it should preserve EV function [70,79]. Moreover,

standardized release criteria for EV preparation have to be established, and stability testing over defined time periods will need to be developed [43].

3. Purpose of the thesis.

This PhD research program has been developed and completed within a collaboration between the Department of Molecular and Developmental Medicine of the University of Siena and two companies: Exosomics SpA for the first year, then Lonza Cell & Gene Therapies for the remaining years.

The first part of this thesis is focused on the relationship between EVs and hypoxia, as pathological stress, and the use of EVs as diagnostic tool for cancer biomarker discovery. In particular, we studied the expression of a promising marker of tumor hypoxia, Carbonic anhydrase IX (CA-IX), in small EVs released by melanoma cells.

At the end of 2021 a part of the company Exosomics was acquired by Lonza Cell and Gene Therapies. The research activity started to be focused to another industrial application of EVs. Thus, the second part of the thesis is related to the production and characterization of EVs from mesenchymal stem cells for cell-free therapy.

4. Part I.

4.1 Introduction.

4.1.1 Hypoxia.

Tissue hypoxia is a condition of altered oxygen homeostasis, in which oxygen demand exceeds supply ensues. It can be a physiological condition, as it happens in intestinal mucosa, renal medulla, bone marrow and lymph nodes, or a pathological state [80,81]. Hypoxia as pathological stress arises when blood supply to a tissue is compromised, as in myocardial infarction, or when a reduction of oxygen levels and nutrients occurs in the cellular microenvironment, as in inflammation and solid cancers. In particular, hypoxia in cancer characterizes the tumor microenvironment and it is a consequence of both high oxygen demand from rapidly proliferating cells and low oxygen supply due to poorly vascularized regions [82,83].

Recent publications suggest a relationship between hypoxia and the release of EVs. In particular, hypoxia can affect the production, size, and molecular content of EVs during cancer. Some studies have demonstrated that hypoxia can enhance the release of EVs in multiple types of cancer [84–87]. Other studies have shown dissimilar observations using different cell models [88,89].

With this mechanism of paracrine communication, cancer cells alter the phenotype of stromal cells and other tumor cells [88,90]. Moreover, hypoxic EVs are reported to have a role in angiogenesis, stemness, activation of cancer associated fibroblasts (CAFs), epithelial-to-mesenchymal transition (EMT) and metastasis, thus mediating the development of cancer [91].

In 2021, we published a review to summarize the functions of EVs released under hypoxia in different cancer models and the EV-associated biomolecules involved in these processes.

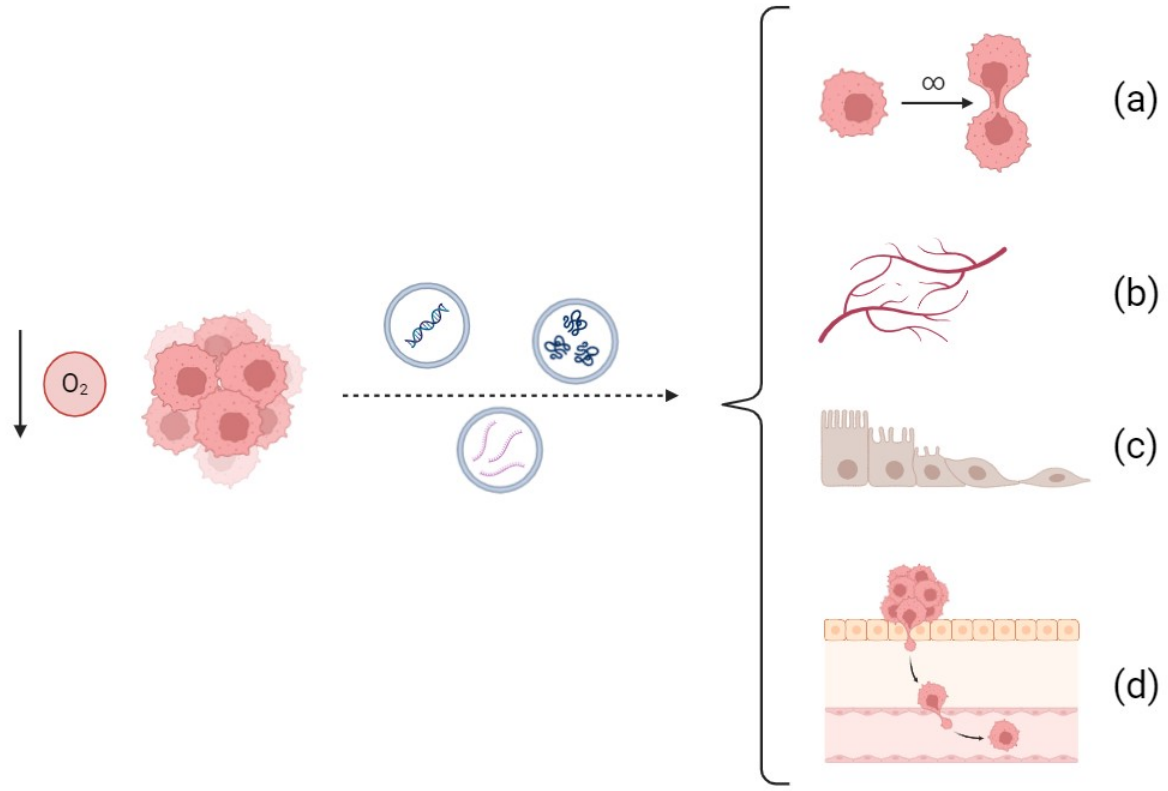

Figure 6. In cancer, hypoxia-derived EVs carry biomolecules involved in proliferation (a), angiogenesis (b), EMT (c) and metastatic behaviour (d) [56].

Cancer disease	Source of EVs	Functions of released EVs	Biomolecules carried by hypoxic EVs	References
Prostate cancer (PCA)	LNCaP and PC3 human PCA cells	Invasiveness, motility and stemness of naïve PCA cells; metalloproteinase activity; remodeling of epithelial adherens junction pathways; induction of CAF-type phenotype in prostate fibroblasts; PCA growth and invasiveness	Proteins: MMP-9, MMP-2, TGF-β2, TNF1α, IL6, TSG101, Akt, ILK1, β-catenin; triglycerides	[88,92]
Epidermoid carcinoma	A431 human squamous carcinoma cells	Angiogenesis; metastasis	not described	[93]
Glioblastoma multiforme (GBM)	U87-MG human GBM cells; plasma of tumor-bearing mice; plasma of GBM patients	Pro-angiogenic effects	mRNAs: ADM, LOX, IGFPB, BCL, BNIP3, NDRG1, PLOD2, PAI1; proteins: IL8, IGFBP1, IGFBP3; MMP9, PTX3, PDGF-AB/AA, CD26, PAI1, CAV1	[94]
	U87-MG human GBM cells	Tumor development; angiogenesis	Tissue Factor (TF)	[95]
Breast cancer	MCF-7, MDA-MB-231, MDA-MB-435 human breast cancer cells	Endothelial cell tubulogenesis; mechanisms of repressing DNA repair	miR-210	[86]
		Focal adhesion formation, invasion and metastasis	not described	[90]
	4T1 mouse breast cancer cells	Angiogenesis	miR-210	[95]
Leukemia	K562 human leukemia cells	HUVECs tube formation	miR-210	[89]
Multiple myeloma	RPMI8226, KMS-11, U266 human multiple myeloma cells	Tube formation; angiogenesis; regulation of FIH molecular pathway	miR-210, miR135b	[96]
Lung cancer	CL1-5 human lung cancer cells	Local and distant angiogenesis; increased vascular permeability; cancer transendothelial migration	miR-23a	[97]
	NCI-H1688 human small cell lung cancer and NCI-H2228 human non-small cell lung cancer	Migration of endothelial and cancer cells; metastasis	TGF-β and IL-10	[98]
	A549 human lung adenocarcinoma cells	Angiogenesis, metastasis, cancer cell survival, migration and tube formation	miR-135b, miR-210	[99]
Ovarian cancer	OVCAR-8, A2780, TR127, TR182 human ovarian cancer cells; patient-derived ascites	Tumor progression, metastasis and chemoresistance	STAT3, FAS proteins	[100]
Oral squamous cell carcinoma (OSCC)	SCC-9, CAL-27 human OSCC cells; serum of OSCC patients	EMT, migration and invasion of target normoxic cells	miR-21; miR-205, miR-148b (to be investigated)	[101]
Nasopharyngeal carcinoma (NPC)	NP69 and AdAH human NPC cells, transfected with latent membrane protein 1 (LMP1)	EMT; cancer progression and invasive potential	HIF1α	[102]

Colorectal cancer (CRC)	HT29 and HCT116 human CRC cells	Endothelial cells proliferation and migration; tumor growth and angiogenesis	Wnt4 protein	[103]
Melanoma	B16-F0 mouse melanoma cells, A375 human melanoma cells, A431 squamous skin carcinoma cells, A549 lung adenocarcinoma cells	Monocyte/macrophage recruitment *in vitro* and *in vivo* and host immunosuppression; tumor cell proliferation	chemokines and growth factors (CSF-1, CCL2, EMAP2, TGFβ, FTH, FTL); miR-let-7a, miR-21a	[104]
Hepatocellular carcinoma (HCC)	Huh7 and MHCC-97H human HCC cells	Proliferation, migration, invasiveness, EMT in normoxic HCC cells	miR-1273f, miR-93-5p, miR-221-3p	[105]
Pancreatic cancer (PC)	PANC-1, BxPC-3 cell lines; serum of PC patients	M2 polarization of macrophages, metastatic behavior of PC cells *in vitro* and *in vivo*	miR-301a-3p	[106]

Table 2. Effects of hypoxia on EVs in different cancer diseases [56].

4.1.2 Hypoxia-Inducible Factors.

Hypoxia-Inducible Factors (HIFs) are a family of transcription factors and are the major components of intracellular hypoxia signalling pathways. They are considered the "master regulators" of oxygen homeostasis: they regulate the expression of thousands of genes involved in crucial aspects of cancer biology, such as cell survival, metabolism, angiogenesis, and invasion. Among HIF-1 transcriptional targets there are also pH-regulating enzymes, such as carbonic anhydrases (CAs), which help maintaining pH homeostasis in cells and are responsible of tumor acidosis [107–113].

HIFs are inactive when oxygen is available, but become active in hypoxic conditions. HIFs consist of heterodimers of an α-subunit (the oxygen-sensitive subunit; α1, α2 or α3) and a constitutively expressed β-subunit (β1 or ARNT), largely insensitive to changes in oxygen tension.

Both the subunits contain helix loop helix and PER-ARNT-SIM (PAS) domains in their NH_2-terminal regions that allow the binding to specific DNA sequences called hypoxia response elements (HREs), in the promoter of target genes [102].

Under normoxic conditions (21% O_2), the α subunit is hydroxylated by prolyl hydroxylases (PHDs) at specific proline and asparagine residues, and consequently recognized by Von Hippel Lindau protein (VHL) and ubiquitinated by E3 ubiquitin ligase complex for proteasome degradation in the cytoplasm [114]. In hypoxic conditions PHDs are inactive, thus α subunit is stabilized and synthesized *de novo* at a high rate [115]. Consequently, it can form the

heterodimer with the β subunit, then translocate to the nucleus and start the transcription of target genes [116].

PHDs are not the unique regulators of HIFα; also the oxygen sensor factor inhibiting HIFα (FIH) can reduce the transcriptional activity of HIFα, by hydroxylation of asparagyl residues. The hydroxylated HIFα cannot bind to its co-activator CBP/p300 [91].

4.1.3 Carbonic Anhydrase IX.

Carbonic anhydrase IX (CA-IX) is a promising marker of tumor hypoxia and its expression is regulated by HIF-1, which binds to a HRE consensus sequence localized in the promoter region of the *CA9* gene [83].

Under normoxic conditions, prolyl hydroxylases (PHDs) hydroxylate the proline sites of HIF-1α protein. This enables the binding of the von Hippel Lindau protein (VHL) to HIF-1α, which leads to the proteasomal degradation of HIF-1α. Under hypoxic conditions, hydroxylation doesn't occur, leading to accumulation of HIF-1.

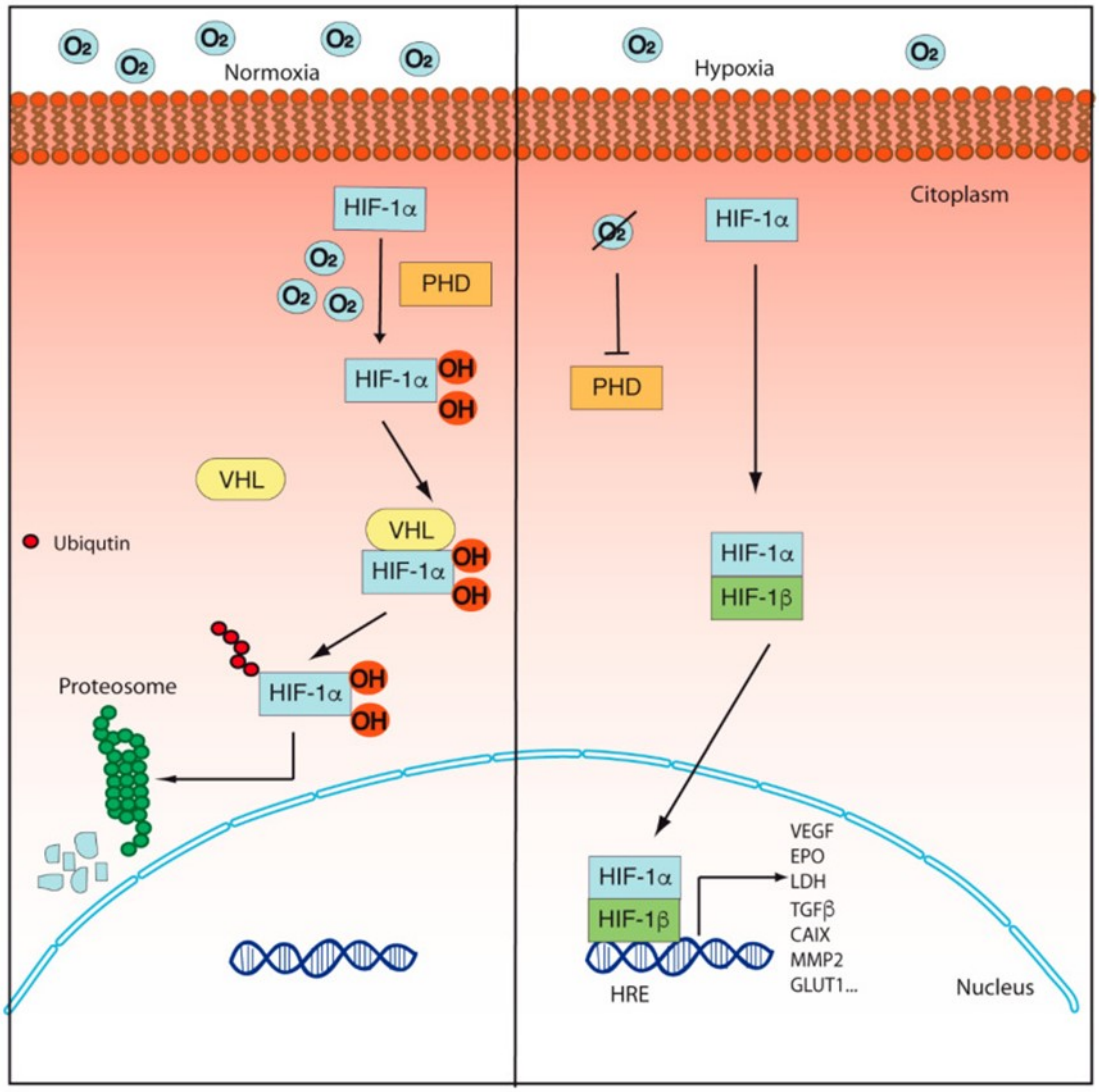

Figure 7. Schematic representation of the HIF-1 pathway. Under normoxic condition, HIF-1α is hydroxylated and rapidly degraded (A). Under hypoxic condition, the HIF-1 complex is stabilized and initiates the transcription of target genes, including CA-IX (B) [117].

CA-IX belongs to the family of carbonic anhydrases (CA) and it is a transmembrane zinc-containing metalloenzyme, that catalyzes the reversible hydration of carbon dioxide to bicarbonate and protons ($H_2O + CO_2 \leftrightarrow H^+ + HCO_3^-$). It is involved in the respiratory gas exchange and acid–base balance, playing a crucial role in maintaining the cell pH homeostasis. It has been demonstrated that CA-IX forms a close interaction with ion-transport systems, the metabolons, contributing to ion-transport and electrolyte-secretion [118,119].

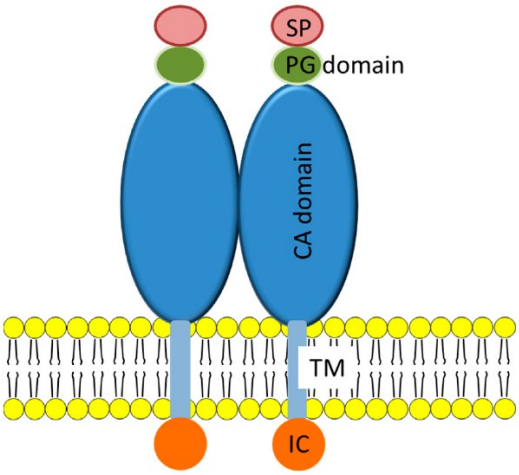

Figure 8. Structure of CA-IX protein [120].

CA-IX is anchored to the extracellular surface by a transmembrane domain (TM), placing its catalytic domain on the extracellular side of the plasma membrane [120].

In normal tissues, the expression of CA-IX is present only in stomach, duodenum, small intestine and gallbladder [119]. Instead, CA-IX overexpression is associated with a variety of solid cancers and it has been found to be highly expressed in invasive melanomas [121,122]. In cancer, CA-IX maintains a favorable intracellular pH for tumor cells, thus increasing their survival and growth, and is correlated with aggressive phenotypes, the maintenance of stemness properties, therapy resistance, and poor prognosis [123–125].

4.1.4 Melanoma.

Cutaneous melanoma is one of the most aggressive types of skin cancer, with poor prognosis. It arises from transformed melanocytes, and despite constituting 1% of skin tumors, it is responsible for over 80% of skin cancer deaths [126].

The World Health Organization (WHO) classifies melanocytic lesions into nine categories according to the associated cumulative sun damage (CSD), which correlates with DNA alterations. Genetic susceptibility is also a relevant risk. The most common genomic alterations are related to pathways controlling cell proliferation and survival (BRAF, NRAS, and KIT, respectively) [127].

The primary treatment is the chirurgical resection of the primitive lesion in order to obtain a good prognosis. For metastatic diseases, new targeted therapies such as BRAF inhibitors have been studied in clinical trials, but since melanoma has great abilities to migrate and invade

other tissues, often patients develop a secondary resistance within a relatively short amount of time [128].

The melanoma tumor microenvironment can be characterized by areas of hypoxia, and this component is associated with an increased ability of invasion and metastatic potential in primary melanoma [129,130]. In addition, melanoma metastasis are not vascularized in the early state and adapt to the initial hypoxic condition, which can lead to an even more aggressive phenotype [131,132]. Hypoxia activates hypoxia-inducible factor-1 (HIF-1), which promotes the transcription of several genes involved in biological mechanisms related to melanoma progression such as angiogenesis, cell proliferation, and metastasis [133,134].

4.1.5 Scope of the work.

In literature, few studies report the relationship between CA-IX and small EVs in different cancer types [135–137]. We investigated, for the first time, the expression of CA-IX protein associated with sEVs in two melanoma *in vitro* models. Our purpose is to demonstrate the potential application of CA-IX-expressing sEVs as biomarkers for cancer diagnosis.

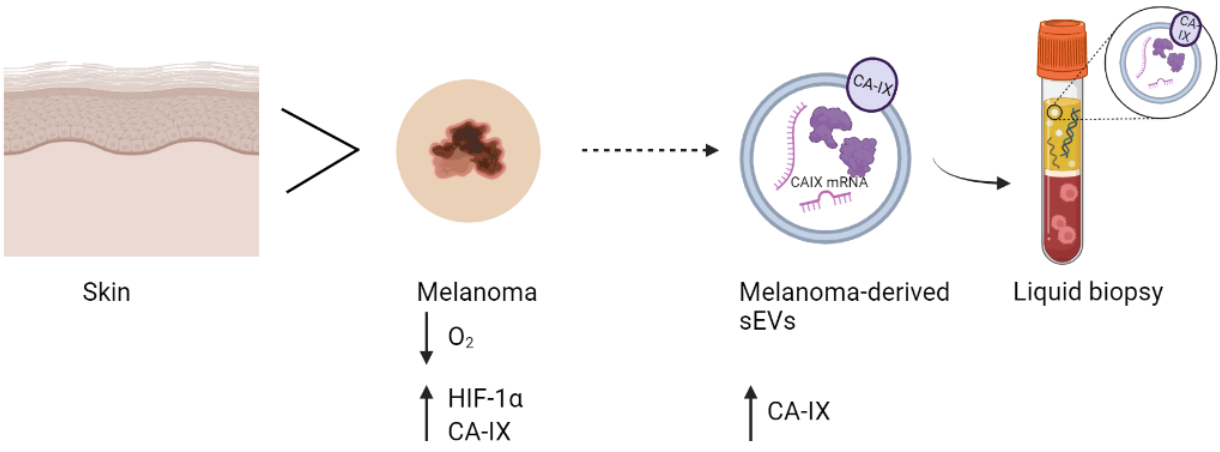

Figure 9. Small EVs released from melanoma cells, under hypoxia, express the hypoxia-induced biomarker CA-IX. CAIX-expressing sEVs can be found in plasma of melanoma patients and exploited for liquid biopsy approach.

4.2 Materials and Methods.

4.2.1 Melanoma cell culture.

Two different human melanoma cell lines, SK-MEL-28 and A375, were provided by Dr. Francesca Chiarini (University of Bologna, Bologna, Italy) and Prof. Luisa Bracci (University of Siena, Bologna, Italy), respectively. The A375 cell line is characterized by a more aggressive phenotype compared to the SK-MEL-28 cell line. Cells were grown in RPMI 1640 or DMEM 10% fetal bovine serum (FBS) with antibiotics and L-glutamine added (Euroclone, Devon, UK). SK-MEL-28 and A375 cells were maintained in a humidified atmosphere at 37 °C, 5% CO_2, 20% O_2 (normoxic condition), and 37 °C, 5% CO_2, 2% O_2 (hypoxic condition).
After 24 hours of culture, the supernatant of each cell line (200 ml), for each condition, was collected for the isolation of small EVs.

4.2.2 Size Exclusion Chromatography.

Size Exclusion Chromatography (SEC) is an efficient method to purify EVs without affecting the original shape and functionality of the vesicles. For each condition, 200 mL of cell conditioned medium (CCM) was pre-cleared by differential centrifugation at 300x g for 10 minutes, 1200x g for 20 minutes, and 10,000x g for 30 minutes at 4 °C. Pre-cleared CCM was concentrated by ultrafiltration with an Amicon® Stirred Cell with Ultracel 100 kDa Ultrafiltration Discs (Merck Millipore, Burlington, MA, USA) to a final volume of 10 mL. Concentrated samples were purified by SEC (qEV10 35 nm, Izon Science, Christchurch, New Zealand). Columns were pre-equilibrated with 1X 0.22 µm filtered PBS, 10 mL of concentrated CCM was loaded in column, then 1X 0.22 µm filtered PBS was used as the mobile phase. The eluate was immediately collected in 60 fractions of 1 mL each. All of the fractions were characterized by micro BCA assay (Thermo Fisher Scientific, Cleveland, OH, USA) and by CD9 sandwich ELISA assay (Exosomics, Siena, Italy). CD9 positive fractions with a low protein concentration were pooled and concentrated to 0.5 mL by 100 kDa ultrafiltration (Amicon® Ultra-15 Centrifugal Filter Unit, Merck Millipore, Burlington, MA, USA). Purified EVs were aliquoted and stored at -80 °C.

4.2.3 EV size and concentration analysis.

To measure the EV size and particle concentration, samples were analyzed using a Flow NanoAnalyzer (nanoFCM Inc., Nottingham, UK), which enables single particle analysis in sheathed flow. The instrument was aligned and calibrated with size and concentration standard beads (nanoFCM Inc., Nottingham, UK), which allowed for the characterization of small EVs between 40 nm and 200 nm. The samples and blank (1X PBS) were read at a constant pressure of 1 kPa for 2 minutes and at a maximum event rate of 12000 events/minute. Between samples, the instrument was cleaned with 1X cleaning solution (nanoFCM Inc., Nottingham, UK) and the capillary rinsed with HPLC-grade water.

4.2.4 RNA Extraction.

Total RNA was extracted from EV samples in order to determine the expression of CA-IX mRNA. RNA was extracted from 6 x 10^9 total particles for each condition. A total of 700 µL of TRIzol™ (Thermo Fisher Scientific, Cleveland, OH, USA) was added to each sample. Samples were vortexed for 30 s and incubated for 5 minutes at RT. Then, 140 µL of pure chloroform was added, the tubes were shaken for 30 seconds and incubated for 10 minutes at RT, then 1 minute in ice. Phases were separated by centrifugation for 10 minutes at 12000x g at 4 °C and the aqueous phase was transferred to a clean tube. Pure ethanol was added to each sample (2:1) and tubes were inverted 4–5 times. The mixture was transferred into a RNA spin column (Epoch Life Science, Missouri City, TX, USA) and centrifuged for 30 seconds at 14000x g at RT, discarding the flow-through. Columns were washed 3 times with 400 µL of Wash Buffer (165 mM NaCl, 33 mM Tris HCl, 3.3 mM EDTA in MilliQ water, pH 7.4–7.5), centrifuging and discarding the flow-through as described above. RNA was eluted with 15 µL of nuclease-free water.

4.2.5 Droplet Digital PCR.

Droplet Digital PCR (ddPCR) is a technique that allows an absolute quantification of a DNA or RNA target, with no need for a standard curve, because the number of targets in a given volume is counted directly. It is characterized by high sensitivity, since it enables the detection of few copies of the target of interest.

Gene expression ddPCR reactions were performed in a duplex configuration using commercially available assays to amplify the beta actin (housekeeping gene) and CA-IX targets (Assay IDs: dHsaCPE5190200; dHsaCPE5055974; Bio-Rad, Hercules, CA, USA), containing HEX and FAM-conjugated reporter probes, respectively. For each sample, a 20 µL one-step ddPCR reaction was prepared (One-Step RT-ddPCR Advanced Kit for Probes, Bio-Rad, Hercules, CA, USA), diluting each assay 1:20 and adding 5 µL of RNA sample. Droplets were generated with a QX200™Droplet Generator (Bio-Rad, Hercules, CA, USA) and transferred to 96-well PCR plates. Amplification conditions were set as follows. Reverse transcription: 42 °C for 60 minutes; enzyme activation: 95 °C for 10 minutes; amplification: 39 cycles of denaturation at 95 °C for 30 seconds and extension at 55 °C for 1 minute, with a ramp rate of 3 °C/s; enzyme inactivation: 98 °C for 10 minutes. Droplets were read in a QX200 Droplet Reader (Bio-Rad, Hercules, CA, USA) and the gene expression data analyzed with QuantaSoft™ Version 1.7 (Bio-Rad, Hercules, CA, USA).

4.2.6 Western Blot.

Western blot is a technique used to separate and identify proteins.

Both cell lines were seeded at a density of 3 x 10^5 cells/well and maintained in normoxia or hypoxia. Cells were lysed with Laemmli buffer with protease inhibitors (Sigma Aldrich, Saint Louis, MO, USA), and after sonication, the total protein amount was determined with micro BCA Protein Assay Reagent Kit (Thermo Fisher Scientific, Cleveland, OH, USA). A total of 30 µg of proteins for each condition was loaded on 10% acrylamide gel. The EV samples were prepared mixing 2 x 10^9 total particles with Laemmli sample buffer 4X (Bio-Rad, Hercules, CA, USA) containing beta-mercaptoethanol and incubated at 95 °C for 10 minutes. Samples were loaded on precast 4–20% Mini-PROTEAN® TGX Gel, 12-well, 20 µL per well (Bio-Rad, Hercules, CA, USA), then the proteins were transferred onto a 0.2 µm nitrocellulose membrane using the Trans-Blot Turbo Transfer System with the Trans-Blot Turbo Transfer Pack (Bio-Rad, Hercules, CA, USA). Western blotting were performed using EveryBlot Blocking Buffer (Bio-Rad, Hercules, CA, USA) for the blocking step and to dilute the primary antibodies and the secondary antibodies. Primary antibodies against HIF-1 (BD Biosciences, San Jose, CA, USA, 1:200 Cat. no. 610958), CA-IX (Cell Signaling, Danvers, MA, USA, 1:500 Cat. no. 5649S), beta actin (Sigma-Aldrich, Saint Louis, MO, USA, 1:50,000 Cat. no. A3854), and Alix (Santa Cruz, Dallas, TX, USA, 1:500, Cat. no. sc-271975) were used. Chemiluminescence was produced

using the SuperSignal™ West Femto Maximum Sensitivity Substrate (Thermo Fisher Scientific, Cleveland, OH, USA).

4.2.7 Biacore Surface Plasmon Resonance (SPR) assay.

Surface plasmon resonance (SPR) is a technology able to measure the molecular interactions between a protein, immobilized on a sensor surface, and a sample containing a potential interacting partner.

The antibody of interest against CA-IX (Exosomics SpA) was immobilized via amine group on a CM4 sensor chip. The antibody was diluted in 10 mM Na acetate pH 5.0 at the concentration of 20 µg/ml and injected for 3 minutes over the dextran matrix, which had been previously activated with a mixture of EDC-NHS for 6 minutes. After antibody injection, a pulse of ethanolamine 1 M was performed to neutralize the activated group.

The recombinant protein CA-IX was diluted at 5 µg/ml, 2.5 µg/ml, 1 µg/ml and 0.1 µg/ml in HBS-EP+ (Cytiva). CA-IX-positive sEVs were diluted at 50 µg/ml, 25 µg/ml and 10 µg/ml in HBS-EP+. Samples were injected for 120 seconds at a flow rate of 30 µl/min and dissociation was followed for 400 seconds, regeneration was achieved with a 30 seconds injection of glycine 10 mM pH 2.0. HBS-EP+ was used as running buffer.

4.2.8 ELISA assay.

A sandwich ELISA measures antigens between two layers of antibodies (a capture and a detection antibody). The target antigen, in this case the EVs, must contain at least two antigenic sites capable of binding to antibodies.

EV samples were analyzed with two types of sandwich ELISA. In the first assay, used to confirm EV identity, the capture and detection antibodies target both the tetraspanin CD9, a canonical small EV marker.

The second assay was used to demonstrate that the CA-IX protein is associated to EV membranes (Exosomics SpA). The capture antibody is against CA-IX and the detection antibody is against a canonical EV marker (target not disclosed). EVs were treated with RIPA buffer, containing the protease inhibitors cocktail (ThermoFisher Scientific, Cleveland, OH, USA), in order to lyse the lipidic membrane [138]. The same number of particles for each condition was loaded onto the plate (1 x 10^9 total particles). OD were read at 450 nm using a microplate reader (CLARIOStar Plus, BMG Labtech, Ortenberg, Germany).

4.2.9 Blood samples and Patient consent.

Plasma samples from patients with unresectable metastatic melanoma stage IIIC–IV were collected for this study from January 2011 to December 2014 and followed-up until December 2016. The study was approved by the Ethical Committee of the Azienda Ospedaliera Universitaria Le Molinette, Torino, Italy, and plasma samples were collected from patients after informed consent (Comitato Etico Interaziendale Titolare A/2.10 del 03-07-2014 Prot. N. 0068188). To obtain plasma for the study, 10 mL of blood was collected in K2-EDTA Vacutainer® tubes (Becton Dickinson, Franklin Lakes, NJ, USA, Cat. no. 366643) using a butterfly system with a needle gauge of 21 (Becton Dickinson, Franklin Lakes, NJ, USA, Cat. no. 367281). Blood tubes were then mixed 8 times and processed within 4 hours from the sampling by centrifugation at 1500x g for 15 minutes at RT. Plasma was aliquoted (1 ml) in labeled cryotubes and stored at - 80 °C prior to use. Before EV isolation, all plasma samples were centrifuged at 1200x g for 20 minutes at 10 °C to eliminate red blood cells and cellular debris.

4.2.10 Immunocapture of EVs from plasma samples.

Immunocapture method allows the pull down of a sub-population of tumor-derived EVs from human biofluids [45]. An anti-CA-IX antibody and an isotype control antibody (Exosomics SpA, Siena, Italy) were used for the selective immunocapture of CA-IX-positive sEVs, and for the capture of a generic population of EVs, respectively, from the plasma of melanoma patients. Latex beads (Magsphere, Pasadena, CA, USA) were coated using 1 µg of antibody per sample. Then, 10 µL of antibody-coated beads were added to the pre-cleared diluted plasma sample (1:1 with 1X PBS). Samples were mixed by pipetting and incubated for 2 hours at RT under rotation. After incubation, samples were centrifuged at 5000x g for 10 minutes at RT. The supernatants were carefully discarded without disturbing the bead pellets. The pellets were washed two times with 1X PBS and spun down by centrifugation at 5000x g for 10 minutes. The final pellets were resuspended in 200 µL of 1X PBS.

4.2.11 Isolation of EVs from plasma samples with SeleCTEV kit.

In order to compare the immunocapture method with another method, able to extract both generic tumor-derived EVs and ctDNA, plasma samples were processed with SeleCTEV kit

(HansaBioMed, Tallinn, Estonia). Starting from the same volume of plasma, samples were diluted 1:1 with 1X Isolation buffer, mixed by pipetting with the Isolation agent and incubated for 2 hours at RT under rotation. After incubation, samples were centrifuged at 16000x g for 15 minutes at RT. The supernatants were carefully discarded without disturbing the pellets. The pellets were washed two times with 1X Isolation buffer and spun down by centrifugation at 7000x g for 7 minutes. The final pellets were resuspended in 200 µL of 1X Isolation buffer.

4.2.12 DNA Extraction.

Bead-bound sEVs from immunocapture and final pellets obtained with SeleCTEV kit were treated with the reagents included in the SeleCTEV Tumor DNA Enrichment Kit (HansaBioMed, Tallinn, Estonia), following the manufacturer's instructions. Pellets were lysed with lysis buffer and digested with proteinase K to release the DNA from protein complexes. The samples were then supplemented with pure ethanol, loaded onto silica membrane spin columns, and centrifuged at 10,000x g for 1 minute. Following centrifugation, the flow-through was discarded. Two washing steps were performed to remove the contaminating solvents and plasma-derived inhibitors. Purified sEV-DNA was eluted in a final volume of 15 µL of elution buffer.

4.2.13 Real time PCR.

PCR amplification of EV-DNA is challenging due to the low abundance and high fragmentation of the template. Therefore, a pre-amplification step was included in the protocol upstream of the quantitative real-time PCR (qPCR) to improve the detection of the BRAF gene.

The following pre-amplification primers and probes were used:

(a) BRAF WT FW: 50-TAGGTGATTTTGGTCTAGCTACAG+T-30;

(b) BRAF WT RW: 50-TTAATCAGTGGAAAAATAGCCTCA-30;

(c) BRAF V600E FW: 50-TAGGTGATTTTGGTCTAGCTACAG+A-30;

(d) BRAF V600E RW: 50-TTAATCAGTGGAAAAATAGCCTCA-30.

The following qPCR primers and probe were used:

(a) WT: FW: 50-TAGGTGATTTTGGTCTAGCTACAG+T-30;

(b) WT RW: 50-TTAATCAGTGGAAAAATAGCCTCA-30;

(c) V600E FW: 50-TAGGTGATTTTGGTCTAGCTACAG+A-30;

(d) V600E RW: 50-TTAATCAGTGGAAAAATAGCCTCA-30.

(e) Probe: 50-FAM-CCGAAGGGGATC+CAGACAA+CTGTTCAAACTGCCTTCGG-3BHQ1-3

All reagents were thawed at RT for at least one hour and briefly mixed without vortexing to avoid inactivation of the enzyme. Each pre-amplification reaction included 7 µL of eluted DNA, 1X Bioron High Fidelity Buffer, 3 mM $MgCl_2$; 200 µM dNTPs, 1.25 units of SNPase polymerase (Bioron GmbH, Römerberg, Germany), and 0.4 µL of primers (10 µM) in a total volume of 20 µL. Each reaction was performed in a PCR-compatible microvial loaded onto a thermal PCR cycler running the following PCR program: 98 °C for 30 seconds, 98 °C for 10 seconds, and 72 °C for 5 minutes, 4 °C on hold. The pre-amplified DNA was diluted in 80 µL of nuclease-free water and immediately used for qPCR analysis. For the amplification of target genes from EV-DNA, each qPCR reaction included 7 µL of pre-amplified DNA, 1X SsoAdvanced Universal Probes Master mix (Biorad, Hercules, CA, USA), 0.625 µL of primers (10 µM), and 0.3125 µL of fluorescent probe (10 µM) in a total volume of 25 µL.

After careful mixing, each reaction was loaded in duplicate on a 96-well PCR plate and the following qPCR program was launched: 95 °C for 3 minutes, 40 cycles at 95 °C for 5 seconds, and 60 °C for 30 seconds, followed by a final hold step at 4 °C.

4.2.14 Statistical analysis.

Two independent biological experiments have been done with A375 and SK-MEL-28 cells, respectively. For each analytical method, analysis of at least two technical replicates are reported as the mean ± standard deviation (SD). Error bars show SD of the mean.

Prism Version 10.00 for Windows (GraphPad Software, La Jolla, CA, USA) was used for statistical analysis of obtained results. A two-tailed Student's t-test was applied to evaluate the statistical difference between two conditions. Statistical comparisons that output p-values < 0.05 were considered significant.

4.3 Results.

All the results described below have been published and presented in a poster session during the 73rd SIF (Italian Society of Physiology) national congress, held in Pisa from 6th to 8th September 2023 [139].

4.3.1 Evaluation of the expression of HIF-1α and Carbonic Anhydrase IX in melanoma cells.

The A375 and SK-MEL-28 human melanoma cell lines were cultivated under a normoxic condition (20% O_2 ~ pO_2 of 140 mmHg) and, for 24 hours, under a hypoxic condition (2% O_2 = pO_2 of 14 mmHg). Cell lysates were analyzed by Western blotting in order to investigate the expression of HIF-1, CA-IX, and a housekeeping protein (beta actin). The results are shown in Figure 10. Both cell lines expressed significantly higher protein levels of HIF-1α under the hypoxic condition, confirming the hypoxic state of cell cultures. As expected, CA-IX protein expression was also induced under hypoxia in the A375 and SK-MEL-28 cells, since its expression is driven by HIF-1α. Moreover, the levels of CA-IX expression were higher in the A375 model compared to SK-MEL-28, and this was an expected result due to the more aggressive phenotype of the A375 cells. Expression levels of the control protein (beta actin) were similar in all of the samples.

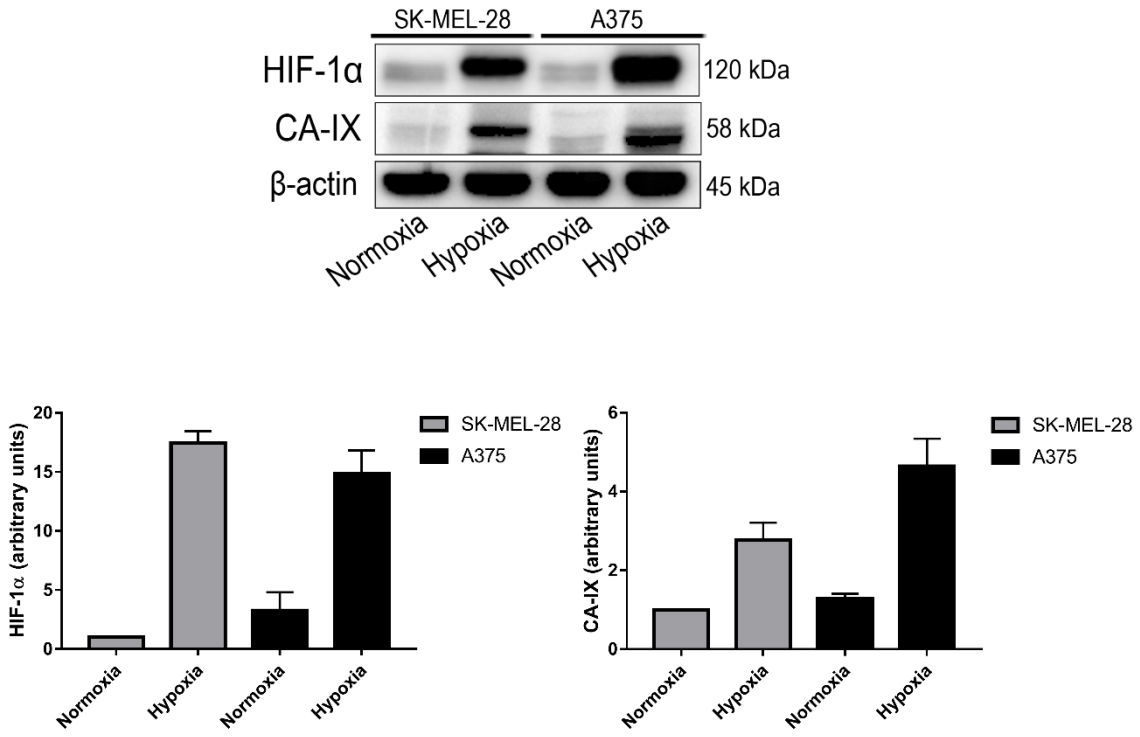

Figure 10. HIF-1α and CA-IX protein expression in A375 and SK-MEL-28 cell lines, after 24 hours exposure to normoxia or hypoxia. Bar charts are representative of two independent experiments and beta actin was used as loading control.

4.3.2 Characterization of small EVs released by melanoma cells.

Equal amounts of CCM from each condition were harvested to purify sEVs by SEC chromatography. 60 fractions of 1 ml each were eluted and analyzed by micro BCA assay, to assess total protein content, and ELISA assay (to assess exosome positive fractions). An example of SEC elution profile of CCM sample from A375 cells is shown in Figure 11.

Fractions positive for CD9 (plot in blue), but with a low protein concentration (plot in green), were pooled and concentrated to 0.5 mL by 100 kDa ultrafiltration.

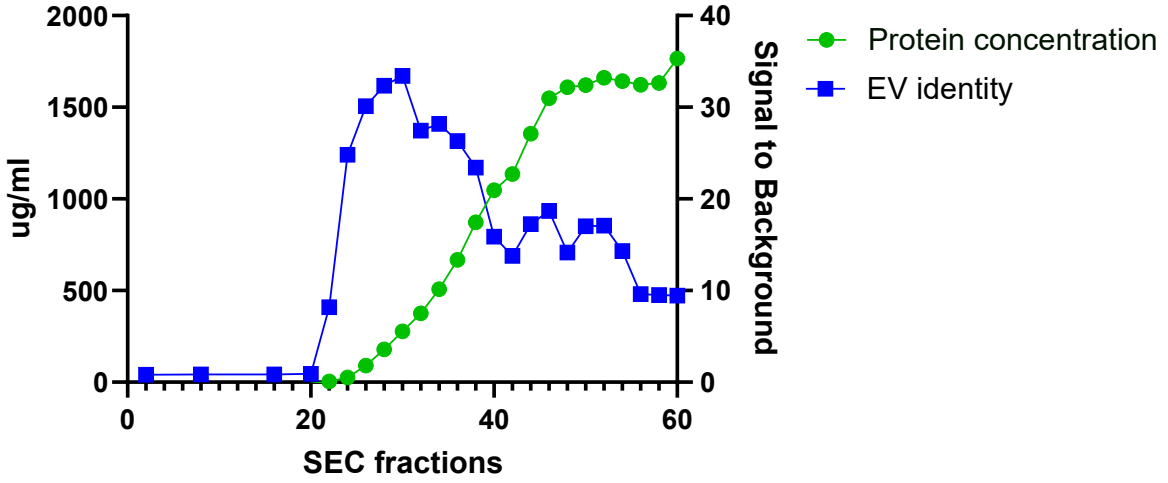

Figure 11. An example of SEC elution profile of A375 CCM, collected after hypoxic treatment. The graph shows the overlay of protein concentration (in green) and positivity for tetraspanin CD9 (in blue) of 60 fractions.

Purified sEVs were analyzed at NanoAnalyzer to assess the particle's concentration and size distribution profile. The concentration and total number of particles released by the A375 cells in normoxia were found to be slightly higher than after hypoxic treatment (Figure 12A). The same trend was observed for the SK-MEL-28 cells (Figure 12A).

All samples had comparable size distribution profiles within the expected size range of sEVs (Figure 12B), with median size values between 64 and 79 nm (Figure 12C).

(A)

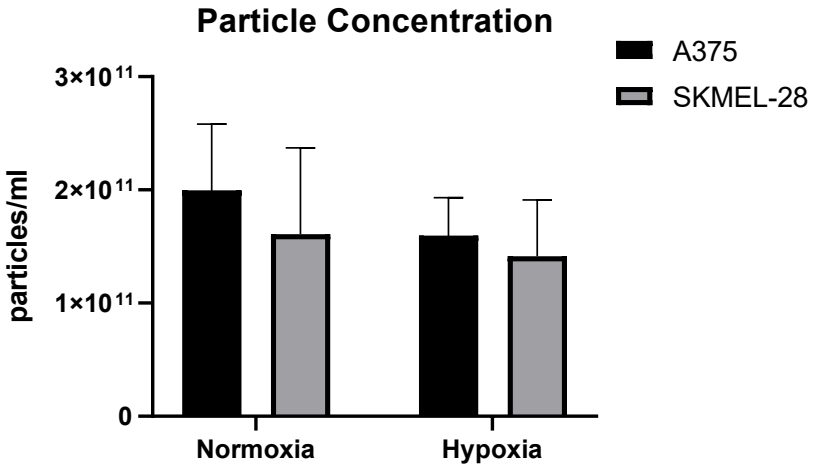

(B)

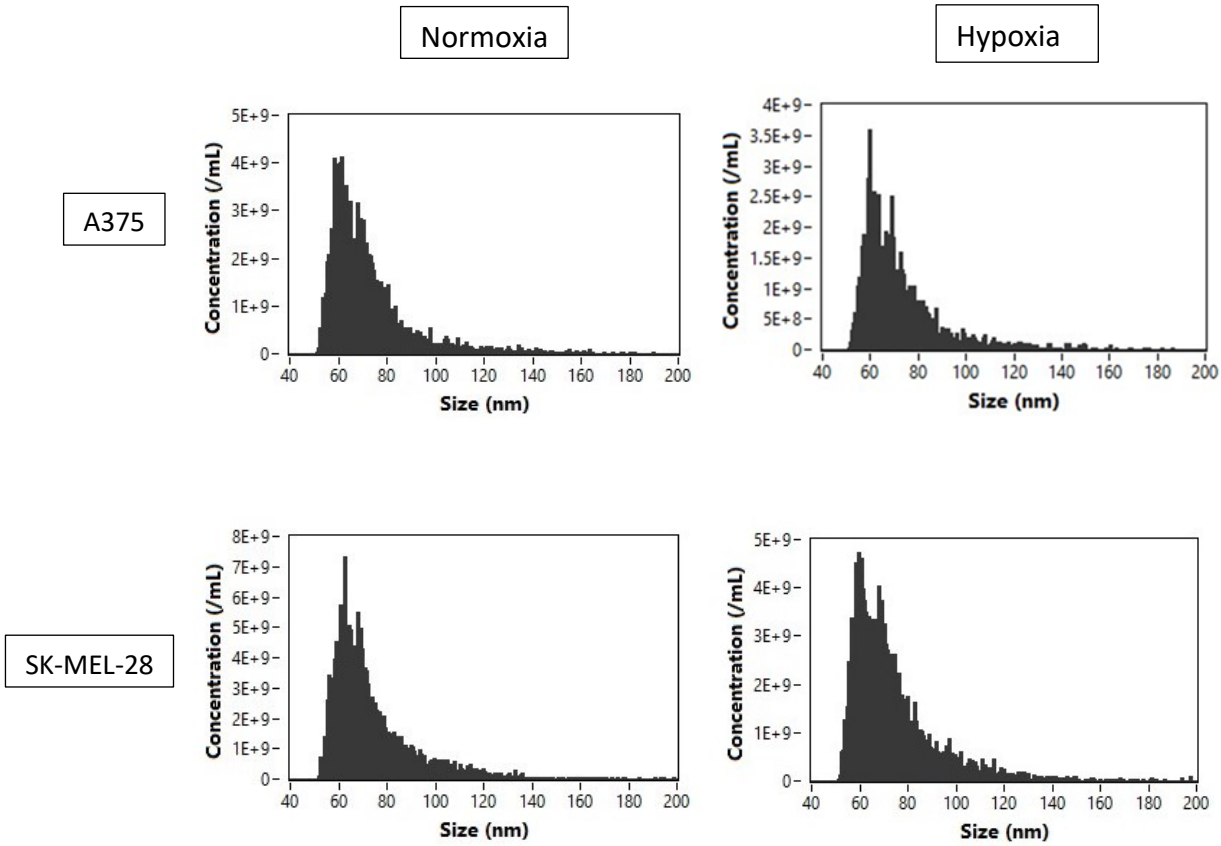

(C)

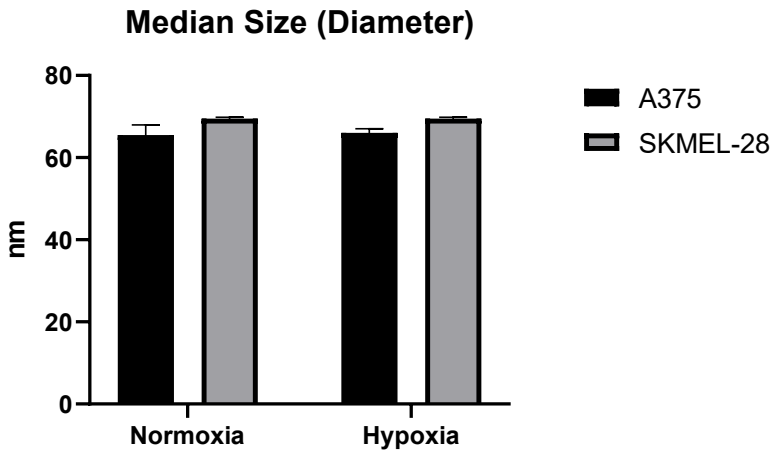

Figure 12. Particle concentration of purified sEVs from A375 and SK-MEL-28 CCM (A). Size distribution profiles by nanoFCM and Median sizes of purified sEVs (B-C). Bar graphs represent the average of two independent experiments.

Next, we investigated whether sEVs carry hypoxia-induced markers after hypoxic treatment. Carbonic anhydrase IX (CA-IX) was selected as a hypoxia-induced marker due to its overexpression in melanoma [140].

To determine the expression of CA-IX mRNA on sEVs, the total RNA was extracted from equal amounts of EVs produced from each condition. Digital droplet PCR was used to quantify the CA-IX and beta actin mRNA copies. Small EVs from the A375 cells were found to carry detectable levels of the CA-IX target even in normoxic condition. Under the hypoxic condition, the expression levels of CA-IX mRNA increased significantly up to 35-fold (Figure 13A, p value < 0.005). Conversely, CA-IX mRNA was not detected in sEVs from the SK-MEL-28 cells in both the normoxic and hypoxic conditions (Figure 13B).

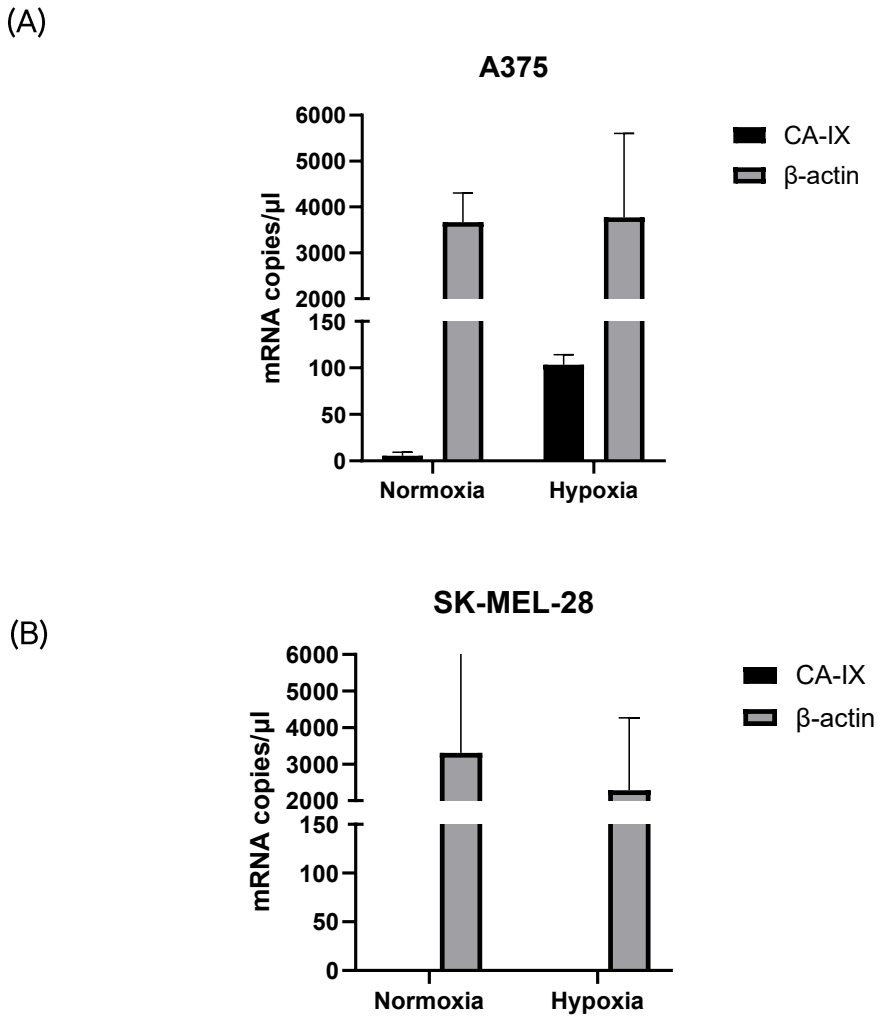

Figure 13. CA-IX and beta actin mRNA copies measured by ddPCR in A375-derived sEVs (A) and SK-MEL-28-derived sEVs (B), under normoxic and hypoxic conditions. Bar graphs are representative of two independent experiments. Beta actin was used as housekeeping gene control.

To evaluate the expression of CA-IX protein, equal numbers of sEVs were lysed and analyzed by Western blotting. Consistent with the mRNA expression data, immunoblotting analysis showed CA-IX protein expressed on sEVs from hypoxic A375 melanoma cells. The canonical EV marker (Alix) was found on sEVs under both normoxic and hypoxic conditions (Figure 14). CA-IX protein was not found on sEVs from hypoxic SK-MEL-28 cells, while Alix was expressed in both conditions (Figure 15).

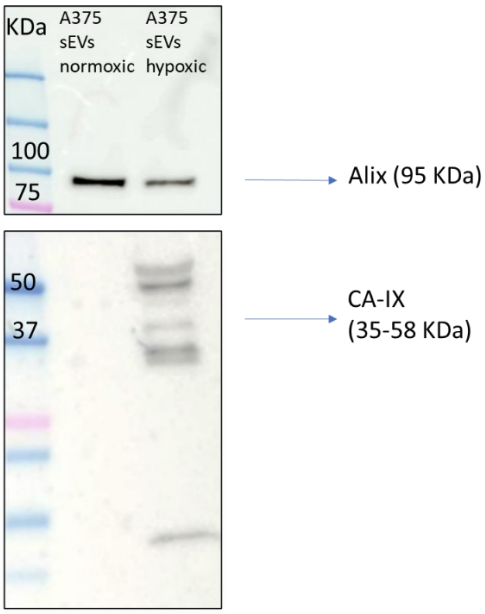

Figure 14. Example of blots showing CA-IX and Alix protein expression in A375-derived sEVs, released under normoxia and hypoxia.

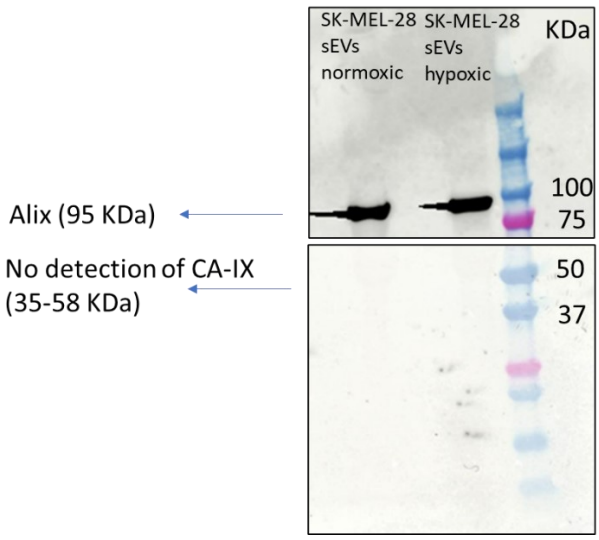

Figure 15. Example of blots showing CA-IX and Alix protein expression in SK-MEL-28-derived sEVs, released under normoxia and hypoxia.

Since a soluble form of CA-IX protein can be present in the CCM or in the sera of patients, we wanted to demonstrate that CA-IX protein is the isoform associated to the membrane of sEVs [141–144].

First, we tested the ability of an anti-CA-IX antibody, kindly provided by Exosomics SpA, to bind the membrane-associated CA-IX, via SPR Biacore assay. To do so, sEVs were purified with the same method (SEC) from CCM of a CA-IX-overexpressing HEK293 cell line (HEK293-pRTS-CA9; Exosomics SpA) and used as the target for a binding kinetic experiment with the selected antibody.

Figure 16 shows the concentration-dependent binding of the antibody to CA-IX-positive sEVs (A) and the concentration-dependent binding of the antibody to the recombinant CA-IX protein (B).

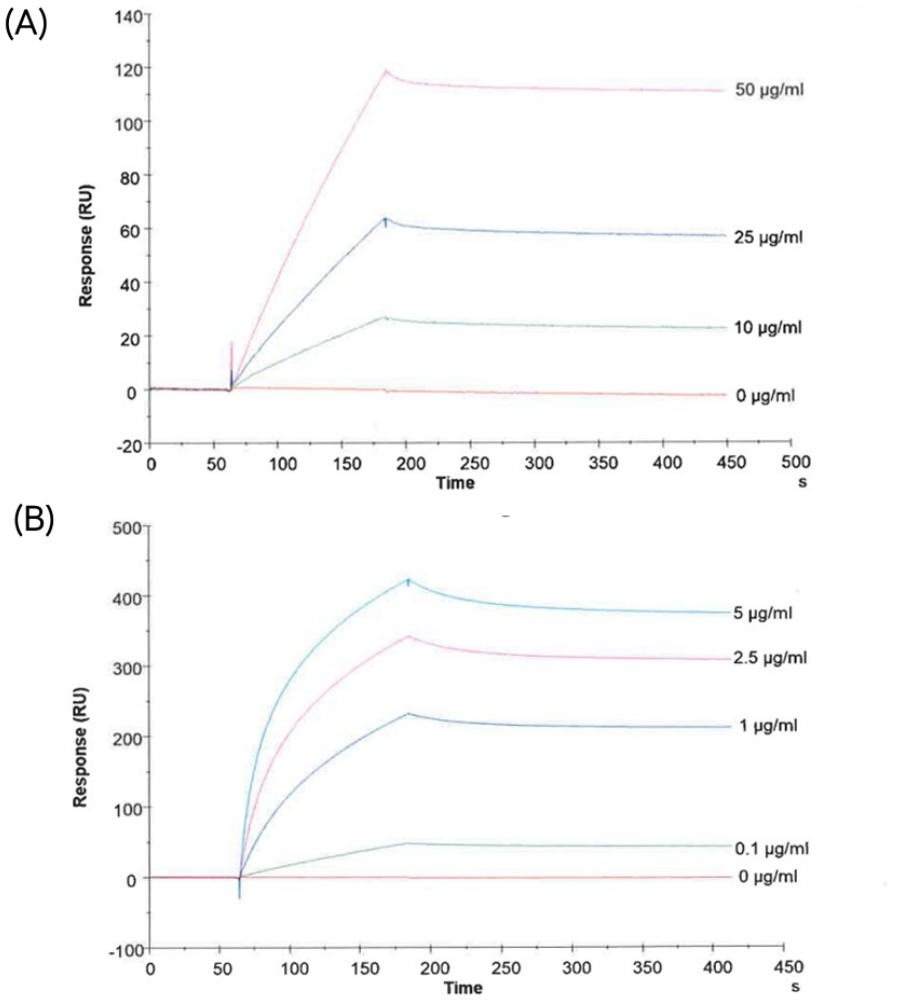

Figure 16. Binding kinetic of an antibody against human CA-IX with CA-IX-positive sEVs from an overexpressing HEK293 cell line (A) and with the recombinant CA-IX protein (B).

The selected antibody was then used to design a specific ELISA assay aimed to reveal CA-IX protein on the EV surface.

First, an ELISA assay was performed to target the tetraspanin CD9 on sEVs from CCM from both conditions, to ascertain the presence of vesicles expressing canonical sEV marker. Consistent with previous results, the amount of CD9-positive particles did not significantly differ between the samples from different cell lines and conditions (Figure 17A).

To specifically detect sEV-associated CA-IX protein, samples were tested by a specific ELISA assay provided by Exosomics SpA. Consistent with our previous data, only hypoxic sEVs from A375 cells resulted in a positive signal, suggesting direct binding to EV-associated CA-IX. After detergent treatment with RIPA buffer, the positive signal from A375 hypoxic sEVs was

abrogated due to the disruption of EV membranes (Figure 17B). These results indicate that CA-IX protein is expressed on the surface of A375 sEVs released under hypoxia.

(A)

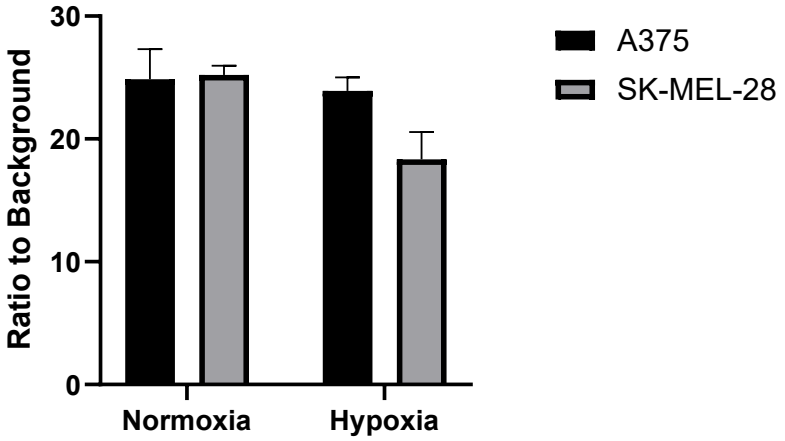

(B)

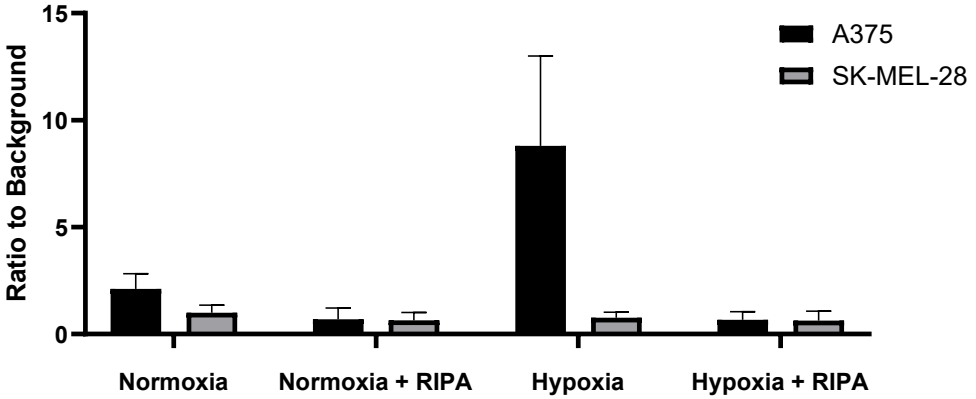

Figure 17. CD9 ELISA assay to confirm EV identity (A). ELISA assay to detect CA-IX protein expression on the EV membrane (B). Bar charts represent the average of two independent experiments.

4.3.3 Application of CA-IX-positive sEVs in liquid biopsy.

To investigate the release of CA-IX-expressing sEVs by melanoma cells *in vivo*, plasma samples from a pool of 5 late stage BRAFV600E-positive melanoma patients were processed using an anti-CA-IX-immunocapture method and a commercially available kit for ctDNA and EV-associated DNA precipitation. DNA was then extracted from the isolated sEVs and used to detect the melanoma specific mutation BRAFV600E by qPCR.

Immunocapture with the anti-CAIX-antibody improved the detection of the melanoma-specific BRAFV600E gene mutation, compared to the generic precipitation method, indicating the enrichment of tumor-derived sEVs carrying the mutation (Figure 18). Mutant BRAFV600 allelic frequency (%) was calculated for the two isolation methods. A statistically significant difference was found between the two methods (p value = 0.04). Consistent with these data, the more generic protocol isolated higher levels of DNA containing the BRAF WT gene, suggesting the co-isolation of more sEVs of non-tumor origin.

(A)

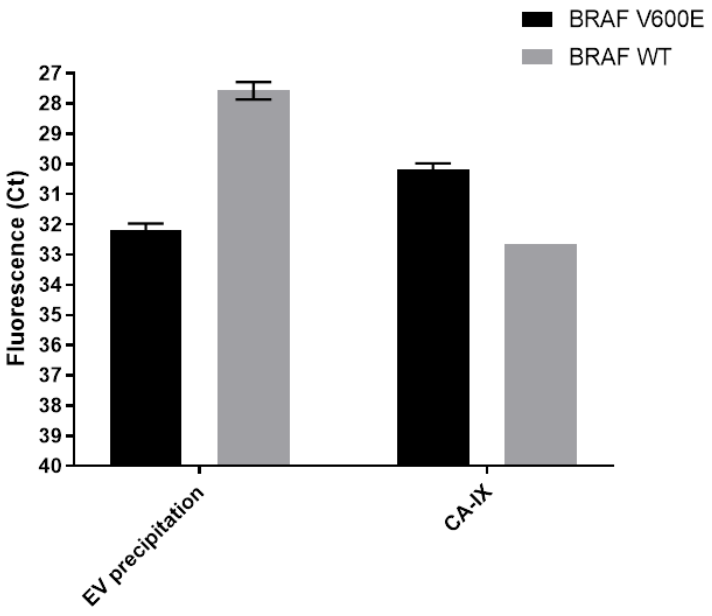

(B)

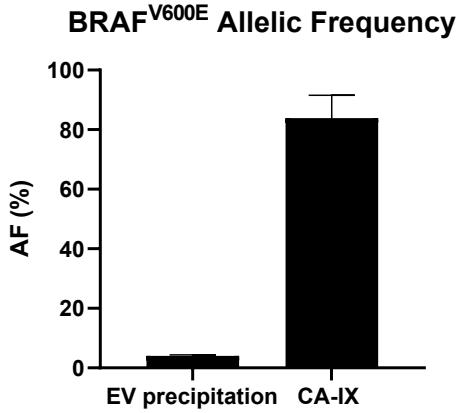

Figure 18. Detection of BRAF WT gene and BRAFV600E mutated gene by qPCR, after generic EV precipitation or CA-IX-based EV immunocapture from 5 plasma samples of late stage melanoma patients. Data are expressed as threshold cycle (Ct) values and plotted on an inverted Y scale (A). Mutant BRAFV600 allelic frequency obtained with the two isolation methods (B).

4.4 Conclusions.

In the first part of the research activity, we investigated how hypoxia influenced the release of sEVs in melanoma and focused on the characterization of sEVs from two representative melanoma cell lines. These cell lines were selected based on the study of Rossi et al. [145]. A375 cells are associated with a highly aggressive phenotype with high migratory capability and invasiveness, while SK-MEL-28 cells have an intermediate phenotype [146]. Both cell lines expressed *bona fide* markers of hypoxia, HIF1α and CA-IX, when grown under low oxygen conditions. Conditioned media from these cell cultures contained sEVs, but their concentration, median size and size distribution did not change significantly during hypoxia. These results are not consistent with other published studies indicating hypoxia as one of the factors that may increase the production and/or release of sEVs and corroborate the idea that these mechanisms are highly cell-specific [86,96].

It is known that hypoxia-induced EVs carry biomolecules involved in cancer progression, which can be exploited as potential biomarkers or as targets for therapy [147,148]. CA-IX is a protein

overexpressed in melanoma and it is associated with the aggressive behavior of different types of tumors; however, only few studies have indicated the association of this protein to sEVs [149–151]. Interestingly, we found that hypoxia significantly increased CA-IX mRNA and protein expression only in sEVs from the most aggressive melanoma cell line, A375, while the expression of this biomarker was not detectable on the SK-MEL-28-derived sEVs under the same conditions. These differences can be explained by the known CA-IX protein expression in higher aggressive tumor phenotypes. The ELISA assay with detergent treatment demonstrated that hypoxia-induced CA-IX protein is associated with the surface of A375 sEVs, and may suggest a role for this isoform in the pathogenesis of melanoma. Consistent with this hypothesis, selective immunocapture of CA-IX-positive sEVs from the plasma of melanoma patients improved the detection of melanoma-specific BRAFV600E mutation, compared to EVs isolated with a more generic method.

However, these preliminary results will need to be confirmed by further experiments in order to increase the statistical significance.

5. Part II.

5.1 Introduction.

It is widely accepted that the therapeutic effects of Mesenchymal Stem/Stromal Cells (MSCs) are mediated significantly by small extracellular vesicles (sEVs) with diameters between 50 nm and 200 nm. In particular, human bone marrow MSC-derived EVs (hbm-MSC-sEVs) have been reported in literature to have protective and reparative effects *in vivo* in different cell models [152]. Thus, there is a growing interest in MSC-EVs because they represent a promising tool for cell-free therapy for a variety of diseases.

5.1.1 EVs from Mesenchymal Stem Cells.

Among stem cells, MSCs have gained significant attention in the field of regenerative medicine as they appear to be safe based on clinical data collected over the last decade [153–157]. MSCs are multipotent, non-hematopoietic adult stem cells, fibroblast-like stem cells, typically found in a variety of human tissues, including bone marrow, adipose tissue, liver, intestine, lung, connective muscle tissue, spleen, skin, placenta, umbilical cords, and other tissues [158]. MSCs are characterized by abilities of self renewal, differentiation, immunomodulatory and trophic support [159]. MSCs exhibit the “trilineage potential” of osteogenic, chondrogenic and adipogenic differentiation capabilities *in vitro* [160].

The effects of MSCs are mediated by paracrine factors: MSCs secrete soluble factors like growth factors, cytokines, chemokines and also extracellular vesicles [161,162]. In particular, sEVs have been reported to be therapeutically efficacious in various preclinical models by virtue of their intrinsic cargo [163–165].

Development of cell-free therapies is important because only less than 1% of transplanted MSCs reach the injured sites and the rest is trapped in the liver, spleen and lung after administration [166]. Moreover, cell therapy administration is not free from safety risks: cellular rejection, toxicity and tumorigenic potential [167,168].

MSC-EVs represent a valid alternative compared to cells because they are easier to manage and can be sterilized by filtration.

MSC-EVs have been applied as new cell-free therapeutic strategies in a variety of disease models including neurological, cardiovascular, immune, renal, musculoskeletal, liver, respiratory, eye and skin diseases, as well as cancers [153,169,170]. The following figure summarizes the main therapeutic effects of MSC-EVs observed in kidney, liver, cardiovascular, and neurological diseases.

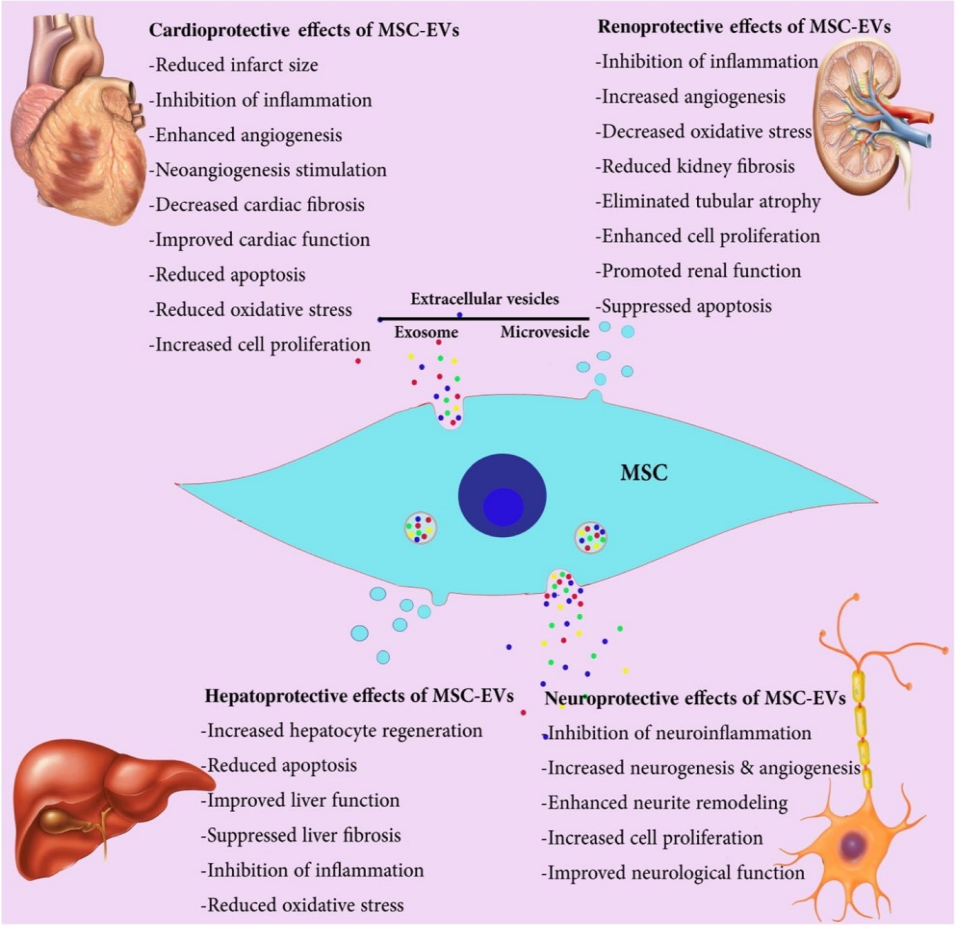

Figure 19. Therapeutic effects of MSC-EVs in kidney, liver, cardiovascular and neurological diseases [162].

One of the most important effects of MSC-EVs is their pro-angiogenic capacity [171,172]. In fact, vascularization is required for tissue repair, since it provides sufficient supply of oxygen, nutrients and growth factors.

Moreover, MSC-EVs can be engineered to transport and deliver therapeutic cargo to target diseased cells and tissues [160,168].

5.1.2 Hypoxia and MSC-EVs.

In the body, most MSCs exist in a hypoxic environment: 1–9% O_2 in bone marrow, 5–9% O_2 in adipose tissue, 1–6% O_2 in umbilical cord blood [173,174]. On the contrary, MSCs for *in vitro* experiments are usually cultured in 21% O_2.

It has been reported that a *in vitro* hypoxic environment improves the proliferation and migration of MSCs during the expansion process, as well as promotes the differentiation ability, compared to MSCs cultured under normoxia [175]. Similarly, hypoxia can also influence the secretion of cytokines, growth factors and EVs [176]. In particular, MSC-EVs generated under hypoxia seem to have improved angiogenic effects and enhanced cytoprotective and anti-inflammatory properties [177,178].

5.1.3 Scope of the work.

In this study, we purified EVs from human bone marrow MSC-derived CCM (from both a 2D culture and a 3D culture), with two EV purification methods: Density Gradient (DG) Ultracentrifugation (UC), considered the gold isolation method in terms of purity, and Size Exclusion liquid Chromatography (SEC). It is known that the choice of EV isolation technique has an impact on the grade of purity of EVs and, consequently, on their biological effects [163,179]. DG-UC should result in a EV final sample with high purity, but the workflow is laborious and time-consuming. On the contrary, SEC is a fast and easy method, it allows to reach a medium-high EV purity, but the final sample is diluted and it requires further processing.

The two types of EVs were fully characterized with several analytical methods, like single-particle analysis, Transmission Electron Microscope (TEM), proteomic and transcriptomic platforms. Then, we evaluated the *in vitro* functionalities of MSC-EVs with cell-based bioactivity assays.

5.2 Materials and Methods.

5.2.1 MSC culture.

Both 2D- and 3D-based cultures of MSCs were performed.

For 2D culture, human bone marrow mesenchymal stem cells (Lonza) were thawed and plated in T-175 cm^2 flasks, in Lonza MSC medium without serum for 3 days, by replacing media after 24 hours plating. After 3 days, cells are passaged into T-275 cm^2 flasks and monitored daily. Once the culture is ~ 80% confluence, cells are harvested and passaged into CF10 flasks. The cell culture is carried on for 5 days to allow cells to become 100% confluent and another 2 days for EV production.

At the end, the conditioned medium is harvested and frozen at -80C.

For 3D culture, a 3 L microcarrier-based bioreactor was used. MSCs were thawed and expanded in T225 flasks. After 3 days of culture, MSCs were harvested, counted and inoculated into the bioreactor. After 8 days, microcarriers were digested and the CCM was harvested, aliquoted and frozen at -80°C.

5.2.2 Density Gradient Ultracentrifugation.

200 ml of MSC-CCM was pre-cleared by differential centrifugation at 300x g for 10 minutes, to remove any cells in suspension, 1200x g for 20 minutes and 10,000x g for 30 minutes at 4 °C, to remove any cell debris and large EVs in suspension. Then, MSC-CCM was concentrated up to 10 ml by ultrafiltration with an Amicon® Stirred Cell with Ultracel 100 kDa Ultrafiltration Discs (Merck Millipore, Burlington, MA, USA).

Small EVs were purified using OptiPrep™ (Merck) cushion density flotation. The iodixanol gradient was prepared by floating 3 ml of 10% w/v iodixanol solution containing NaCl (150 mM) and Tris HCl (25 mM, pH 7.4) over 3 ml of 55% w/v iodixanol solution. Concentrated CCM (5 ml) was floated on top of the iodixanol cushion and ultracentrifuged using a Fiberlite F65L rotor for 3.5 hours at 100,000× g. Eleven fractions (1 ml each) were collected from the top of the gradient and kept at -80 °C.

5.2.3 Size Exclusion Chromatography.

200 mL of MSC-CCM was processed as described in paragraph 4.2.2, using a colum qEV10 70 nm (Izon Science, Christchurch, New Zealand). All the fractions were characterized by the micro BCA assay (Thermo Fisher Scientific, Cleveland, OH, USA) and by a sandwich ELISA assay targeting a mix of three tetraspanins CD9, CD63 and CD81 (Exbio, Czech Republic). Positive fractions for tetraspanins, but with low protein concentration, were pooled and concentrated to 0.5 mL by 100 kDa ultrafiltration (Amicon® Ultra-15 Centrifugal Filter Unit, Merck Millipore, Burlington, MA, USA). Purified EVs were aliquoted and stored at -80 °C.

5.2.4 Transmission Electron Microscopy.

Transmission Electron Microscopy (TEM) was used to verify EV morphology and integrity. Each EV sample (3 µl, corresponding to 0.12–0.16 µg) was loaded for 2 minutes onto a 300 mesh formvar coated copper grid. After blotting the excess, the grid was negatively stained with 2% aqueous ammonium molybdate for 30 seconds and analyzed using a Thermo Fisher Scientific Tecnai G2 Spirit transmission electron microscope operating at 120 kV equipped with a EMSIS Veleta 2048X2048 CCD camera.

5.2.5 NanoAnalyzer analysis.

EV samples were analyzed using a Flow NanoAnalyzer (nanoFCM Inc., Nottingham, UK) to measure the EV size and particle concentration, as described in paragraph 4.2.3.
In addition, EV samples were stained with CellTrace CFSE Cell Proliferation kit (Thermo Fisher Scientific) to evaluate EV integrity. The same amount of particles were incubated with CFSE 10 µM for 1.5 hours at 37°C under shaking. Then, the excess of dye was removed with a SEC qEV original column (Izon).
To confirm EV identity, samples were stained with a mix of three tetraspanin antibodies (CD9, CD63 and CD81) conjugated with a fluorophore. The same amount of particles were incubated with antibodies for 1 hour at 37°C under shaking. Then, the excess of dye was removed with centrifugal filters (Pall). Fluorescent samples were analyzed using Flow NanoAnalyzer in order to assess the % of positive events.

5.2.6 Western Blot.

Western Blot assay of purified EVs was run to check the expression of canonical EV markers and negative EV marker. The same number of particles for each sample was prepared following the same procedure described in paragraph 4.2.6.

Primary antibodies against CD81 (BD Biosciences, San Jose, CA, USA, 1:500, Cat. no. 555675), Alix (Santa Cruz, Dallas, TX, USA, 1:500, Cat. no. sc-271975) and Calnexin (Santa Cruz, Dallas, TX, USA, 1:200, Cat. no. 11397) were used.

5.2.7 Mass Spectrometry.

To measure total protein content, EV samples were quantified using microBCA assay (Thermo Fisher Scientific). The same amount of proteins per sample were used for acetone-based precipitation. Samples were precipitated with chilled acetone (Merck), mixed by vortexing and incubated at -20 ˚C overnight.

The precipitated protein pellets were dried and solubilized with urea 8 M Tris-HCl 100 mM pH 8.5 (Merck). Protein quantification was repeated with microBCA assay.

To do the protein digestion step, a minimum of 10 µg of proteins were digested with Trypsin Gold Mass Spectrometry Grade (Promega) at 37°C overnight.

The resultant peptides were resuspended in 0.1% trifluoroacetic acid water at a final concentration of 1 µg/µL. A total of 3 µL (equal to 3 µg of starting material) were injected into Nano LC-MS (Q Exactive HF X-UHPLC Nano).

Peptide separation was carried out at 35 °C using a PepMap RSLC C18 column, 75 µm × 15 cm, 2 µm, 100 Å (Thermo Fisher) at a flow rate of 300 nl/minute. The mobile phases A and B used for the analysis are 0.1% formic acid in water and 0.1% formic acid in acetonitrile, respectively. Protein identification was performed by Proteome Discoverer 2.5 (Thermo Scientific). The peptide spectra were matched against Homo sapiens database downloaded from Uniprot (TaxId: 9606). The analysis was based on at least one unique peptide with a minimum length of seven amino acids and a false discovery rate (FDR) of 0.01. The default peak-picking settings were used to process the raw MS files in MaxQuant (version 1.6.1.0) and its integrated search engine Andromeda [180,181]. The protein relative quantification and calculation of statistical significance was carried out using two-tailed Student's t-test and error correction (p-value < 0.05) with the method of Benjamini–Hochberg. Moreover, a volcano plot, showing a summary

distribution of differentially expressed proteins was designed with Perseus software (version 1.6.1.1) [182]. The obtained proteins were compared with the Exocarta database to check for their presence in the top 100 proteins that are often identified in exosomes [36]. Moreover, by means of Uniprot database, proteins belonging to the GOs extracellular exosome [GO:0070062] and extracellular region [GO:0005576] were identified.

5.2.8 miRNA Whole Transcriptome Assay (WTA).

The miRNA Whole Transcriptome Assay (WTA) is a next-generation sequencing (NGS)-based application that measures the expression of 2083 human microRNAs (miRNAs) directly from EVs, without the RNA extraction step. The preparation of sequencing libraries was done with a semi-automated system (HTG molecular EdgeSeq). EV samples were lysed at 95 °C with Lysis Buffer (HTG molecular) and then loaded on sample plate (HTG molecular) for the quantitative nuclease protection assay. Then, sequencing adapters were added to the probes via PCR. The resulting PCR products were cleaned and quantified by qPCR. Then, the normalized pool of libraries was run on MiSeq® sequencer (Illumina).
Data analysis was done using Reveal software (HTG), which performed differential expression analysis with DESeq2 package (version 1.30.1) available from Bioconductor [183].
GO analysis was done with miRNA Enrichment Analysis and Annotation Tool (miEAA) [184].

5.2.9 Scratch Wound Healing assay.

Scratch wound healing assay was used to evaluate the impact of MSC-EVs on cell migration *in vitro*. Human umbilical vein endothelial cells (HUVECs; Lonza) were seeded in a 24-well plate, in EGM™ Medium (Lonza). After 24 hours, cells were starved in order to synchronize them and inhibit cell proliferation. When cells are 85-90% confluent, a scratch is performed in the center of the cell monolayer. The cell debris were washed with PBS. Then, cells were treated with medium containing MSC-EVs (doses are expressed as ratio cell:EV). Each condition was performed in three technical replicates. Pictures were taken under microscope at 0, 18 and 24 hours after creating the scratch. Scratch area at different timepoints were measured using ImageJ software. Results are expressed as % rate of gap closure at time 18 hours or 24 hours, compared to time 0. The % rate will be calculated using this formula: (1 – Ax/A0)%, where A0 and Ax represent the empty scratch area at 0 hours and x hours (x = 18 hours or 24 hours).

5.2.10 MTT Proliferation assay.

HUVECs (Lonza) were seeded into 96-well plates, in EGM medium (Lonza) and cultured overnight. Cells were starved for at least 16 hours in order to synchronize them. Then, cells were incubated with different amounts of EVs (expressed as ratio cell:EV) for 24 hours. Each condition was performed in six replicates. Cell proliferation was analyzed using the Cell Proliferation Kit I (MTT; Roche). 10 µl of MTT solution was added to the cells and incubated at 37 °C for 4 hours. Solubilization buffer was added to dissolve the purple crystals overnight at 37 °C. Then, the absorbance was read at 570 nm (reference wavelengh > 650 nm) using a microplate reader (CLARIOStar Plus, BMG Labtech, Ortenberg, Germany). The background was removed by subtracting the absorbance recorded from a well without cells.

5.2.11 Tube formation assay.

HUVEC cells pre-screened for angiogenesis (Lonza) are cultured using EGM™-2 Medium, containing VEGF (Lonza). Cells are first seeded in 6-well plate at a density of 6 x 10^5 cells/well. After 24 hours, they are starved for at least 16 hours to ensure that all cells are synchronized at the same cell cycle stage. Then, cells are pre-treated with MSC SEC-derived EVs or DG-derived EVs (1:1000 ratio cell : EV) for 24 hours.

The day after, cells are detached and plated at a density of 3 x 10^4 cells/well in triplicate for each condition in 96-well plates coated with 75 µL of Matrigel Basement Membrane Matrix (Corning).

Pictures were taken under microscope after 2, 4, 10 and 20 hours. Images were analyzed using ImageJ software with the Angiogenesis Analyzer plugin for quantification of tube networks [185].

5.2.11 Statistical analysis.

Purification of MSC-derived EVs from 2D and 3D cell culture has been done in triplicate for each isolation method.

Prism Version 10.00 for Windows (GraphPad Software, La Jolla, CA, USA) was used for statistical analysis. Results of analytical methods are reported as the mean ± standard deviation (SD) of at least two technical replicates. Error bars show SD of the mean.

A two-tailed Student's t-test was applied to evaluate the statistical difference between two conditions. Statistical comparisons that output p-values < 0.05 were considered significant.

5.3 Results.

Preliminary results have been presented in a poster session during the 3rd EVIta Symposium, held in Urbino from September 13th to 15th 2023.

5.3.1 Purification of MSC-EVs.

In order to evaluate the impact of the EV purification method on final EV sample, concentrated CCM was purified with two methods: DG-UC and SEC. Since SEC protocols required the loading of 10 ml of concentrated CCM while DG-UC only 5 ml, two DG purifications were pooled into one final EV sample. Ten fractions of 1 ml were recovered by DG-UC. Particle concentration (Particles/ml) was measured in each fraction with NanoAnalyzer, while presence of the three tetraspanins CD9-CD63-CD81 was assessed by ELISA assay. Figure 20 shows the overlay of the two results.

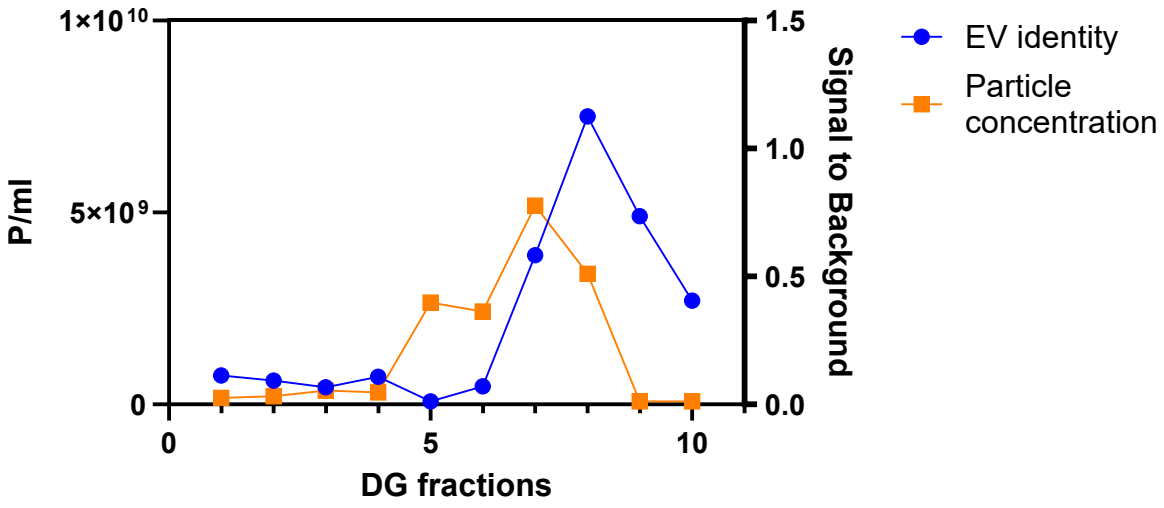

Figure 20. Overlay of Particle concentration (in orange) and positivity for three tetraspanins (in blue) of 10 fractions obtained with DG-UC from MSC CCM.

Fractions 7 and 8, were selected as they had the highest particle concentration and tetraspanins signal. Then, the two fractions were stained with CFSE to evaluate EV integrity,

and with a mix of three fluorescent antibodies against CD9-CD63-CD81 to quantitatively assess the expression of these EV biomarkers. 5(6)-CFDA-SE (CFSE) is a non-fluorescent molecule carrying two acetate groups that facilitate the transit through the EV membrane. Once inside the EVs, it is converted into fluorescent-CFSE by intracellular esterases removing the acetate groups. CFSE positive particles are intact vesicles that contain cellular esterases.

Figure 21 shows a higher % staining with CFSE for fraction 7 compared to fraction 8 (64.7% for fraction 7 and 32.2% for fraction 8). Moreover, fraction 8 was characterized by higher threshold value of FITC channel (206 compared to 21 for fraction 7; 15-17 for unstained samples). The higher threshold may be due to excess of unpurified dye, and related to the presence of protein contaminants. Figure 22 shows a higher % staining with the mix of tetraspanins antibodies for fraction 7 compared to fraction 8 (68.7% for fraction 7 compared to 51.7% for fraction 8).

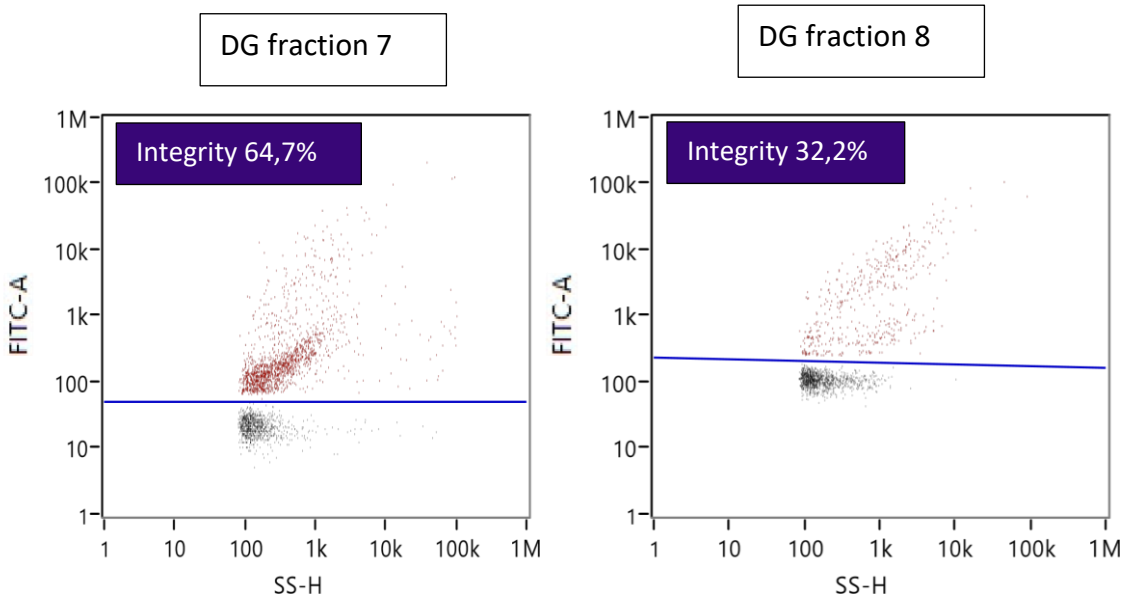

Figure 21. NanoAnalyzer dot plots of fractions 7 and 8 stained with CFSE, representative of EV integrity.

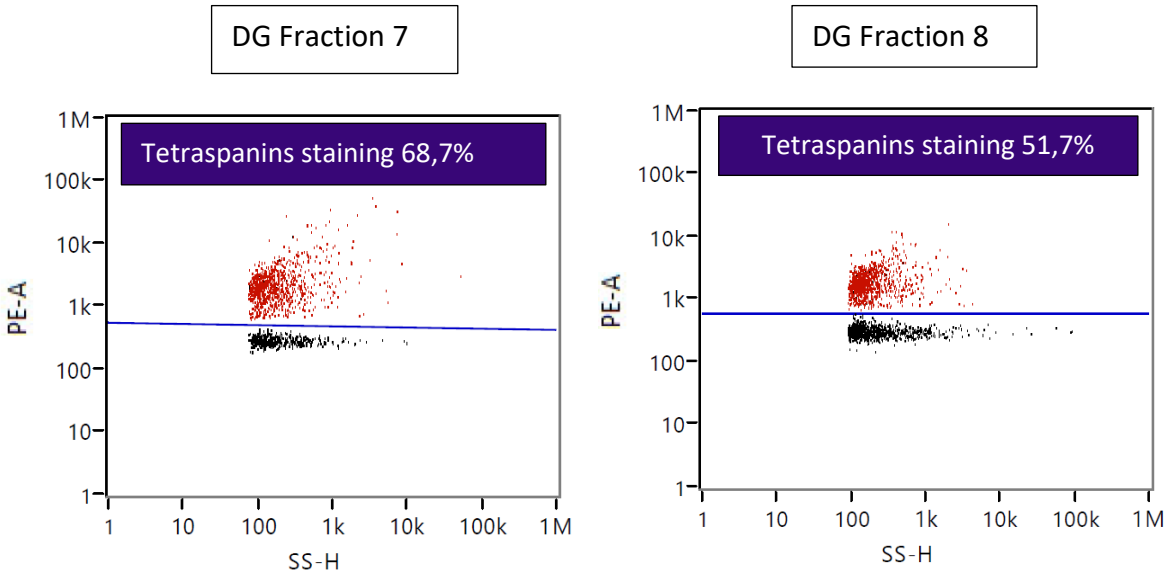

Figure 22. NanoAnalyzer dot plots of fractions 7 and 8 stained with a mix of three fluorescent antibodies against tetraspanins (CD9-CD63-CD81).

Based on abovementioned results, fraction 7 was identified as the fraction with the highest % of intact EVs and with the lowest amount of impurities. Hence, fractions 7 from two independent DG purifications were pooled, washed with PBS and further purified by ultracentrifugation to eliminate iodixanol from final EV sample.

Figure 23 shows an example of SEC elution profile: fractions positive for the three tetraspanins CD9-CD63-CD81 (blue line), but with a low protein concentration (green line), were pooled and concentrated to a final volume of 0.5 mL using 100 kDa ultrafiltration device.

The described workflow was followed for both the two sources of CCM (2D and 3D), and the purification runs were done in triplicate.

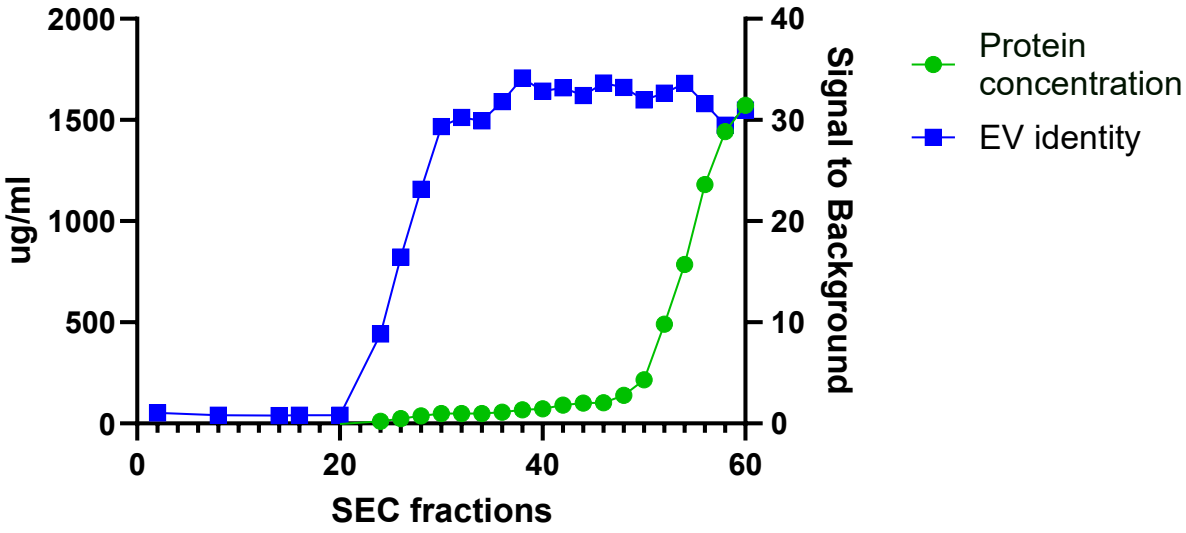

Figure 23. Example of SEC elution profile of MSC CCM-derived from 2D culture. The graph shows the overlay of protein concentration (in green) and positivity for three tetraspanins (in blue) of 60 fractions.

5.3.2 Characterization of MSC-EVs.

First of all, MSC-EVs were characterized with NanoAnalyzer to determine particle concentration and particle size. The instrument is calibrated with size standard beads which allow the characterization of a population of sEVs (40-200 nm).

Particle concentrations obtained from 3D culture were higher compared to 2D culture, consistent with the existing literature, even if the difference observed was not statistically significant [43,69,74,75]. SEC purified samples from 2D cultures had higher particle concentration than DG-UC purified, though the difference was not statistically significant. Mean EV sizes were similar between 2D and 3D cultures and purification methods (Figure 24B).

Purity index was calculated dividing the mean particle concentration by the mean total protein concentration (micro BCA assay) [179]. As expected, DG method yielded the highest purity index (Figure 25; a detailed comparison of purification methods is described in paragraph 1.4 and Table 1).

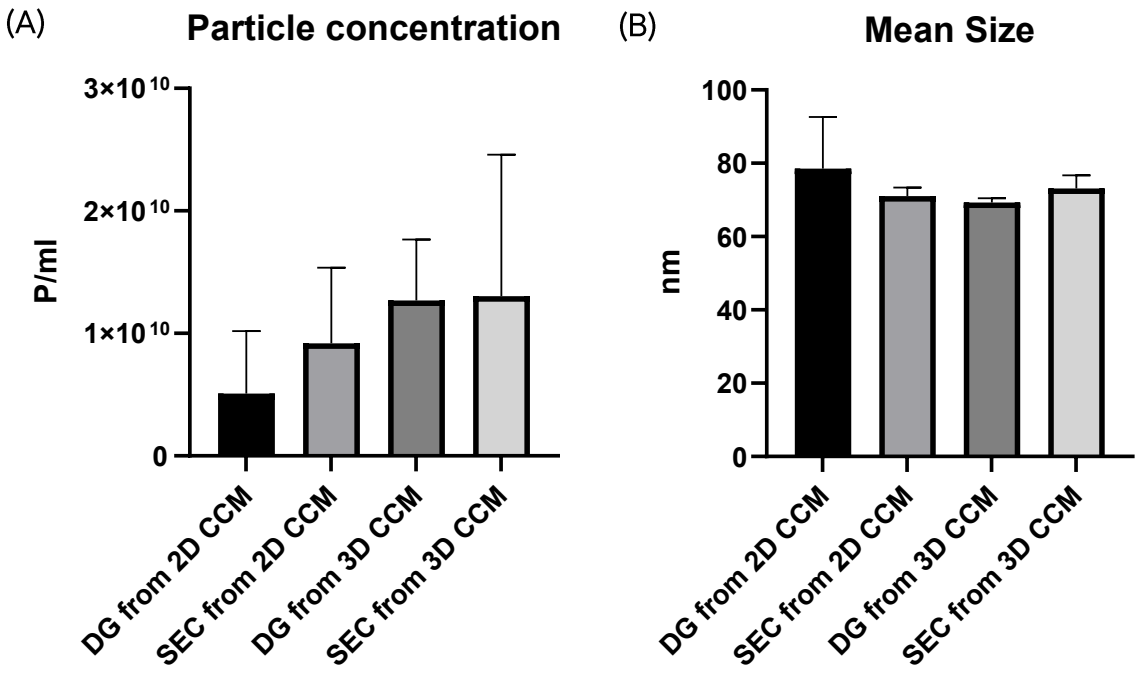

Figure 24. Particle concentration (A) and particle mean size (B) measured at NanoAnalyzer, of EV samples purified with SEC and DG-UC, from 2D and 3D cultures. Bar charts are representative of three independent experiments.

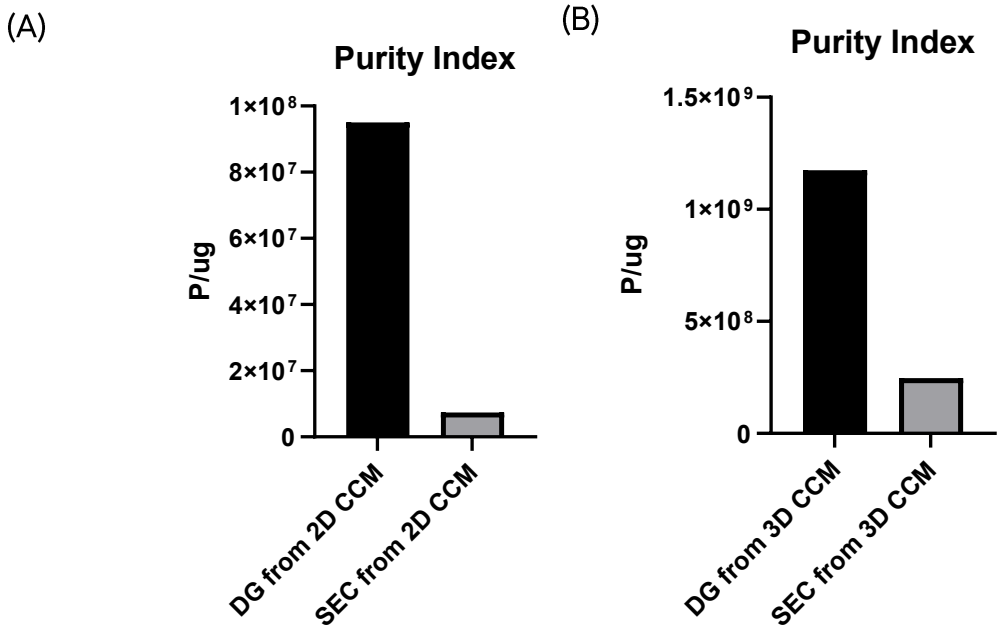

Figure 25. Purity indexes of EV samples obtained from 2D cultures (A) and 3D cultures (B).

Then, purified EVs were stained with CFSE to quantify the % of intact EVs. To reduce background noise, the excess of dye was removed with SEC prior to analysis with NanoAnalyzer. All samples showed % of CFSE staining above 60%: 2D-EVs purified with SEC:

74.3%, purified with DG: 64.7%; 3D-EVs purified with SEC: 70.2%, purified with DG: 70.5%. Examples of NanoAnalyzer dot plots are shown in Figure 26 (samples from 3D culture).

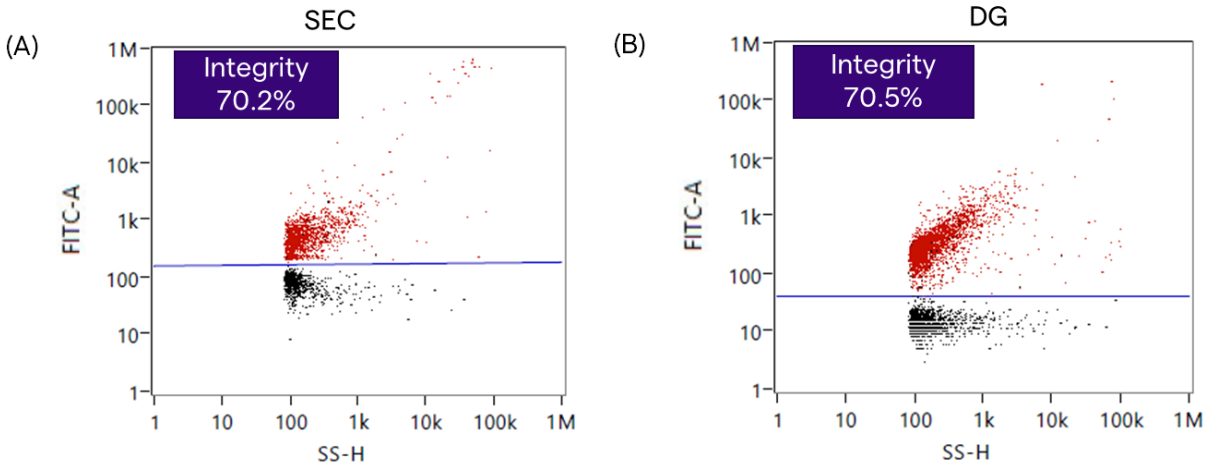

Figure 26. Example of NanoAnalyzer dot plots of EV samples from 3D culture stained with CFSE.

EV integrity was also investigated with Transmission Electron Microscopy (TEM). TEM confirmed the presence of lipid bilayer-surrounded vesicles in all EV samples.

Figure 27 shows MSC-EVs derived from 2D culture, purified with SEC cromatography (A) and DG Ultracentrifugation (B). The pictures of samples obtained from the two purification methods show similar size and integrity of EVs.

Figure 28 shows MSC-EVs derived from 3D culture, purified with SEC (A) and DG-UC (B). The pictures of samples obtained from the two purification methods show similar size and integrity of small EVs.

Compared to 3D samples, 2D samples show less particle concentration, as expected from data obtained with NanoAnalyzer, and different sizes of EVs (a population of MVs of 200 nm size and a population of sEVs).

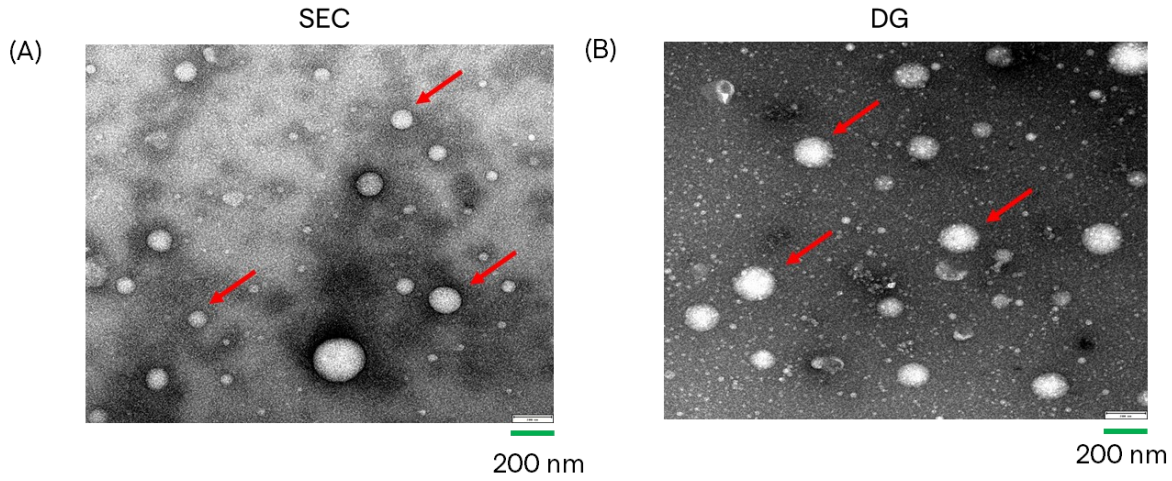

Figure 27. TEM images of MSC-EVs from 2D CCM, purified with SEC (A) and with DG (B).

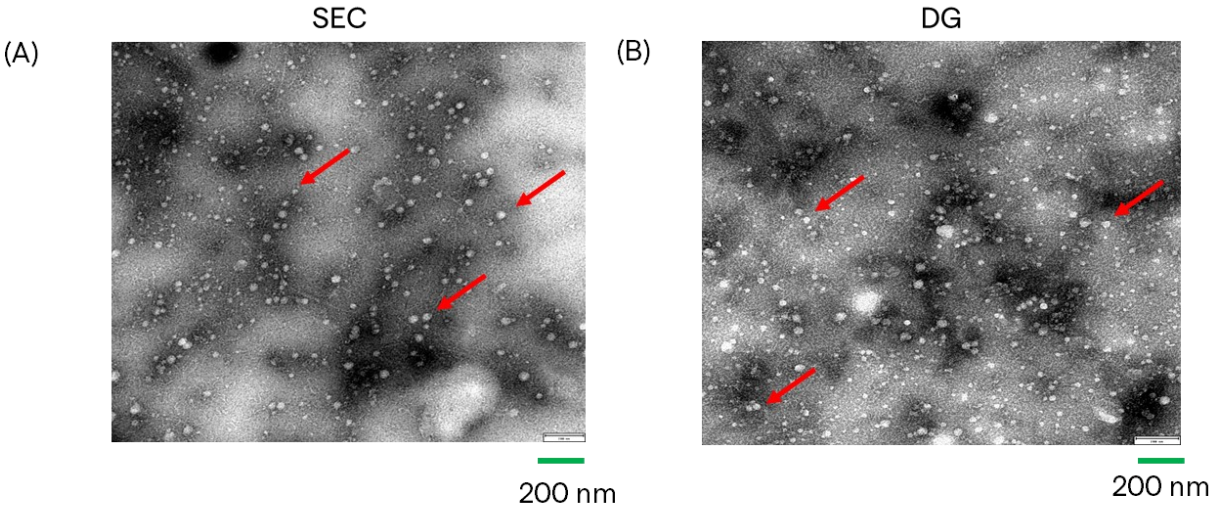

Figure 28. TEM images of MSC-EVs from 3D CCM, purified with SEC (A) and with DG (B).

Samples were characterized also in terms of EV identity, using two orthogonal methods (NanoAnalyzer and Western Blot). Samples were stained with a mix of three fluorescent antibodies targeting tetraspanins (CD9-CD63-CD81) and, after the removal of unbound antibodies, analyzed with NanoAnalyzer. Tetraspanins-positive percentages were higher in samples deriving from DG, compared to those from SEC: 2D sample purified with SEC: 47.4%, purified with DG: 68.7%; 3D sample purified with SEC: 44.1%, purified with DG: 67.5%. Examples of NanoAnalyzer dot plots are shown in Figure 29 (samples from 2D culture). DG samples showed higher percentages compared to SEC samples, and this can be explained with the higher purity index of these EVs (Figure 25).

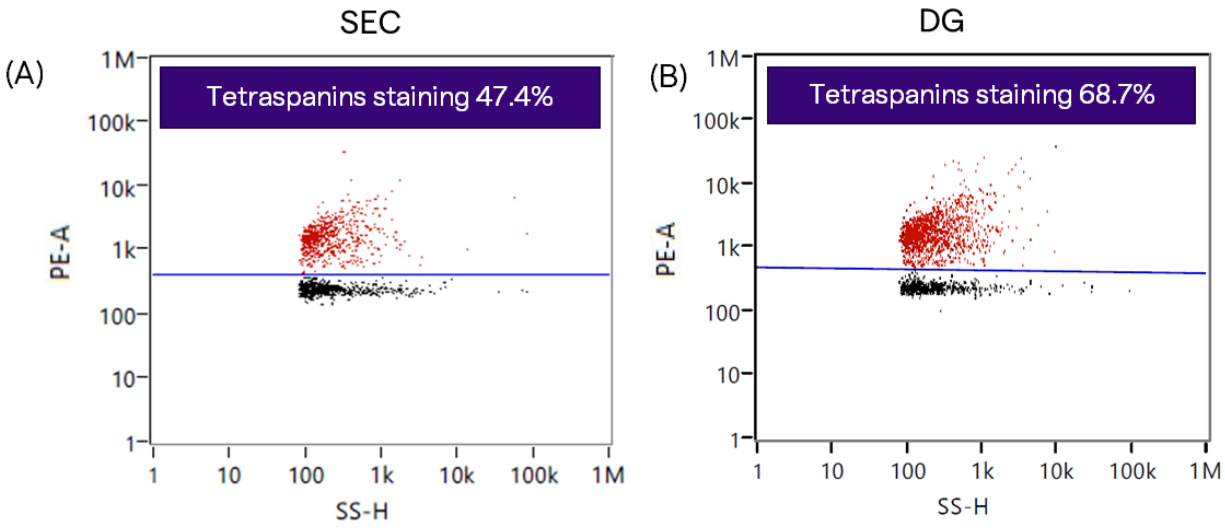

Figure 29. Example of NanoAnalyzer dot plots of EV samples stained with a mix of three fluorescent antibodies against CD9-CD63-CD81.

Single stainings of EV samples with fluorescent antibodies against each tetraspanin were also performed. Figure 30 shows the % of staining for each tetraspanin, in SEC-derived EVs and DG-derived EVs. Similar expression patterns were found in the two samples: CD63 and CD9 are the most and the least expressed tetraspanin, respectively.

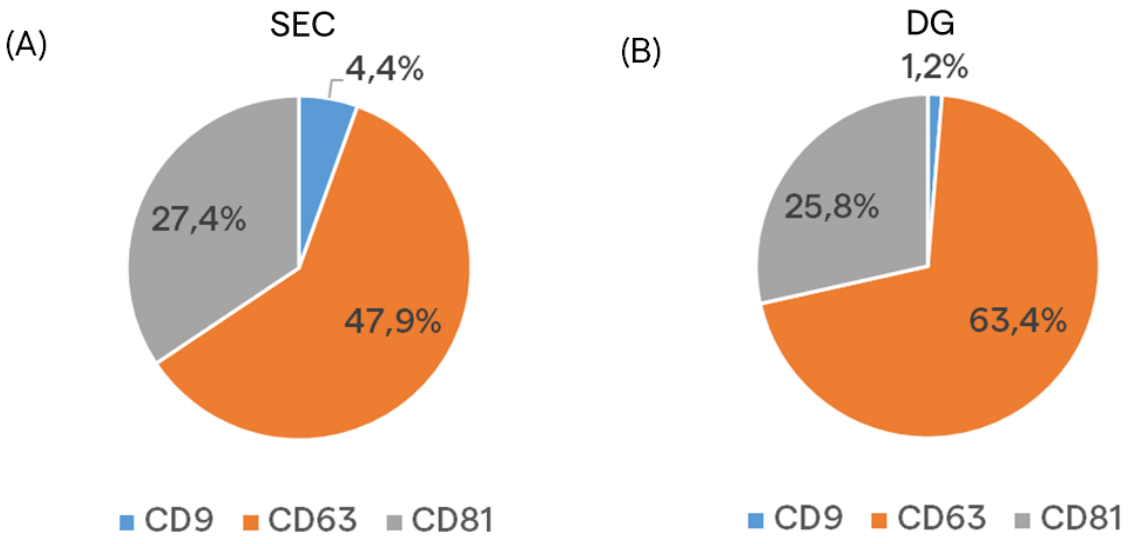

Figure 30. Pie charts representing the % staining of the single tetraspanins on EV samples purified with SEC (A) and DG (B), from 3D MSC-CCM.

SEC-derived EVs and DG-derived EVs were analyzed in Western Blot, loading the same number of particles, to confirm the presence of canonical small EV markers (CD81 and Alix) and the absence of non-EV marker (calnexin). MSC cell lysate was loaded as positive control for calnexin blot. Results obtained confirmed the protein expression of EV markers on both the two EV preparations, and the absence of calnexin protein expression (Figure 31).

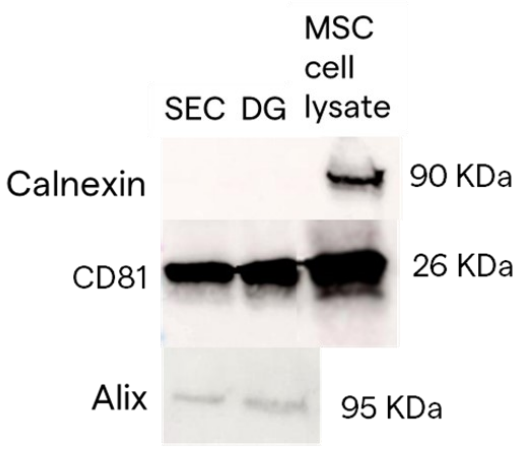

Figure 31. Blots representing CD81 and Alix protein expression in EV samples obtained from SEC and DG-UC. Calnexin protein expression was used as EV negative control.

5.3.3 Characterization of MSC-EV cargo.

5.3.3.1 Proteomic analysis.

MSC-derived EVs purified from 2D CCM, with SEC and DG, were further characterized, on total protein cargo.

Starting from the same amount of total proteins, mass spectrometry was performed to determine the proteomic analysis of the two EV preparations in duplicate, following the procedure described in paragraph 5.2.7.

Protein hits were identified using both one-peptide and two-peptide thresholds.

Using the one-peptide threshold, a total of 194 proteins were identified in SEC-EVs and 161 proteins in DG-EVs. Jaccard coefficient, indicating similarity index between samples, was 46.69% (Figure 32A). Narrowing the analysis to EV-related proteins, based on ExoCarta

database, 107 proteins were identified in SEC-EVs and 99 proteins in DG-EVs. Jaccard coefficient was 51.47% (Figure 32B).

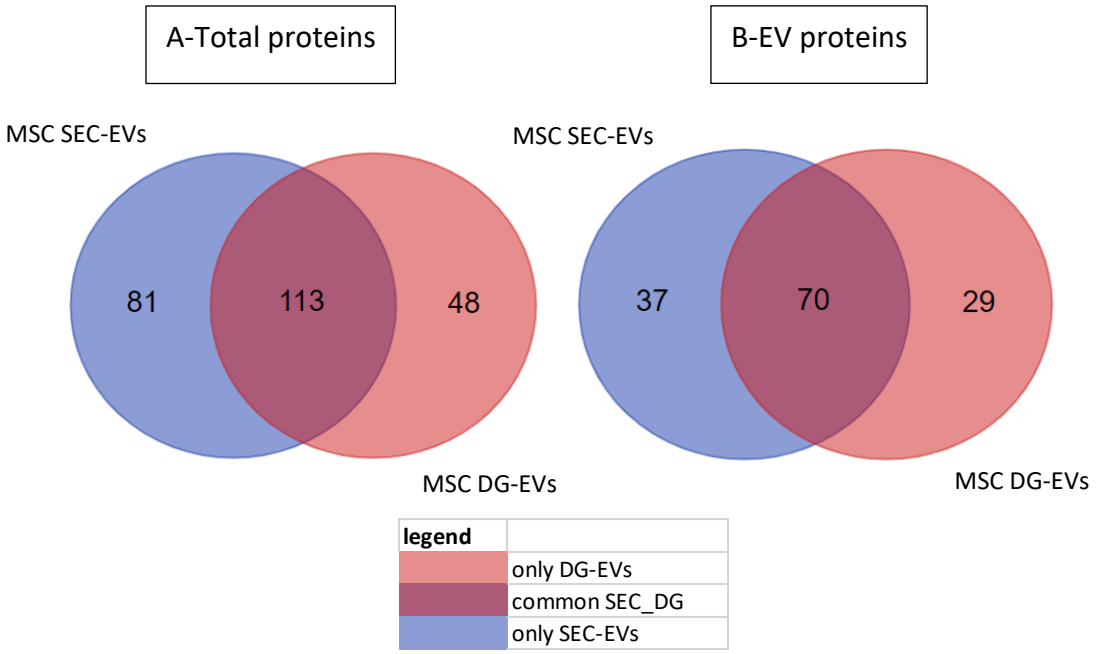

Figure 32. Venn charts of total proteins (A) and EV-related proteins (B) detected in MSC SEC-EVs, in DG-EVs and in common between the two groups. Analysis has been done considering 1 peptide.

Using the two-peptide threshold, 150 proteins were identified in SEC-EVs and 135 proteins in DG-EVs. Jaccard coefficient was 55.37% (Figure 33A). If we consider only EV-related proteins, 95 proteins were found in SEC-EVs and 93 proteins in DG-EVs. Jaccard coefficient was 56.67% (Figure 33B).

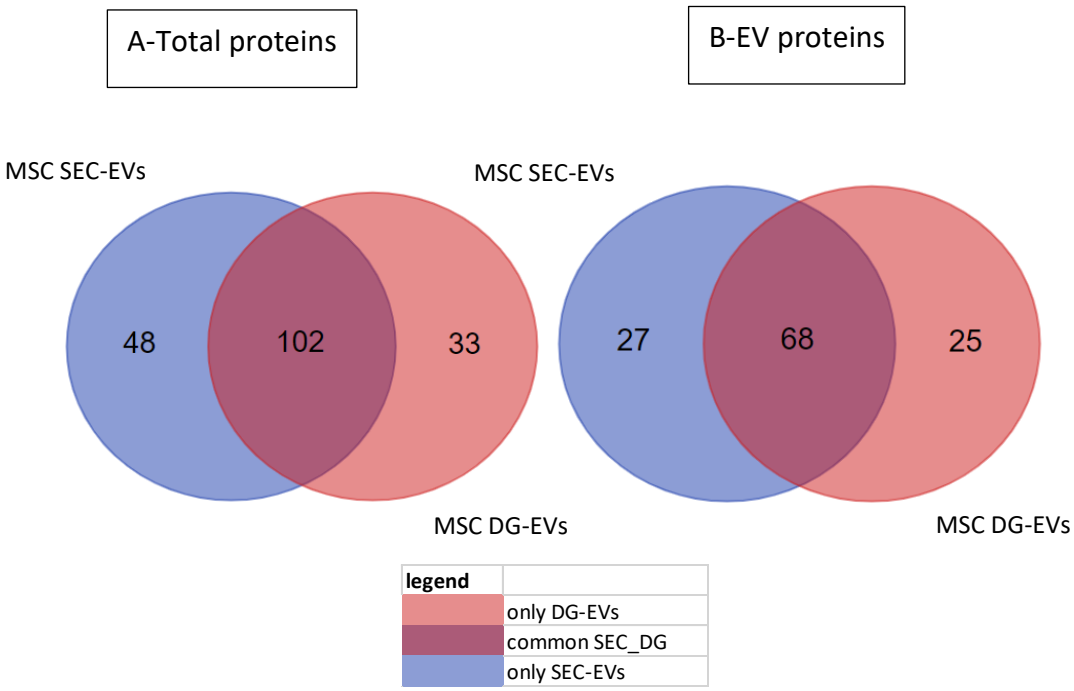

Figure 33. Venn charts of total proteins (A) and EV-related proteins (B) detected in MSC SEC-EVs, in DG-EVs and in common between the two groups. Analysis has been done considering 2 peptides.

Due to the intrinsic limitations of the SEC purification method, it is expected to find more co-isolated proteins in SEC-derived EVs, compare to DG-EVs. However, if we consider only EV-related proteins, the two samples are closer to each other.

Similarity index values have to be considered medium-high, since due to the intrinsic variability of the analytical technique, running replicates of the same sample should result in a Jaccard coefficient of maximum 70-80%.

Protein similarity between the two samples was also calculated using Spearman correlation coefficient which was 0.76, indicating medium-high correlation (Figure 34).

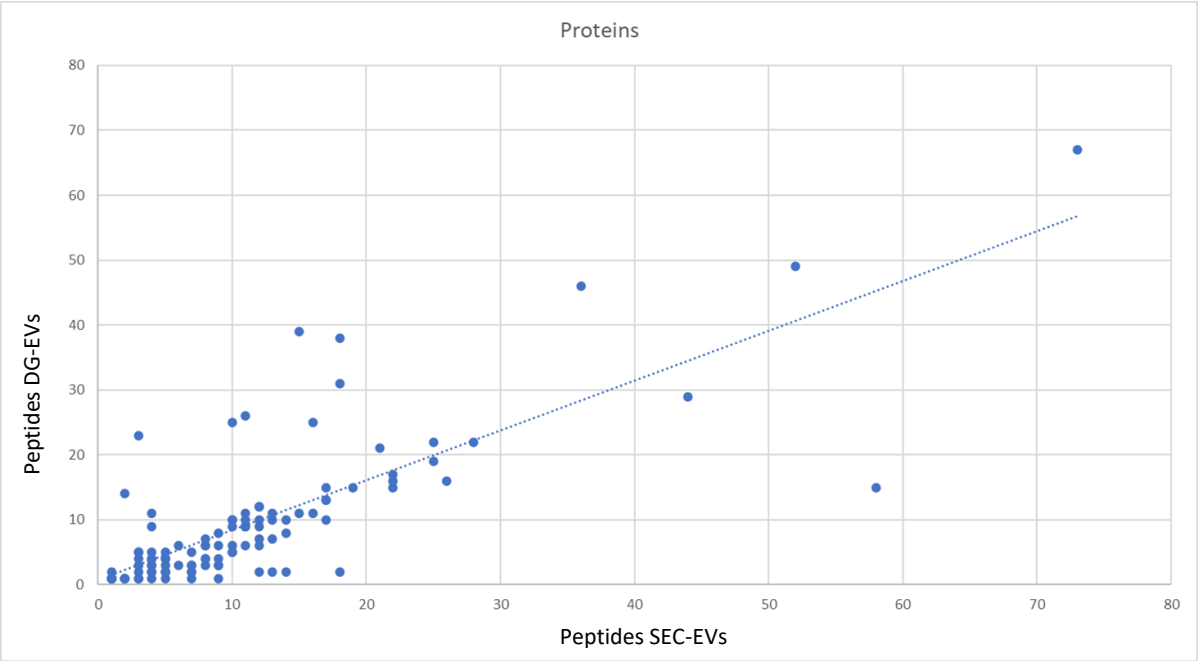

Figure 34. Correlation between the number of peptides that recognize proteins in SEC-EVs and DG-EVs, for the population of common proteins.

Considering also proteins identified with 1 peptide, Cellular Component (CC) Gene Ontology (GO) analysis has been done for the proteins commonly detected in SEC-EVs and DG-EVs (113 proteins). Proteins were significantly enriched in «Extracellular» and «Exosomes» GO annotations (Figure 35).

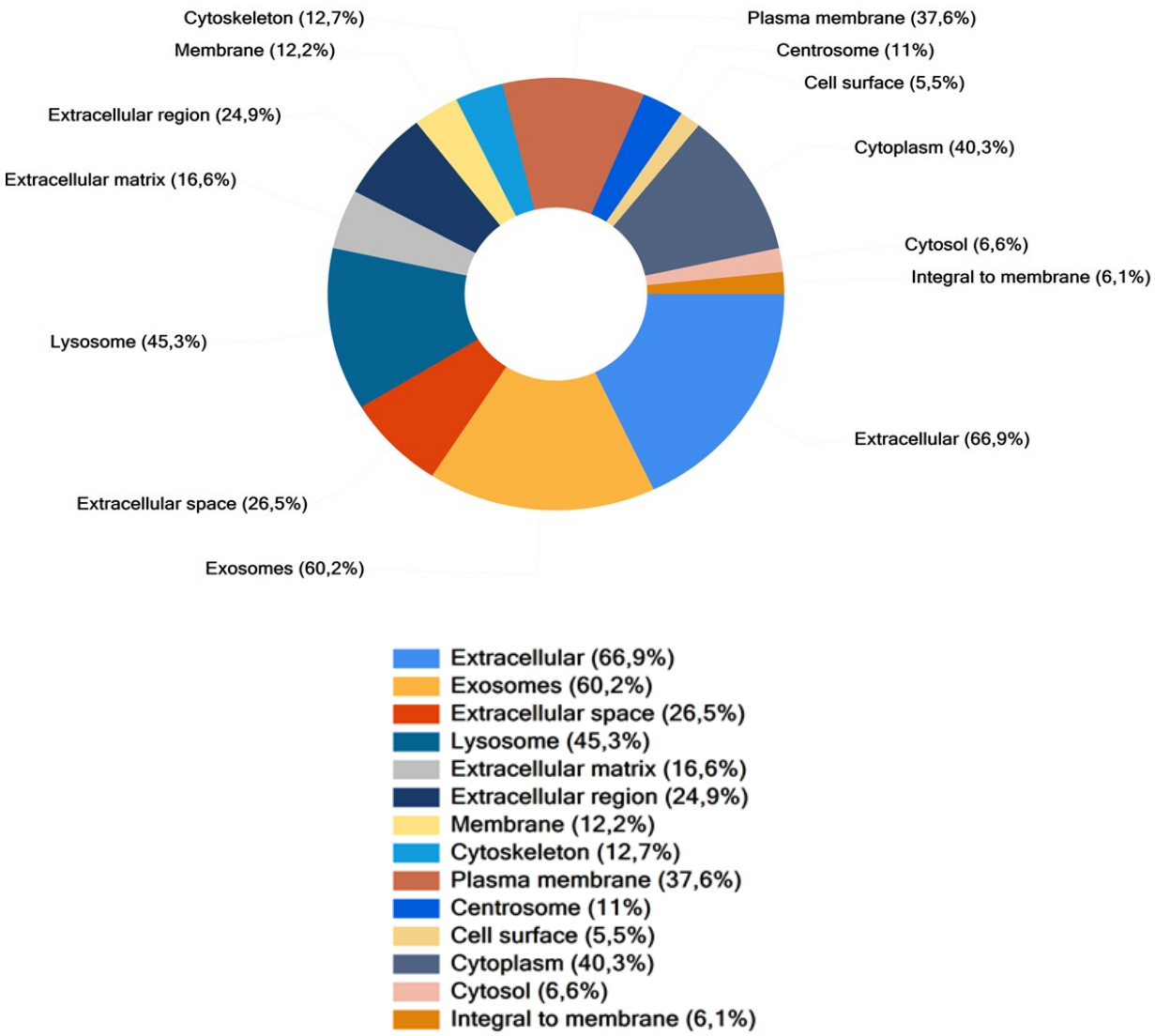

Figure 35. Cellular component analysis of proteins found in common between SEC-EVs and DG-EVs.

Biological Process and Biological Pathways GO analysis have been done for the proteins commonly detected in SEC-EVs and DG-EVs (Figures 36-37).

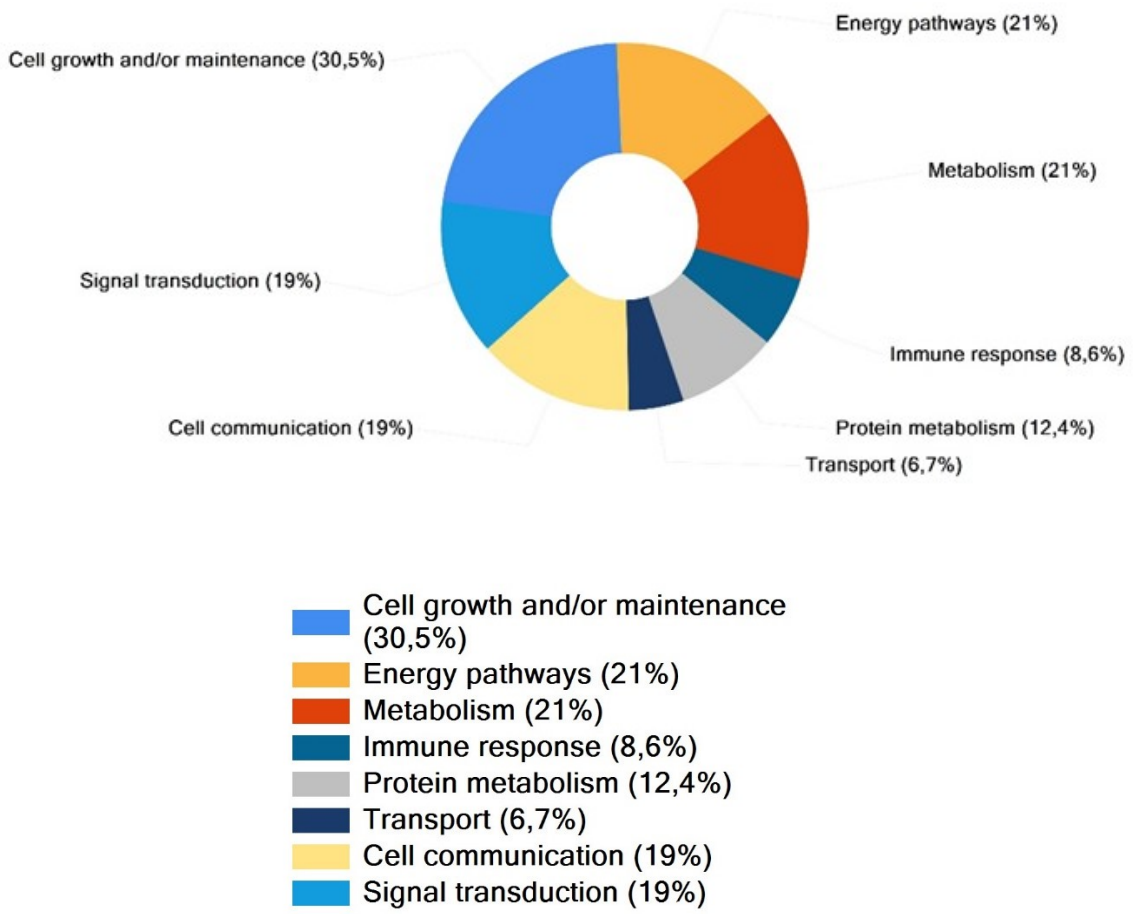

Figure 36. Biological process analysis of proteins found in common between SEC-EVs and DG-EVs.

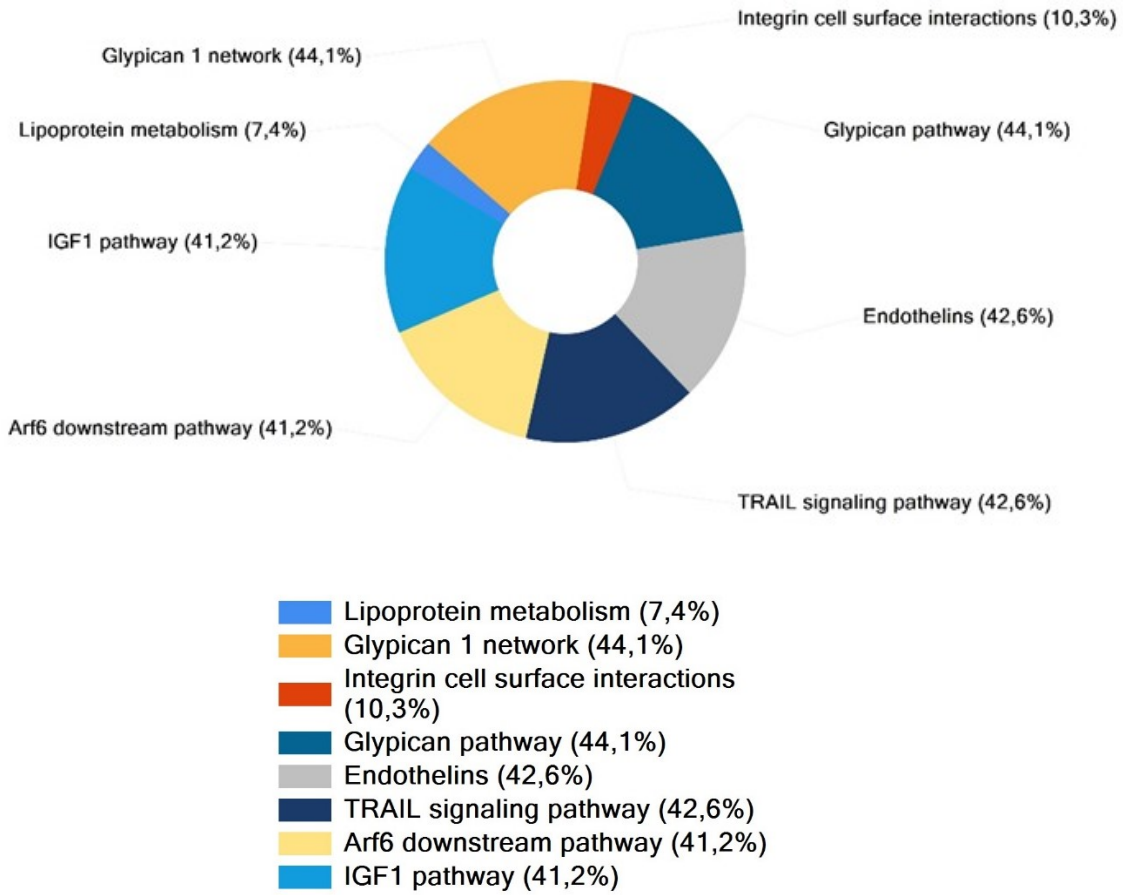

Figure 37. Biological pathways analysis of proteins found in common between SEC-EVs and DG-EVs.

Among the common proteins identified in SEC and DG-EVs, few proteins are up-regulated in SEC-EVs or in DG-EVs (Figure 38). Table 3 reports the 31 proteins that are up-regulated in SEC-EVs (in blue) and in DG-EVs (in orange). SEC-EVs are enriched in proteins involved in cell adhesion (BGH3, EMILIN1), innate immunity (C1RL) and inflammatory response (ATRN). DG-EVs are enriched in proteins involved in cell growth (HTRA1), cell adhesion (EDIL3), cell differentiation (AMPN), angiogenesis (AMPN; EDIL3).

ID	Description	Species	Genes	Significance
EDIL3_HUMAN	EGF-likerepeatanddiscoidinI-likedomain-containingprotein3	Homosapiens	EDIL3	up_DG-EVs
ATRN_HUMAN	Attractin	Homosapiens	ATRN	up_SEC-EVs
APOM_HUMAN	ApolipoproteinM	Homosapiens	APOM	up_SEC-EVs
CERU_HUMAN	Ceruloplasmin	Homosapiens	CP	up_SEC-EVs
HPTR_HUMAN	Haptoglobin-relatedprotein	Homosapiens	HPR	up_SEC-EVs
ANGT_HUMAN	Angiotensinogen	Homosapiens	AGT	up_SEC-EVs
APOH_HUMAN	Beta-2-glycoprotein1	Homosapiens	APOH	up_SEC-EVs
A2GL_HUMAN	Leucine-richalpha-2-glycoprotein	Homosapiens	LRG1	up_SEC-EVs
ALBU_HUMAN	Albumin	Homosapiens	ALB	up_DG-EVs
TRFE_HUMAN	Serotransferrin	Homosapiens	TF	up_DG-EVs
K2C1_HUMAN	Keratin,typeIIcytoskeletal1	Homosapiens	KRT1	up_DG-EVs
PAI1_HUMAN	Plasminogenactivatorinhibitor1	Homosapiens	SERPINE1	up_DG-EVs
THBG_HUMAN	Thyroxine-bindingglobulin	Homosapiens	SERPINA7	up_SEC-EVs
HPLN1_HUMAN	Hyaluronanandproteoglycanlinkprotein 1	Homosapiens	HAPLN1	up_SEC-EVs
K1C10_HUMAN	Keratin,typeIcytoskeletal10	Homosapiens	KRT10	up_DG-EVs
K2C5_HUMAN	Keratin,typeIIcytoskeletal5	Homosapiens	KRT5	up_DG-EVs
AMPN_HUMAN	AminopeptidaseN	Homosapiens	ANPEP	up_DG-EVs
CBPN_HUMAN	CarboxypeptidaseNcatalyticchain	Homosapiens	CPN1	up_SEC-EVs
CO5A1_HUMAN	Collagenalpha-1(V)chain	Homosapiens	COL5A1	up_SEC-EVs
PGS1_HUMAN	Biglycan	Homosapiens	BGN	up_SEC-EVs
K1C9_HUMAN	Keratin,typeIcytoskeletal9	Homosapiens	KRT9	up_DG-EVs
K22E_HUMAN	Keratin,typeIIcytoskeletal2epidermal	Homosapiens	KRT2	up_DG-EVs
BTD_HUMAN	Biotinidase	Homosapiens	BTD	up_SEC-EVs
LUM_HUMAN	Lumican	Homosapiens	LUM	up_SEC-EVs
SPP24_HUMAN	Secretedphosphoprotein24	Homosapiens	SPP2	up_SEC-EVs
BGH3_HUMAN	Transforminggrowthfactor-beta-inducedproteinig-h3	Homosapiens	TGFBI	up_SEC-EVs
TARSH_HUMAN	TargetofNesh-SH3	Homosapiens	ABI3BP	up_SEC-EVs
PDC6I_HUMAN	Programmedcelldeath6-interactingprotein	Homosapiens	PDCD6IP	up_DG-EVs
HTRA1_HUMAN	SerineproteaseHTRA1	Homosapiens	HTRA1	up_DG-EVs
C1RL_HUMAN	ComplementC1rsubcomponent-likeprotein	Homosapiens	C1RL	up_SEC-EVs
EMIL1_HUMAN	EMILIN-1	Homosapiens	EMILIN1	up_SEC-EVs

Table 3. Proteins up-regulated in SEC-EVs (blue) and DG-EVs (orange).

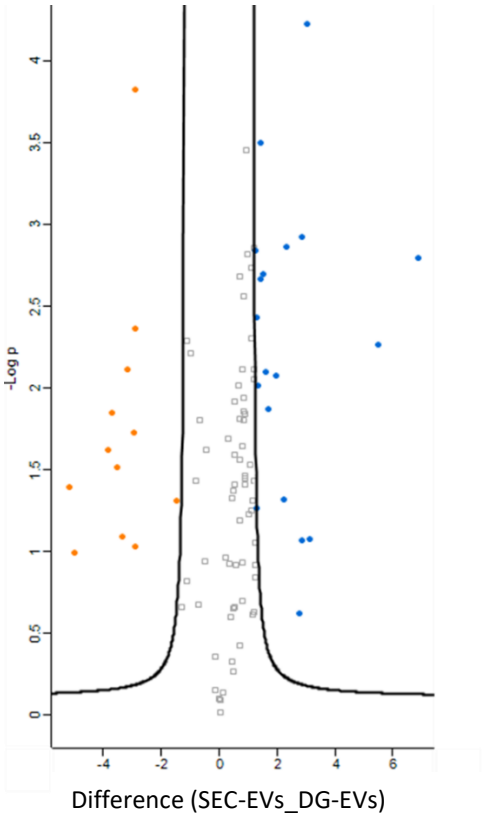

Figure 38. Volcano Plot showing significantly differentially expressed proteins in SEC-EVs (blue) and DG-EVs (orange).

5.3.3.2 Transcriptomic analysis.

MSC-derived EVs purified from 2D CCM, with SEC and DG, were further characterized on total miRNA cargo.

Starting from the same number of total EVs, we performed the transcriptomic analysis of 2083 human miRNAs for the two EV preparations running three technical replicates, following the procedure described in paragraph 5.2.8.

The Reveal software analysis gives information about the quality of the sequencing, in particular the quality and quantity of RNA, the number of sequences and the genetic variability. All the replicates for both the two EV samples passed the QC criteria.

The correlation between the replicates of the same sample and between all replicates of the two samples were high (Pearson coefficient > 0.92; Figures 39-40).

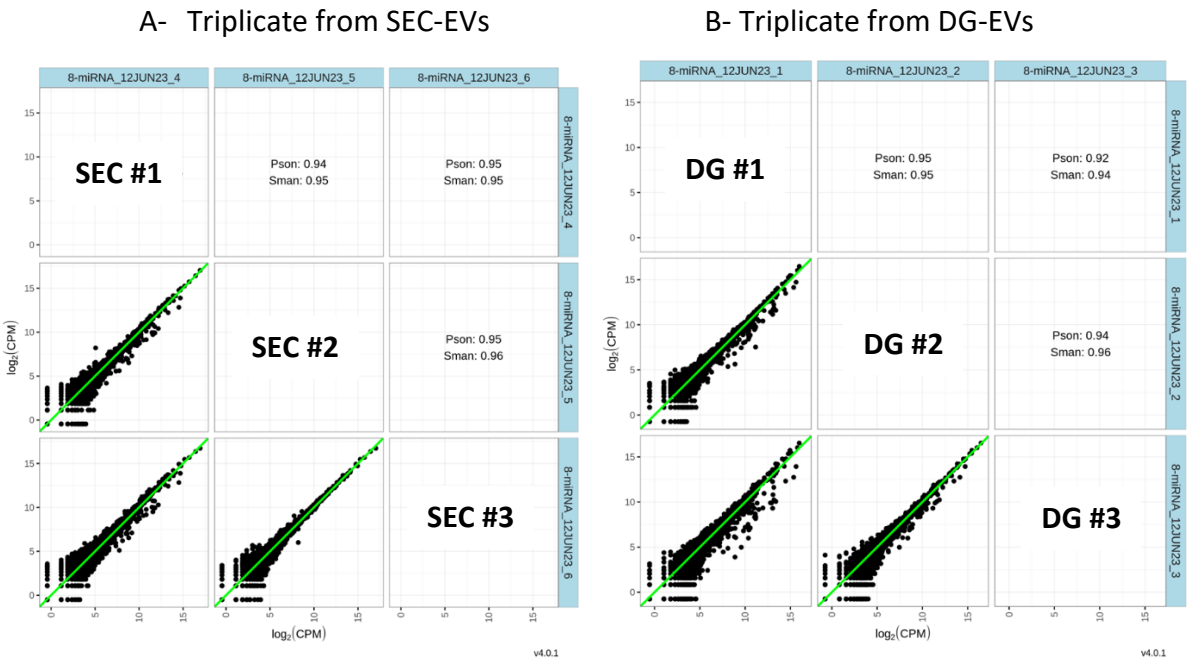

Figure 39. Pair-wise correlation scatterplots of three technical replicates of SEC-EVs (A) and DG-EVs (B).

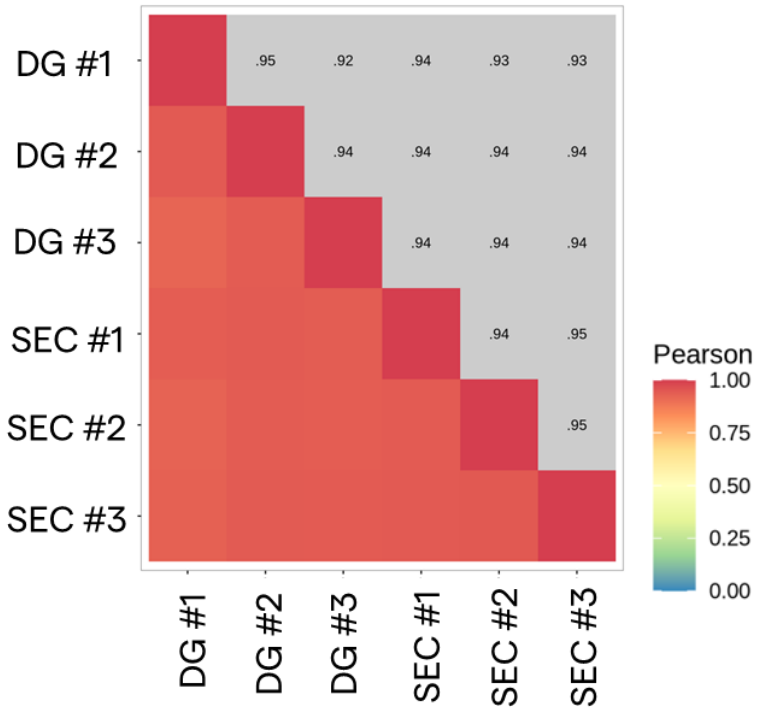

Figure 40. Correlation heatmap of technical replicates of SEC-EVs and DG-EVs.

Differential expression analysis was performed with DESeq2 method, usind DG-EVs as reference group [186]. Few deregulated probes (66) were found between SEC-EVs and DG-

EVs: red dots are down-regulated miRNAs in SEC-EVs, blue dots are up-regulated miRNAs in SEC-EVs, compared to DG-EVs (Figure 41). Colored dots are miRNAs with an adjusted p value < 0.05 [187].

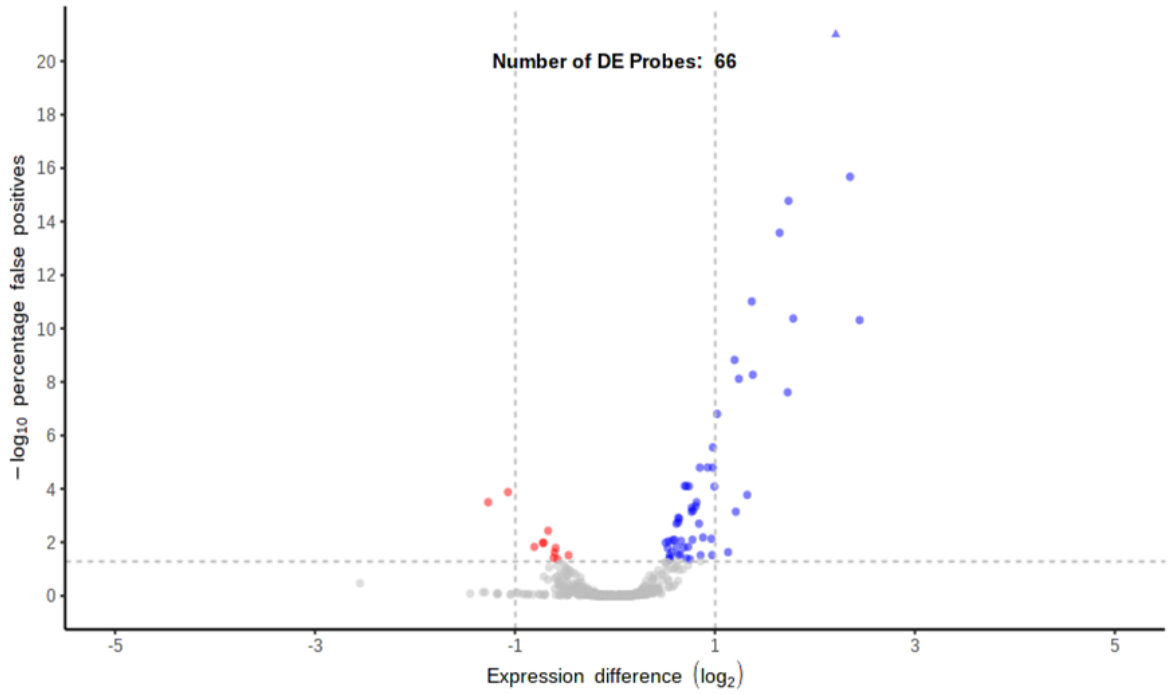

Figure 41. Volcano plot representing differentially expressed probes using DG-EVs as reference group.

Analysis for enrichment pathways of the 66 deregulated miRNAs has been done with the miRNA Enrichment Analysis and Annotation Tool (miEAA) [184]. In particular, GO Cellular component (miRPathDB) analysis was carried out and identified 8 statistically significant enriched subcategories (Figure 42).

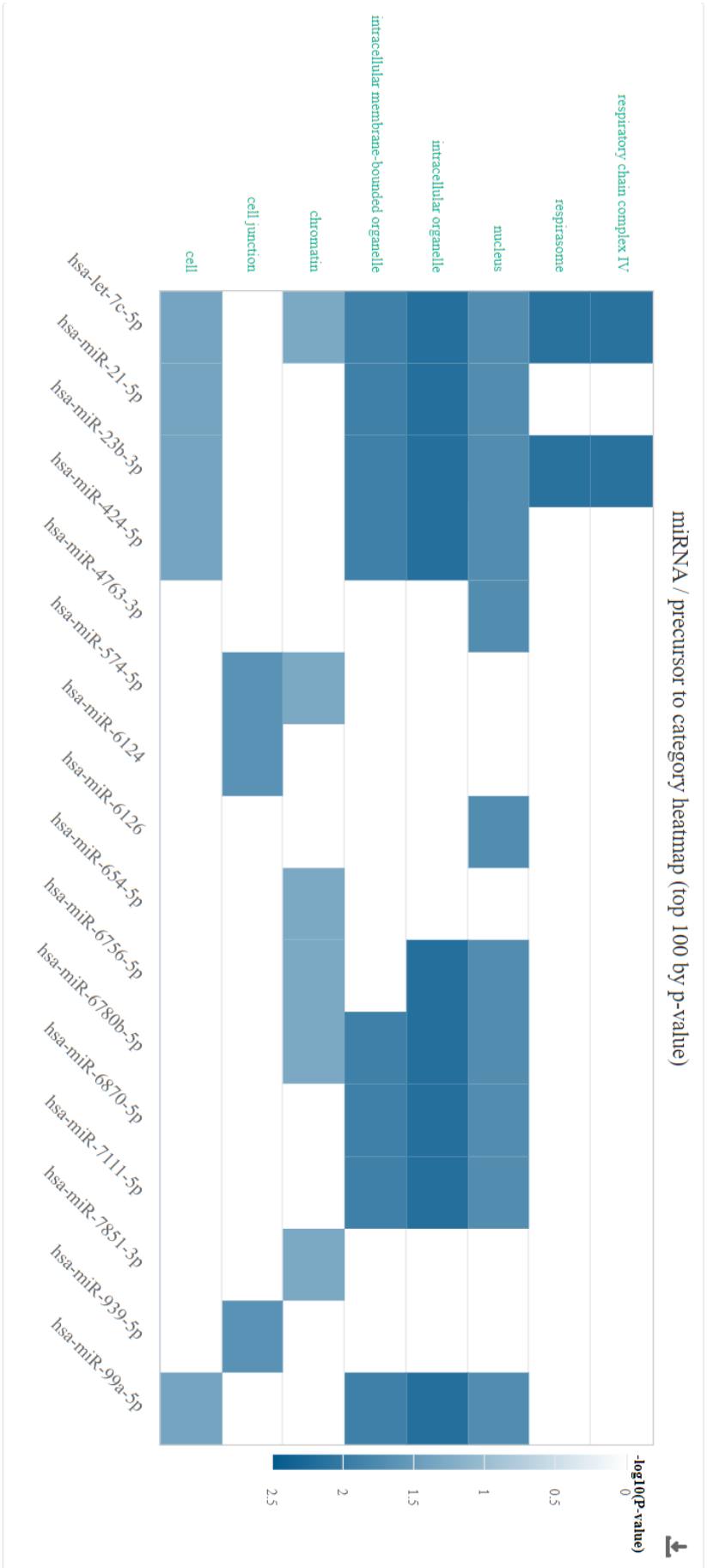

Figure 42. Heatmap showing GO CC analysis of deregulated probes found in MSC-EVs.

Analysis with the tool Localization (RNALocate) found only two statistically significant subcategories (Cytoplasm; Nucleus). Interestingly, even if not statistically significant, more than half of total deregulated probes (37) are annotated for the following categories: Microvesicle; Exosome; Extracellular vesicle; Circulating (hsa-let-7c-5p; hsa-miR-1236-5p; hsa-miR-1273h-5p; hsa-miR-1275; hsa-miR-1290; hsa-miR-149-3p; hsa-miR-197-5p; hsa-miR-198; hsa-miR-199a-3p; hsa-miR-21-5p; hsa-miR-23b-3p; hsa-miR-3162-5p; hsa-miR-3197; hsa-miR-3652; hsa-miR-3940-5p; hsa-miR-424-5p; hsa-miR-4253; hsa-miR-4463; hsa-miR-4507; hsa-miR-451a; hsa-miR-4758-5p; hsa-miR-5010-5p; hsa-miR-5585-3p; hsa-miR-564; hsa-miR-574-5p; hsa-miR-6124; hsa-miR-6126; hsa-miR-6131; hsa-miR-654-5p; hsa-miR-6746-5p; hsa-miR-6821-5p; hsa-miR-6870-5p; hsa-miR-7108-5p; hsa-miR-7851-3p; hsa-miR-885-3p; hsa-miR-939-5p; hsa-miR-99a-5p).

GO Biological process (miRPathDB) and GO Molecular function (miRPathDB) analysis resulted in no enriched pathways of interest (Figures 43-44).

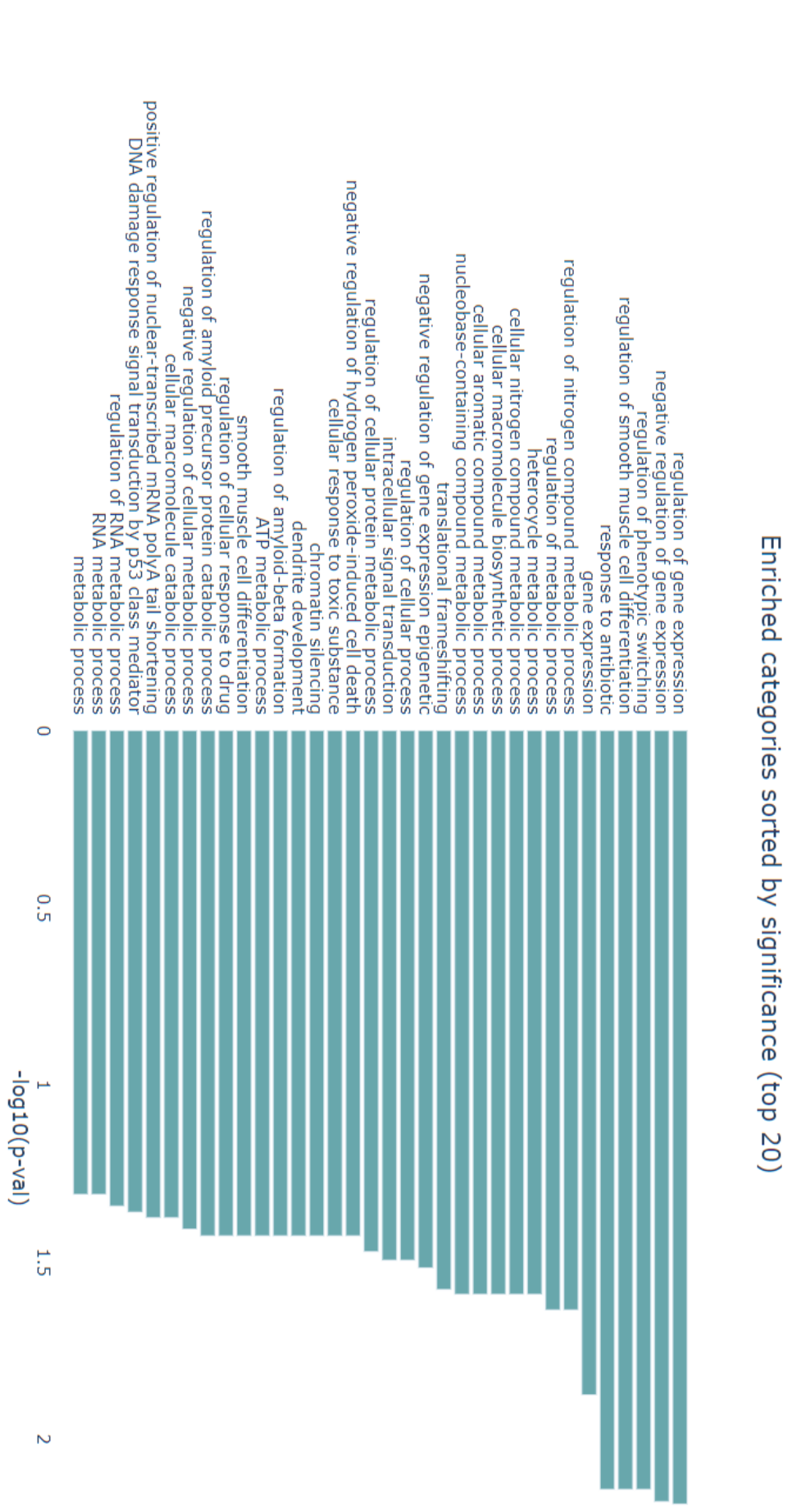

Figure 43. Heatmap showing GO Biological process analysis of deregulated probes found in MSC-EVs.

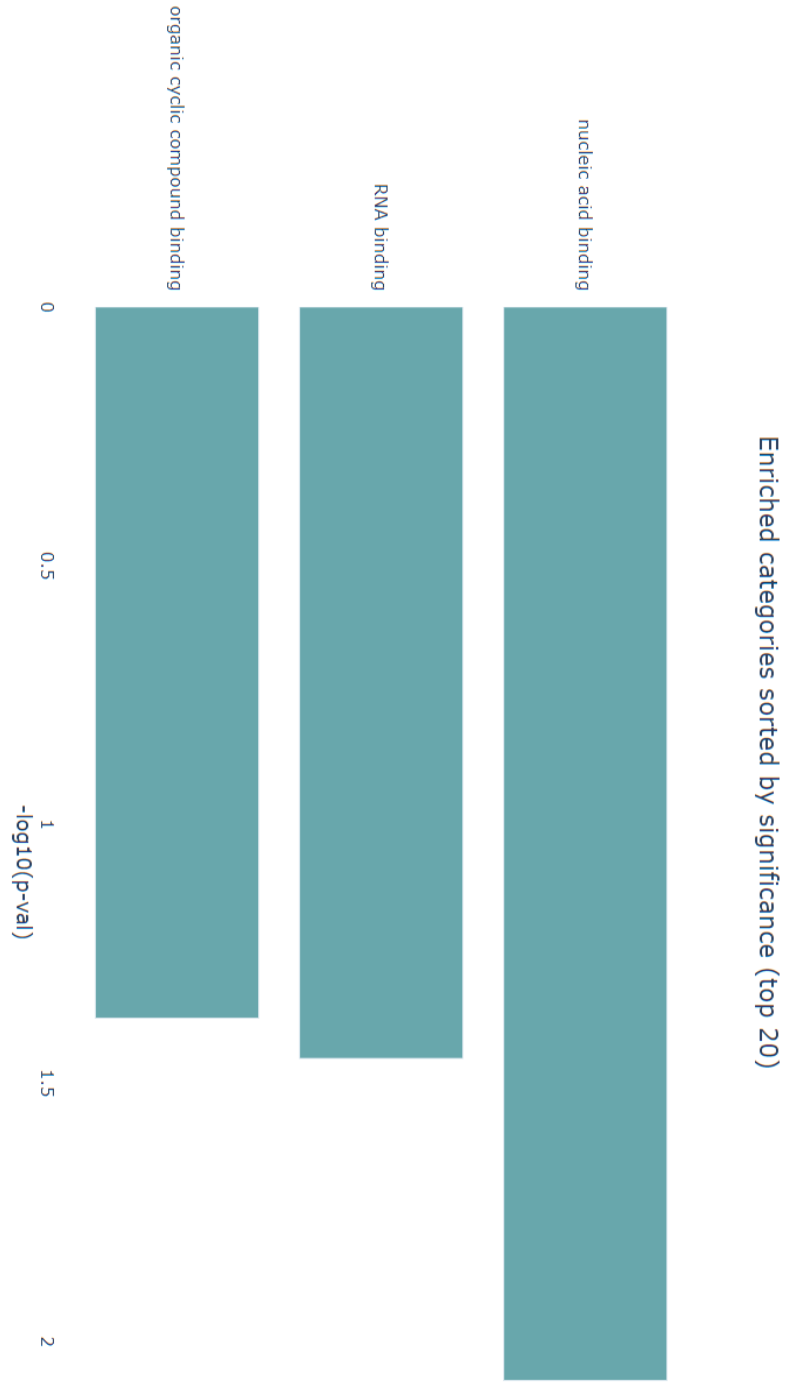

Figure 44. Heatmap showing GO Molecular function analysis of deregulated probes found in MSC-EVs.

5.3.4 *In vitro* functional properties of MSC-EVs.

MSC-EVs can be uptaken by endothelial cells and stimulate cell proliferation and migration *in vitro* [188–190]. Human Umbilical Vein Endothelial Cells (HUVECs) are endothelial cells widely used as model for both wound healing and tube formation assays. Hence, we sought to evaluate the functional properties of SEC- and DG-UC purified MSC-EVs on these two assays.

The impact of MSC-EVs on cell migration was assessed with the wound healing assay. Protocol assay, described in paragraph 5.2.9, includes a starvation step to synchronize cells and halt cell proliferation, thus the gap closure will be achieved mainly by cell migration.
Baseline growth of HUVEC cells in complete medium showed that the cells are able to close the gap after 24 hours. We wanted to investigate if the treatment with MSC-EVs increases the rate of gap closure after scratching.
In literature, there is no standardized protocol to estimate the dose of MSC-EVs for wound healing assay. In fact, some studies reported doses expressed as micrograms of MSC-EVs, others as number of particles. In addition, MSC-EVs were purified with different methods, and the concentration is assessed with different techniques, leading to different measurements of particles [188,191,192].
To calculate the dose of EVs, we used the particle concentration measured at NanoAnalyzer, which measures at single particle level and takes into account the population of small EVs. In order to translate same doses in different cell-based assays, we considered the ratio between cell : number of EVs. We tested different ratios (1: 10, 1:100, 1:1000, 1:2000, 1:3000) with both SEC-EVs and DG-EVs from 2D culture and 3D culture, in triplicate.
SEC-derived MSC-EVs enhanced cell migration starting from 1: 1000 ratio, but even at the highest dose (ratio 1: 3000) without a statistically significant difference compared to untreated cells. Instead, DG-derived MSC-EVs enhanced cell migration with a statistically significant difference compared to untreated cells, starting from 1:2000 ratio (Figures 45 and 46).

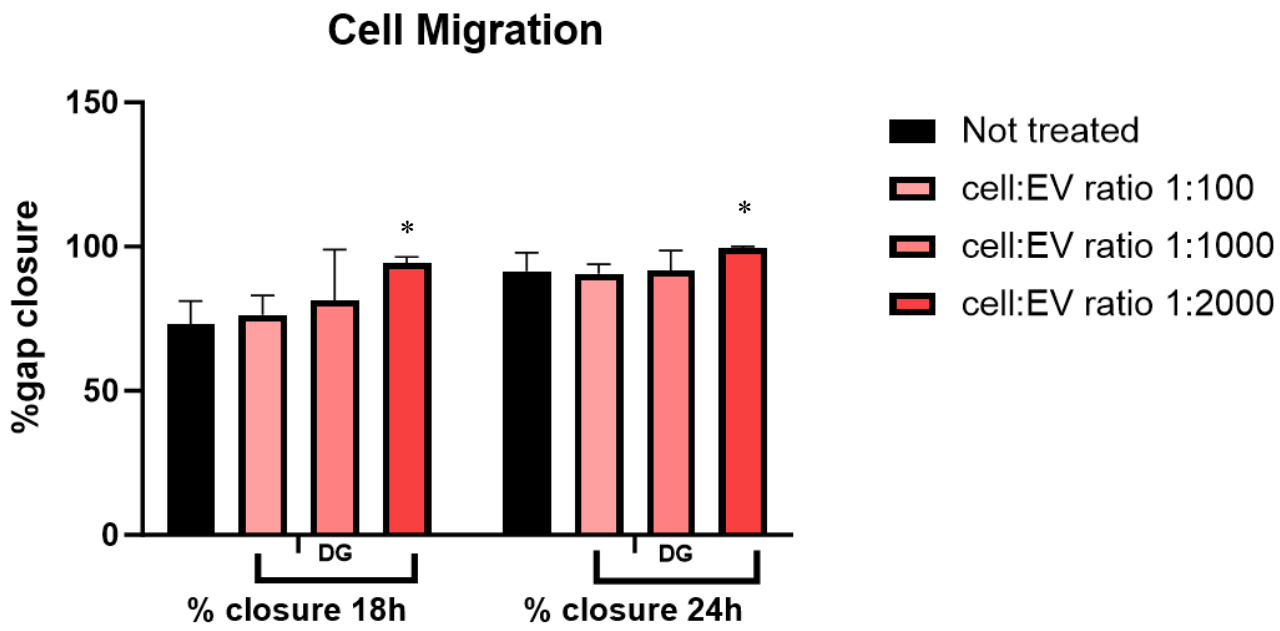

*Figure 45. Rate of wound closure calculated for not treated HUVEC cells and cells treated with DG-sEVs. Bar chart is representative of three technical replicates. * indicates a statistically significant difference (p value < 0.05).*

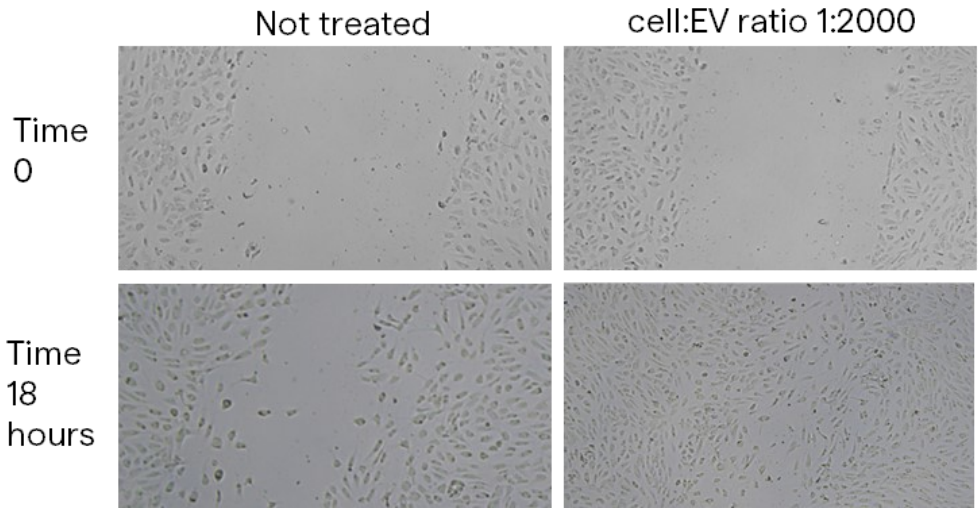

Figure 46. Images of the wound space at time 0 and time 18 h, without treatment or with treatment with DG-sEVs at ratio cell:EV 1:2000.

To evaluate HUVEC proliferation in response to the pre-treatment of 24 hours with MSC-sEVs, a colorimetric MTT-based assay was used as described in paragraph 5.2.10.
Both DG and SEC-purified EVs significanlty increased cell proliferation, starting with as little as 1000 EVs per cell with the DG sample (Figure 47).

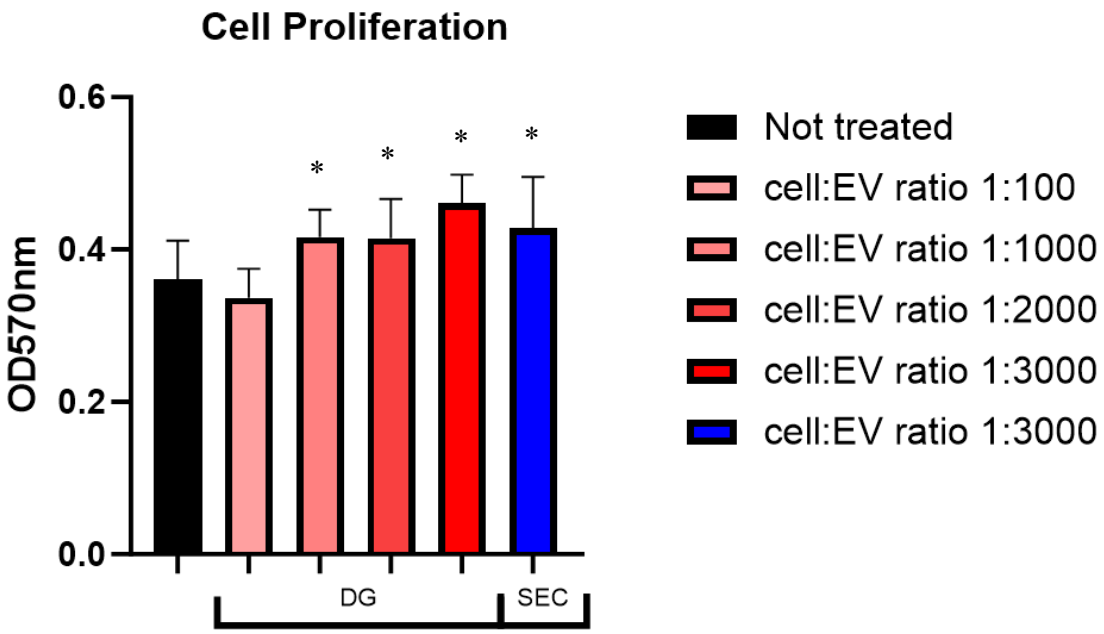

*Figure 47.MTT-based colorimetric assay to quantify HUVEC cell proliferation, with or without a pre-treatment with MSC-sEVs. Bar chart is representative of six technical replicates. * indicates a statistically significant difference (p value < 0.05).*

Tube formation assay was used to evaluate the impact of MSC-EVs on angiogenesis, a phenomenon that includes different processes, such as endothelial cell proliferation, differentiation and migration. Pre-screened HUVECs, in complete medium, seeded on 3D gel are able to form tube-like structures within 2-4 hours and to grow according to a meshed network [185,193]. Since the tube formation starts in few hours after cell seeding on Matrigel, we decided to perform a pre-treatment of 24 hours with MSC-EVs, in order to allow them to be internalized by endothelial cells.
It has been demonstrated that the kinetic of the meshing network structuration of endothelial cells on Matrigel starts by the formation of a multitude of small and unstable meshes. Size of meshes then progressively increases by fusion of two adjacent meshes, which occurred by

segments (tube) regression or disruption [194]. We observed this behaviour for both not treated HUVECs and pre-treated HUVECs (Figure 48, looking from the left to the right).

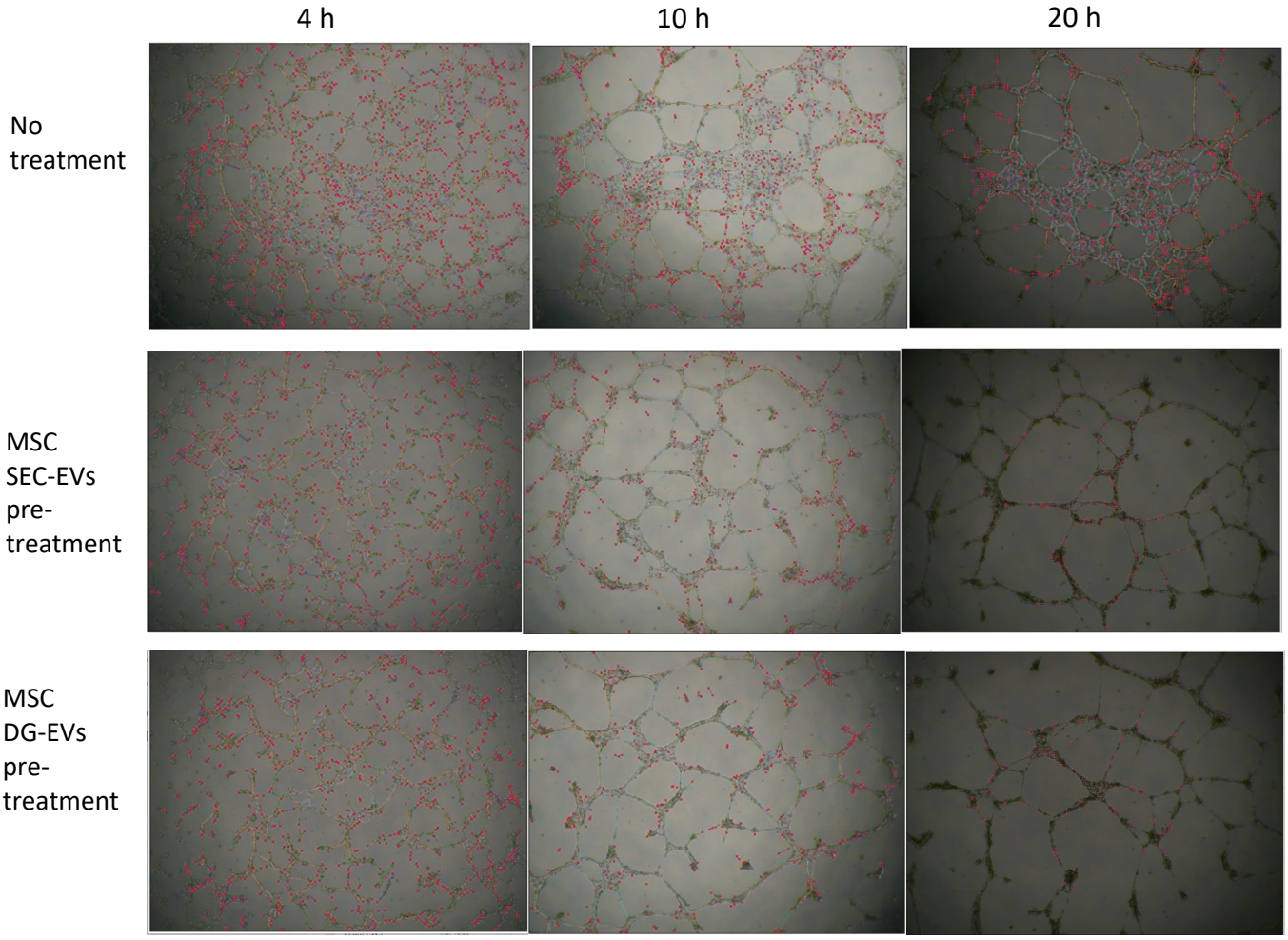

Figure 48. HUVEC network analysis of pictures taken at 4, 10 and 20 hours after cell seeding on Matrigel.

The pre-treatment with MSC-EVs, both SEC-derived and DG-derived EVS, seems to have an impact on HUVEC tube formation. In fact, it resulted, for all analyzed timepoints, in a significant decrease of most of the parameters quantified by Angiogenesis Analyzer for ImageJ (extremities, nodes, junctions, master junctions, segments, master segments, branches, meshes, segments lenght, branches lenght), except for «mesh index» and «mean mesh size», which are, conversely, significantly increased (p value < 0.05). Mesh index, which is the mean distance separating two master junctions, represents a further indication of mesh size.

Figures 49 and 50 show some representative angiogenesis network parameters, quantified with ImageJ at time 10 hours.

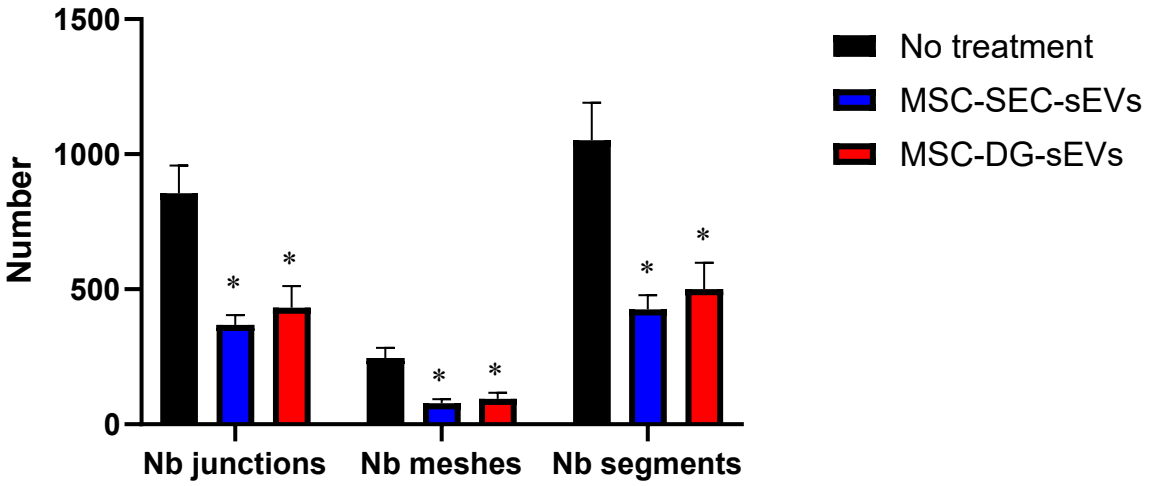

*Figure 49. Quantification of representative angiogenesis network parameters at 10 hours in HUVEC cells without and with pre-treatment with MSC-EVs. Bar chart is representative of three technical replicates. * indicates a statistically significant difference (p value < 0.05).*

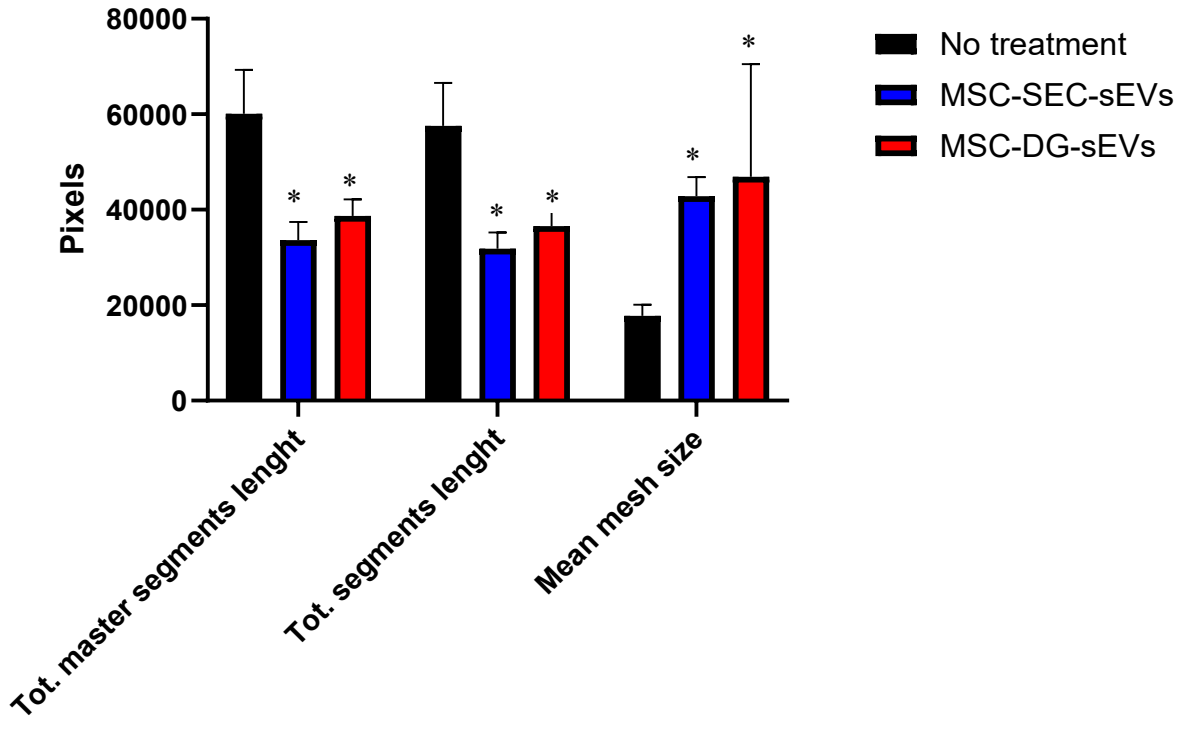

*Figure 50. Quantification of representative network parameters at 10 hours in HUVEC cells without and with pre-treatment with MSC-EVs. Bar chart is representative of three technical replicates. * indicates a statistically significant difference (p value < 0.05).*

Our data suggest the formation of more complete networks, with less tubes but with bigger meshes, in wells with HUVECs pre-treated with MSC-EVs. In untreated wells, clusters of cells not organized in tube-like structures are visible even after 20 hours from cell seeding (Figure 48).

It is challenging to compare these data with previously published reports. In fact, most studies on *in vitro* pro-angiogenic functionalities of MSC-EVs reported only the increase of some metrics, like nodes or segments lenght, after treatment with EVs, while neglecting others such as mesh size [190,191,195,196].

However, these data warrant further work to better establish dose ranges and demonstrate the effective internalization of EVs by the cells.

5.4 Conclusions.

In this study we performed a deep characterization of EVs from human bone marrow MSC, described in literature to have therapeutic and beneficial effects in different diseases. MSC-EVs were purified from both a static 2D culture and from a 3D culture using a bioreactor system. Consistent with several studies reported in literature, higher yields of EVs from 3D culture were obtained [68,75–77]. Moreover, average EV size was more homogeneous in 3D-derived sample, corresponding to small EVs subtype (Figure 28).

To investigate *in vitro* functional properties of these EVs, two different EV purification methods, SEC and DG-UC, were evaluated in order to see also the impact of sample purity on the molecular content and functional effects of EV *in vitro*.

Density gradient ultracentrifugation was selected as gold standard method to obtain high EV purity, while SEC chromatography was identified as less laborious method yielding, however, a medium-high final EV purity. As expected, DG-derived EVs had a higher purity index compared to SEC-derived EVs (Figure 25). In fact, protein contaminants could not be fully separated from EVs by SEC.

Despite the different purity indexes, both EV types resulted in similar integrity and expression of canonical EV markers (Figures 26, 29-31).

As a consequence of the higher purity of DG-EVs, less particles were needed to obtain functional effects *in vitro*, including increasing endothelial cell migration and proliferation.

Bioinformatic analysis of proteome and miRNA cargo, limited to the 2D EV samples, did not show significant differences in the two EV preparation.

In conclusion, the two EV preparations, from both 2D and 3D sources, showed similar effects on endothelial cells *in vitro.* DG method is to be preferred for small studies of proof of concept, but SEC method is a valid alternative for high-throughput analysis.

Future studies are warranted to evaluate if MSC-EVs released under hypoxic conditions have improved functional properties *in vitro* and *in vivo*.

6. References.

1. Théry, C.; Witwer, K.W.; Aikawa, E.; Alcaraz, M.J.; Anderson, J.D.; Andriantsitohaina, R.; Antoniou, A.; Arab, T.; Archer, F.; Atkin-Smith, G.K.; et al. Minimal Information for Studies of Extracellular Vesicles 2018 (MISEV2018): A Position Statement of the International Society for Extracellular Vesicles and Update of the MISEV2014 Guidelines. *Journal of Extracellular Vesicles* **2018**, *7*, 1535750, doi:10.1080/20013078.2018.1535750.
2. van Niel, G.; D'Angelo, G.; Raposo, G. Shedding Light on the Cell Biology of Extracellular Vesicles. *Nature Reviews Molecular Cell Biology* **2018**, *19*, 213–228, doi:10.1038/nrm.2017.125.
3. Kim, D.-K.; Kang, B.; Kim, O.Y.; Choi, D.; Lee, J.; Kim, S.R.; Go, G.; Yoon, Y.J.; Kim, J.H.; Jang, S.C.; et al. EVpedia: An Integrated Database of High-Throughput Data for Systemic Analyses of Extracellular Vesicles. *Journal of Extracellular Vesicles* **2013**, *2*, 20384, doi:10.3402/jev.v2i0.20384.
4. Yáñez-Mó, M.; Siljander, P.R.-M.; Andreu, Z.; Bedina Zavec, A.; Borràs, F.E.; Buzas, E.I.; Buzas, K.; Casal, E.; Cappello, F.; Carvalho, J.; et al. Biological Properties of Extracellular Vesicles and Their Physiological Functions. *Journal of Extracellular Vesicles* **2015**, *4*, 27066, doi:10.3402/jev.v4.27066.
5. Théry, C. Exosomes: Secreted Vesicles and Intercellular Communications. F1000 Biol Rep 3(15). *F1000 biology reports* **2011**, *3*, 15, doi:10.3410/B3-15.
6. Chargaff, E. CELL STRUCTURE AND THE PROBLEM OF BLOOD COAGULATION. *Journal of Biological Chemistry* **1945**, *160*, 351–359.
7. Wolf, P. The Nature and Significance of Platelet Products in Human Plasma. *British Journal of Haematology* **1967**, *13*, 269–288, doi:10.1111/j.1365-2141.1967.tb08741.x.
8. Aaronson, S.A.; Behrens, U.; Orner, R.; Haines, T.H. Ultrastructure of Intracellular and Extracellular Vesicles, Membranes, and Myelin Figures Produced by Ochromonas Danica. *Journal of ultrastructure research* **1971**, *35 5*, 418–430.
9. Käppeli O; Finnerty W R Partition of Alkane by an Extracellular Vesicle Derived from Hexadecane-Grown Acinetobacter. *Journal of Bacteriology* **1979**, *140*, 707–712, doi:10.1128/jb.140.2.707-712.1979.
10. Nunez, E.A.; Wallis, J.; Gershon, M.D. Secretory Processes in Follicular Cells of the Bat Thyroid. III. The Occurrence of Extracellular Vesicles and Colloid Droplets during Arousal from Hibernation. *American Journal of Anatomy* **1974**, *141*, 179–201, doi:10.1002/aja.1001410203.
11. Pan, B.-T.; Johnstone, R.M. Fate of the Transferrin Receptor during Maturation of Sheep Reticulocytes in Vitro: Selective Externalization of the Receptor. *Cell* **1983**, *33*, 967–978, doi:10.1016/0092-8674(83)90040-5.
12. Johnstone, R.M.; Adam, M.; Hammond, J.R.; Orr, L.; Turbide, C. Vesicle Formation during Reticulocyte Maturation. Association of Plasma Membrane Activities with Released Vesicles (Exosomes). *Journal of Biological Chemistry* **1987**, *262*, 9412–9420, doi:10.1016/S0021-9258(18)48095-7.
13. Raposo, G.; Nijman, H.W.; Stoorvogel, W.; Liejendekker, R.; Harding, C.V.; Melief, C.J.; Geuze, H.J. B Lymphocytes Secrete Antigen-Presenting Vesicles. *Journal of Experimental Medicine* **1996**, *183*, 1161–1172, doi:10.1084/jem.183.3.1161.
14. Bard, M.P.; Hegmans, J.P.; Hemmes, A.; Luider, T.M.; Willemsen, R.; Severijnen, L.-A.A.; van Meerbeeck, J.P.; Burgers, S.A.; Hoogsteden, H.C.; Lambrecht, B.N. Proteomic Analysis of Exosomes Isolated from Human Malignant Pleural Effusions. *Am J Respir Cell Mol Biol* **2004**, *31*, 114–121, doi:10.1165/rcmb.2003-0238OC.
15. Subra, C.; Laulagnier, K.; Perret, B.; Record, M. Exosome Lipidomics Unravels Lipid Sorting at the Level of Multivesicular Bodies. *Biochimie* **2007**, *89*, 205–212, doi:10.1016/j.biochi.2006.10.014.

16. Denzer, K.; Kleijmeer, M.J.; Heijnen, H.F.G.; Stoorvogel, W.; Geuze, H.J. Exosome: From Internal Vesicle of the Multivesicular Body to Intercellular Signaling Device. *Journal of cell science* **2000**, *113 Pt 19*, 3365–3374.
17. Skog, J.; Würdinger, T.; van Rijn, S.; Meijer, D.H.; Gainche, L.; Curry, W.T.; Carter, B.S.; Krichevsky, A.M.; Breakefield, X.O. Glioblastoma Microvesicles Transport RNA and Proteins That Promote Tumour Growth and Provide Diagnostic Biomarkers. *Nature Cell Biology* **2008**, *10*, 1470–1476, doi:10.1038/ncb1800.
18. Couch, Y.; Buzàs, E.I.; Di Vizio, D.; Gho, Y.S.; Harrison, P.; Hill, A.F.; Lötvall, J.; Raposo, G.; Stahl, P.D.; Théry, C.; et al. A Brief History of Nearly EV-Erything – The Rise and Rise of Extracellular Vesicles. *Journal of Extracellular Vesicles* **2021**, *10*, e12144, doi:10.1002/jev2.12144.
19. Gould, S.J.; Raposo, G. As We Wait: Coping with an Imperfect Nomenclature for Extracellular Vesicles. *Journal of Extracellular Vesicles* **2013**, *2*, 20389, doi:10.3402/jev.v2i0.20389.
20. Minciacchi, V.R.; Freeman, M.R.; Di Vizio, D. Extracellular Vesicles in Cancer: Exosomes, Microvesicles and the Emerging Role of Large Oncosomes. *Seminars in Cell & Developmental Biology* **2015**, *40*, 41–51, doi:10.1016/j.semcdb.2015.02.010.
21. Raposo, G.; Stoorvogel, W. Extracellular Vesicles: Exosomes, Microvesicles, and Friends. *Journal of Cell Biology* **2013**, *200*, 373–383, doi:10.1083/jcb.201211138.
22. Monerah Al Soraj; Salma Bargal; Yunus A. Luqmani Extracellular Vesicles: A Mechanism to Reverse Metastatic Behaviour as a New Approach to Cancer Therapy. In *Tumor Metastasis*; Ke Xu, Ed.; IntechOpen: Rijeka, 2016; p. Ch. 5 ISBN 978-953-51-2631-7.
23. Zhang, H.; Freitas, D.; Kim, H.S.; Fabijanic, K.; Li, Z.; Chen, H.; Mark, M.T.; Molina, H.; Martin, A.B.; Bojmar, L.; et al. Identification of Distinct Nanoparticles and Subsets of Extracellular Vesicles by Asymmetric Flow Field-Flow Fractionation. *Nature Cell Biology* **2018**, *20*, 332–343, doi:10.1038/s41556-018-0040-4.
24. Zhang, Q.; Higginbotham, J.N.; Jeppesen, D.K.; Yang, Y.-P.; Li, W.; McKinley, E.T.; Graves-Deal, R.; Ping, J.; Britain, C.M.; Dorsett, K.A.; et al. Transfer of Functional Cargo in Exomeres. *Cell Reports* **2019**, *27*, 940-954.e6, doi:10.1016/j.celrep.2019.01.009.
25. Zhang, Q.; Jeppesen, D.K.; Higginbotham, J.N.; Graves-Deal, R.; Trinh, V.Q.; Ramirez, M.A.; Sohn, Y.; Neininger, A.C.; Taneja, N.; McKinley, E.T.; et al. Supermeres Are Functional Extracellular Nanoparticles Replete with Disease Biomarkers and Therapeutic Targets. *Nature Cell Biology* **2021**, *23*, 1240–1254, doi:10.1038/s41556-021-00805-8.
26. Abels, E.R.; Breakefield, X.O. Introduction to Extracellular Vesicles: Biogenesis, RNA Cargo Selection, Content, Release, and Uptake. *Cellular and Molecular Neurobiology* **2016**, *36*, 301–312, doi:10.1007/s10571-016-0366-z.
27. Venturella, M.; Carpi, F.M.; Zocco, D. Standardization of Blood Collection and Processing for the Diagnostic Use of Extracellular Vesicles. *Current Pathobiology Reports* **2019**, *7*, 1–8, doi:10.1007/s40139-019-00189-3.
28. György, B.; Pálóczi, K.; Kovács, A.; Barabás, E.; Bekő, G.; Várnai, K.; Pállinger, É.; Szabó-Taylor, K.; Szabó, T.G.; Kiss, A.A.; et al. Improved Circulating Microparticle Analysis in Acid-Citrate Dextrose (ACD) Anticoagulant Tube. *Thrombosis Research* **2014**, *133*, 285–292, doi:10.1016/j.thromres.2013.11.010.
29. Coumans, F.A.W.; Brisson, A.R.; Buzas, E.I.; Dignat-George, F.; Drees, E.E.E.; El-Andaloussi, S.; Emanueli, C.; Gasecka, A.; Hendrix, A.; Hill, A.F.; et al. Methodological Guidelines to Study Extracellular Vesicles. *Circulation Research* **2017**, *120*, 1632–1648, doi:10.1161/CIRCRESAHA.117.309417.
30. Vila-Liante, V.; Sánchez-López, V.; Martínez-Sales, V.; Ramón-Nuñez, L.A.; Arellano-Orden, E.; Cano-Ruiz, A.; Rodríguez-Martorell, F.J.; Gao, L.; Otero-Candelera, R. Impact of Sample Processing on the Measurement of Circulating Microparticles: Storage and Centrifugation Parameters. **2016**, *54*, 1759–1767, doi:10.1515/cclm-2016-0036.
31. Gandham, S.; Su, X.; Wood, J.; Nocera, A.L.; Alli, S.C.; Milane, L.; Zimmerman, A.; Amiji, M.; Ivanov, A.R. Technologies and Standardization in Research on Extracellular Vesicles. *Trends in Biotechnology* **2020**, *38*, 1066–1098, doi:10.1016/j.tibtech.2020.05.012.

32. YAMADA, T.; INOSHIMA, Y.; MATSUDA, T.; ISHIGURO, N. Comparison of Methods for Isolating Exosomes from Bovine Milk. *Journal of Veterinary Medical Science* **2012**, *74*, 1523–1525, doi:10.1292/jvms.12-0032.
33. Štukelj, R.; Schara, K.; Bedina - Zavec, A.; Šuštar, V.; Pajnič, M.; Pađen, L.; Krek, J.L.; Kralj-Iglič, V.; Mrvar-Brečko, A.; Janša, R. Effect of Shear Stress in the Flow through the Sampling Needle on Concentration of Nanovesicles Isolated from Blood. *European Journal of Pharmaceutical Sciences* **2017**, *98*, 17–29, doi:10.1016/j.ejps.2016.10.007.
34. Chen, C.; Skog, J.; Hsu, C.-H.; Lessard, R.T.; Balaj, L.; Wurdinger, T.; Carter, B.S.; Breakefield, X.O.; Toner, M.; Irimia, D. Microfluidic Isolation and Transcriptome Analysis of Serum Microvesicles. *Lab Chip* **2010**, *10*, 505–511, doi:10.1039/B916199F.
35. Van Deun, J.; Mestdagh, P.; Agostinis, P.; Akay, Ö.; Anand, S.; Anckaert, J.; Martinez, Z.A.; Baetens, T.; Beghein, E.; Bertier, L.; et al. EV-TRACK: Transparent Reporting and Centralizing Knowledge in Extracellular Vesicle Research. *Nature Methods* **2017**, *14*, 228–232, doi:10.1038/nmeth.4185.
36. Keerthikumar, S.; Chisanga, D.; Ariyaratne, D.; Al Saffar, H.; Anand, S.; Zhao, K.; Samuel, M.; Pathan, M.; Jois, M.; Chilamkurti, N.; et al. ExoCarta: A Web-Based Compendium of Exosomal Cargo. *Journal of Molecular Biology* **2016**, *428*, 688–692, doi:10.1016/j.jmb.2015.09.019.
37. Pathan, M.; Fonseka, P.; Chitti, S.V.; Kang, T.; Sanwlani, R.; Van Deun, J.; Hendrix, A.; Mathivanan, S. Vesiclepedia 2019: A Compendium of RNA, Proteins, Lipids and Metabolites in Extracellular Vesicles. *Nucleic Acids Research* **2019**, *47*, D516–D519, doi:10.1093/nar/gky1029.
38. Tauro, B.J.; Greening, D.W.; Mathias, R.A.; Ji, H.; Mathivanan, S.; Scott, A.M.; Simpson, R.J. Comparison of Ultracentrifugation, Density Gradient Separation, and Immunoaffinity Capture Methods for Isolating Human Colon Cancer Cell Line LIM1863-Derived Exosomes. *Methods* **2012**, *56*, 293–304, doi:10.1016/j.ymeth.2012.01.002.
39. Witwer, K.W.; Buzás, E.I.; Bemis, L.T.; Bora, A.; Lässer, C.; Lötvall, J.; Nolte-'t Hoen, E.N.; Piper, M.G.; Sivaraman, S.; Skog, J.; et al. Standardization of Sample Collection, Isolation and Analysis Methods in Extracellular Vesicle Research. *Journal of Extracellular Vesicles* **2013**, *2*, 20360, doi:10.3402/jev.v2i0.20360.
40. Van Deun, J.; Mestdagh, P.; Sormunen, R.; Cocquyt, V.; Vermaelen, K.; Vandesompele, J.; Bracke, M.; De Wever, O.; Hendrix, A. The Impact of Disparate Isolation Methods for Extracellular Vesicles on Downstream RNA Profiling. *Journal of Extracellular Vesicles* **2014**, *3*, 24858, doi:10.3402/jev.v3.24858.
41. Kalra, H.; Adda, C.G.; Liem, M.; Ang, C.-S.; Mechler, A.; Simpson, R.J.; Hulett, M.D.; Mathivanan, S. Comparative Proteomics Evaluation of Plasma Exosome Isolation Techniques and Assessment of the Stability of Exosomes in Normal Human Blood Plasma. *PROTEOMICS* **2013**, *13*, 3354–3364, doi:10.1002/pmic.201300282.
42. Roux, Q.; Van Deun, J.; Dedeyne, S.; Hendrix, A. The EV-TRACK Summary Add-on: Integration of Experimental Information in Databases to Ensure Comprehensive Interpretation of Biological Knowledge on Extracellular Vesicles. *Journal of Extracellular Vesicles* **2020**, *9*, 1699367, doi:10.1080/20013078.2019.1699367.
43. Reiner, A.T.; Witwer, K.W.; van Balkom, B.W.M.; de Beer, J.; Brodie, C.; Corteling, R.L.; Gabrielsson, S.; Gimona, M.; Ibrahim, A.G.; de Kleijn, D.; et al. Concise Review: Developing Best-Practice Models for the Therapeutic Use of Extracellular Vesicles. *Stem Cells Translational Medicine* **2017**, *6*, 1730–1739, doi:10.1002/sctm.17-0055.
44. Alvarez, M.L.; Khosroheidari, M.; Kanchi Ravi, R.; DiStefano, J.K. Comparison of Protein, microRNA, and mRNA Yields Using Different Methods of Urinary Exosome Isolation for the Discovery of Kidney Disease Biomarkers. *Kidney International* **2012**, *82*, 1024–1032, doi:10.1038/ki.2012.256.
45. Mondal, S.K.; Whiteside, T.L. Immunoaffinity-Based Isolation of Melanoma Cell-Derived and T Cell-Derived Exosomes from Plasma of Melanoma Patients. In *Melanoma: Methods and Protocols*; Hargadon, K.M., Ed.; Springer US: New York, NY, 2021; pp. 305–321 ISBN 978-1-07-161205-7.

46. Nordin, J.Z.; Lee, Y.; Vader, P.; Mäger, I.; Johansson, H.J.; Heusermann, W.; Wiklander, O.P.B.; Hällbrink, M.; Seow, Y.; Bultema, J.J.; et al. Ultrafiltration with Size-Exclusion Liquid Chromatography for High Yield Isolation of Extracellular Vesicles Preserving Intact Biophysical and Functional Properties. *Nanomedicine: Nanotechnology, Biology and Medicine* **2015**, *11*, 879–883, doi:10.1016/j.nano.2015.01.003.
47. Brennan, K.; Martin, K.; FitzGerald, S.P.; O'Sullivan, J.; Wu, Y.; Blanco, A.; Richardson, C.; Mc Gee, M.M. A Comparison of Methods for the Isolation and Separation of Extracellular Vesicles from Protein and Lipid Particles in Human Serum. *Scientific Reports* **2020**, *10*, 1039, doi:10.1038/s41598-020-57497-7.
48. Muller, L.; Hong, C.-S.; Stolz, D.B.; Watkins, S.C.; Whiteside, T.L. Isolation of Biologically-Active Exosomes from Human Plasma. *Journal of Immunological Methods* **2014**, *411*, 55–65, doi:10.1016/j.jim.2014.06.007.
49. Irmer, B.; Chandrabalan, S.; Maas, L.; Bleckmann, A.; Menck, K. Extracellular Vesicles in Liquid Biopsies as Biomarkers for Solid Tumors. *Cancers* **2023**, *15*, doi:10.3390/cancers15041307.
50. Ilié, M.; Hofman, P. Pros: Can Tissue Biopsy Be Replaced by Liquid Biopsy? *Translational Lung Cancer Research; Vol 5, No 4 (August 29, 2016): Translational Lung Cancer Research* **2016**.
51. van Niel, G.; Porto-Carreiro, I.; Simoes, S.; Raposo, G. Exosomes: A Common Pathway for a Specialized Function. *The Journal of Biochemistry* **2006**, *140*, 13–21, doi:10.1093/jb/mvj128.
52. Valadi, H.; Ekström, K.; Bossios, A.; Sjöstrand, M.; Lee, J.J.; Lötvall, J.O. Exosome-Mediated Transfer of mRNAs and microRNAs Is a Novel Mechanism of Genetic Exchange between Cells. *Nature Cell Biology* **2007**, *9*, 654–659, doi:10.1038/ncb1596.
53. Thakur, B.K.; Zhang, H.; Becker, A.; Matei, I.; Huang, Y.; Costa-Silva, B.; Zheng, Y.; Hoshino, A.; Brazier, H.; Xiang, J.; et al. Double-Stranded DNA in Exosomes: A Novel Biomarker in Cancer Detection. *Cell Research* **2014**, *24*, 766–769, doi:10.1038/cr.2014.44.
54. Kosaka, N.; Iguchi, H.; Ochiya, T. Circulating microRNA in Body Fluid: A New Potential Biomarker for Cancer Diagnosis and Prognosis. *Cancer Science* **2010**, *101*, 2087–2092, doi:10.1111/j.1349-7006.2010.01650.x.
55. Lv, L.-L.; Wu, W.-J.; Feng, Y.; Li, Z.-L.; Tang, T.-T.; Liu, B.-C. Therapeutic Application of Extracellular Vesicles in Kidney Disease: Promises and Challenges. *Journal of Cellular and Molecular Medicine* **2018**, *22*, 728–737, doi:10.1111/jcmm.13407.
56. Venturella, M.; Criscuoli, M.; Carraro, F.; Naldini, A.; Zocco, D. Interplay between Hypoxia and Extracellular Vesicles in Cancer and Inflammation. *Biology* **2021**, *10*, doi:10.3390/biology10070606.
57. Johnsen, K.B.; Gudbergsson, J.M.; Skov, M.N.; Pilgaard, L.; Moos, T.; Duroux, M. A Comprehensive Overview of Exosomes as Drug Delivery Vehicles — Endogenous Nanocarriers for Targeted Cancer Therapy. *Biochimica et Biophysica Acta (BBA) - Reviews on Cancer* **2014**, *1846*, 75–87, doi:10.1016/j.bbcan.2014.04.005.
58. Kalluri, R.; LeBleu, V.S. The Biology, Function, and Biomedical Applications of Exosomes. *Science* **2020**, *367*, eaau6977, doi:10.1126/science.aau6977.
59. Fitts, C.A.; Ji, N.; Li, Y.; Tan, C. Exploiting Exosomes in Cancer Liquid Biopsies and Drug Delivery. *Advanced Healthcare Materials* **2019**, *8*, 1801268, doi:10.1002/adhm.201801268.
60. Szebeni, J.; Muggia, F.; Gabizon, A.; Barenholz, Y. Activation of Complement by Therapeutic Liposomes and Other Lipid Excipient-Based Therapeutic Products: Prediction and Prevention. *Advanced Drug Delivery Reviews* **2011**, *63*, 1020–1030, doi:10.1016/j.addr.2011.06.017.
61. Szebeni, J.; Bedőcs, P.; Rozsnyay, Z.; Weiszhár, Z.; Urbanics, R.; Rosivall, L.; Cohen, R.; Garbuzenko, O.; Báthori, G.; Tóth, M.; et al. Liposome-Induced Complement Activation and Related Cardiopulmonary Distress in Pigs: Factors Promoting Reactogenicity of Doxil and AmBisome. *Nanomedicine: Nanotechnology, Biology and Medicine* **2012**, *8*, 176–184, doi:10.1016/j.nano.2011.06.003.
62. Cheng, L.; Sharples, R.A.; Scicluna, B.J.; Hill, A.F. Exosomes Provide a Protective and Enriched Source of miRNA for Biomarker Profiling Compared to Intracellular and Cell-Free Blood. *Journal of Extracellular Vesicles* **2014**, *3*, 23743, doi:10.3402/jev.v3.23743.

63. Gehrmann, U.; Näslund, T.I.; Hiltbrunner, S.; Larssen, P.; Gabrielsson, S. Harnessing the Exosome-Induced Immune Response for Cancer Immunotherapy. *Seminars in Cancer Biology* **2014**, *28*, 58–67, doi:10.1016/j.semcancer.2014.05.003.
64. Hee Kim, S.; Bianco, N.; Menon, R.; Lechman, E.R.; Shufesky, W.J.; Morelli, A.E.; Robbins, P.D. Exosomes Derived from Genetically Modified DC Expressing FasL Are Anti-Inflammatory and Immunosuppressive. *Molecular Therapy* **2006**, *13*, 289–300, doi:10.1016/j.ymthe.2005.09.015.
65. Milosevits, G.; Szebeni, J.; Krol, S. Exosomes: Potential Model for Complement-Stealth Delivery Systems. **2015**, *7*, 207–218, doi:10.1515/ejnm-2015-0005.
66. Gu, X.; Erb, U.; Büchler, M.W.; Zöller, M. Improved Vaccine Efficacy of Tumor Exosome Compared to Tumor Lysate Loaded Dendritic Cells in Mice. *International Journal of Cancer* **2015**, *136*, E74–E84, doi:10.1002/ijc.29100.
67. Bu, N.; Wu, H.; Sun, B.; Zhang, G.; Zhan, S.; Zhang, R.; Zhou, L. Exosome-Loaded Dendritic Cells Elicit Tumor-Specific CD8+ Cytotoxic T Cells in Patients with Glioma. *Journal of Neuro-Oncology* **2011**, *104*, 659–667, doi:10.1007/s11060-011-0537-1.
68. Haraszti, R.A.; Miller, R.; Stoppato, M.; Sere, Y.Y.; Coles, A.; Didiot, M.-C.; Wollacott, R.; Sapp, E.; Dubuke, M.L.; Li, X.; et al. Exosomes Produced from 3D Cultures of MSCs by Tangential Flow Filtration Show Higher Yield and Improved Activity. *Molecular Therapy* **2018**, *26*, 2838–2847, doi:10.1016/j.ymthe.2018.09.015.
69. Kourembanas, S. Exosomes: Vehicles of Intercellular Signaling, Biomarkers, and Vectors of Cell Therapy. *Annu. Rev. Physiol.* **2015**, *77*, 13–27, doi:10.1146/annurev-physiol-021014-071641.
70. Yan, L.; Wu, X. Exosomes Produced from 3D Cultures of Umbilical Cord Mesenchymal Stem Cells in a Hollow-Fiber Bioreactor Show Improved Osteochondral Regeneration Activity. *Cell Biology and Toxicology* **2020**, *36*, 165–178, doi:10.1007/s10565-019-09504-5.
71. Wiklander, O.P.B.; Brennan, M.Á.; Lötvall, J.; Breakefield, X.O.; EL Andaloussi, S. Advances in Therapeutic Applications of Extracellular Vesicles. *Science Translational Medicine* **2019**, *11*, eaav8521, doi:10.1126/scitranslmed.aav8521.
72. Nassar, W.; El-Ansary, M.; Sabry, D.; Mostafa, M.A.; Fayad, T.; Kotb, E.; Temraz, M.; Saad, A.-N.; Essa, W.; Adel, H. Umbilical Cord Mesenchymal Stem Cells Derived Extracellular Vesicles Can Safely Ameliorate the Progression of Chronic Kidney Diseases. *Biomaterials Research* **2016**, *20*, 21, doi:10.1186/s40824-016-0068-0.
73. de Almeida Fuzeta, M.; de Matos Branco, A.D.; Fernandes-Platzgummer, A.; da Silva, C.L.; Cabral, J.M.S. Addressing the Manufacturing Challenges of Cell-Based Therapies. In *Current Applications of Pharmaceutical Biotechnology*; Silva, A.C., Moreira, J.N., Lobo, J.M.S., Almeida, H., Eds.; Springer International Publishing: Cham, 2020; pp. 225–278 ISBN 978-3-030-40464-2.
74. Gao, W.; Liang, T.; He, R.; Ren, J.; Yao, H.; Wang, K.; Zhu, L.; Xu, Y. Exosomes from 3D Culture of Marrow Stem Cells Enhances Endothelial Cell Proliferation, Migration, and Angiogenesis via Activation of the HMGB1/AKT Pathway. *Stem Cell Research* **2021**, *50*, 102122, doi:10.1016/j.scr.2020.102122.
75. Zhang, S.; Chu, W.C.; Lai, R.C.; Lim, S.K.; Hui, J.H.P.; Toh, W.S. Exosomes Derived from Human Embryonic Mesenchymal Stem Cells Promote Osteochondral Regeneration. *Osteoarthritis and Cartilage* **2016**, *24*, 2135–2140, doi:10.1016/j.joca.2016.06.022.
76. Cao, J.; Wang, B.; Tang, T.; Lv, L.; Ding, Z.; Li, Z.; Hu, R.; Wei, Q.; Shen, A.; Fu, Y.; et al. Three-Dimensional Culture of MSCs Produces Exosomes with Improved Yield and Enhanced Therapeutic Efficacy for Cisplatin-Induced Acute Kidney Injury. *Stem Cell Research & Therapy* **2020**, *11*, 206, doi:10.1186/s13287-020-01719-2.
77. de Almeida Fuzeta, M.; Bernardes, N.; Oliveira, F.D.; Costa, A.C.; Fernandes-Platzgummer, A.; Farinha, J.P.; Rodrigues, C.A.V.; Jung, S.; Tseng, R.-J.; Milligan, W.; et al. Scalable Production of Human Mesenchymal Stromal Cell-Derived Extracellular Vesicles Under Serum-/Xeno-Free Conditions in a Microcarrier-Based Bioreactor Culture System. *Frontiers in Cell and Developmental Biology* **2020**, *8*.
78. Batrakova, E.V.; Kim, M.S. Using Exosomes, Naturally-Equipped Nanocarriers, for Drug Delivery. *Journal of Controlled Release* **2015**, *219*, 396–405, doi:10.1016/j.jconrel.2015.07.030.

79. Kordelas, L.; Rebmann, V.; Ludwig, A.-K.; Radtke, S.; Ruesing, J.; Doeppner, T.R.; Epple, M.; Horn, P.A.; Beelen, D.W.; Giebel, B. MSC-Derived Exosomes: A Novel Tool to Treat Therapy-Refractory Graft-versus-Host Disease. *Leukemia* **2014**, *28*, 970–973, doi:10.1038/leu.2014.41.
80. Taylor, C.T.; Colgan, S.P. Regulation of Immunity and Inflammation by Hypoxia in Immunological Niches. *Nature Reviews Immunology* **2017**, *17*, 774–785, doi:10.1038/nri.2017.103.
81. Vanderkooi, J.M.; Erecinska, M.; Silver, I.A. Oxygen in Mammalian Tissue: Methods of Measurement and Affinities of Various Reactions. *American Journal of Physiology-Cell Physiology* **1991**, *260*, C1131–C1150, doi:10.1152/ajpcell.1991.260.6.C1131.
82. Bernards, R.; Weinberg, R.A. Metastasis Genes: A Progression Puzzle. *Nature* **2002**, *418*, 823–823, doi:10.1038/418823a.
83. Vaupel, P.; Mayer, A. Hypoxia in Cancer: Significance and Impact on Clinical Outcome. *Cancer and Metastasis Reviews* **2007**, *26*, 225–239, doi:10.1007/s10555-007-9055-1.
84. Hu, C.; Chen, M.; Jiang, R.; Guo, Y.; Wu, M.; Zhang, X. Exosome-Related Tumor Microenvironment. *J Cancer* **2018**, *9*, 3084–3092, doi:10.7150/jca.26422.
85. Yaghoubi, S.; Najminejad, H.; Dabaghian, M.; Karimi, M.H.; Abdollahpour-Alitappeh, M.; Rad, F.; Mahi-Birjand, M.; Mohammadi, S.; Mohseni, F.; Sobhani Lari, M.; et al. How Hypoxia Regulate Exosomes in Ischemic Diseases and Cancer Microenvironment? *IUBMB Life* **2020**, *72*, 1286–1305, doi:10.1002/iub.2275.
86. King, H.W.; Michael, M.Z.; Gleadle, J.M. Hypoxic Enhancement of Exosome Release by Breast Cancer Cells. *BMC Cancer* **2012**, *12*, 421, doi:10.1186/1471-2407-12-421.
87. Patton, M.C.; Zubair, H.; Khan, M.A.; Singh, S.; Singh, A.P. Hypoxia Alters the Release and Size Distribution of Extracellular Vesicles in Pancreatic Cancer Cells to Support Their Adaptive Survival. *Journal of Cellular Biochemistry* **2020**, *121*, 828–839, doi:10.1002/jcb.29328.
88. Ramteke, A.; Ting, H.; Agarwal, C.; Mateen, S.; Somasagara, R.; Hussain, A.; Graner, M.; Frederick, B.; Agarwal, R.; Deep, G. Exosomes Secreted under Hypoxia Enhance Invasiveness and Stemness of Prostate Cancer Cells by Targeting Adherens Junction Molecules. *Molecular Carcinogenesis* **2015**, *54*, 554–565, doi:10.1002/mc.22124.
89. Tadokoro, H.; Umezu, T.; Ohyashiki, K.; Hirano, T.; Ohyashiki, J.H. Exosomes Derived from Hypoxic Leukemia Cells Enhance Tube Formation in Endothelial Cells *. *Journal of Biological Chemistry* **2013**, *288*, 34343–34351, doi:10.1074/jbc.M113.480822.
90. Wang, T.; Gilkes, D.M.; Takano, N.; Xiang, L.; Luo, W.; Bishop, C.J.; Chaturvedi, P.; Green, J.J.; Semenza, G.L. Hypoxia-Inducible Factors and RAB22A Mediate Formation of Microvesicles That Stimulate Breast Cancer Invasion and Metastasis. *Proc Natl Acad Sci U S A* **2014**, *111*, E3234-42.
91. Hypoxia-Induced Signaling Promotes Prostate Cancer Progression: Exosomes Role as Messenger of Hypoxic Response in Tumor Microenvironment. *Critical Reviews™ in Oncogenesis* **2015**, *20*, 419–434.
92. Schlaepfer, I.R.; Nambiar, D.K.; Ramteke, A.; Kumar, R.; Dhar, D.; Agarwal, C.; Bergman, B.; Graner, M.; Maroni, P.; Singh, R.P.; et al. Hypoxia Induces Triglycerides Accumulation in Prostate Cancer Cells and Extracellular Vesicles Supporting Growth and Invasiveness Following Reoxygenation. *Oncotarget; Vol 6, No 26* **2015**.
93. Park, J.E.; Tan, H.S.; Datta, A.; Lai, R.C.; Zhang, H.; Meng, W.; Lim, S.K.; Sze, S.K. Hypoxic Tumor Cell Modulates Its Microenvironment to Enhance Angiogenic and Metastatic Potential by Secretion of Proteins and Exosomes *. *Molecular & Cellular Proteomics* **2010**, *9*, 1085–1099, doi:10.1074/mcp.M900381-MCP200.
94. Kucharzewska, P.; Christianson, H.C.; Welch, J.E.; Svensson, K.J.; Fredlund, E.; Ringnér, M.; Mörgelin, M.; Bourseau-Guilmain, E.; Bengzon, J.; Belting, M. Exosomes Reflect the Hypoxic Status of Glioma Cells and Mediate Hypoxia-Dependent Activation of Vascular Cells during Tumor Development. *Proceedings of the National Academy of Sciences* **2013**, *110*, 7312–7317, doi:10.1073/pnas.1220998110.
95. Jung, K.O.; Youn, H.; Lee, C.-H.; Kang, K.W.; Chung, J.-K. Visualization of Exosome-Mediated miR-210 Transfer from Hypoxic Tumor Cells. *Oncotarget; Vol 8, No 6* **2016**.

96. Umezu, T.; Tadokoro, H.; Azuma, K.; Yoshizawa, S.; Ohyashiki, K.; Ohyashiki, J.H. Exosomal miR-135b Shed from Hypoxic Multiple Myeloma Cells Enhances Angiogenesis by Targeting Factor-Inhibiting HIF-1. *Blood* **2014**, *124*, 3748–3757, doi:10.1182/blood-2014-05-576116.
97. Hsu, Y.-L.; Hung, J.-Y.; Chang, W.-A.; Lin, Y.-S.; Pan, Y.-C.; Tsai, P.-H.; Wu, C.-Y.; Kuo, P.-L. Hypoxic Lung Cancer-Secreted Exosomal miR-23a Increased Angiogenesis and Vascular Permeability by Targeting Prolyl Hydroxylase and Tight Junction Protein ZO-1. *Oncogene* **2017**, *36*, 4929–4942, doi:10.1038/onc.2017.105.
98. Wang, Y.; Yi, J.; Chen, X.; Zhang, Y.; Xu, M.; Yang, Z. The Regulation of Cancer Cell Migration by Lung Cancer Cell-Derived Exosomes through TGF-β and IL-10. *Oncol Lett* **2016**, *11*, 1527–1530, doi:10.3892/ol.2015.4044.
99. Chen, J.; Xu, R.; Xia, J.; Huang, J.; Su, B.; Wang, S. Aspirin Inhibits Hypoxia-Mediated Lung Cancer Cell Stemness and Exosome Function. *Pathology - Research and Practice* **2019**, *215*, 152379, doi:10.1016/j.prp.2019.03.008.
100. Dorayappan, K.D.P.; Wanner, R.; Wallbillich, J.J.; Saini, U.; Zingarelli, R.; Suarez, A.A.; Cohn, D.E.; Selvendiran, K. Hypoxia-Induced Exosomes Contribute to a More Aggressive and Chemoresistant Ovarian Cancer Phenotype: A Novel Mechanism Linking STAT3/Rab Proteins. *Oncogene* **2018**, *37*, 3806–3821, doi:10.1038/s41388-018-0189-0.
101. Li, L.; Li, C.; Wang, S.; Wang, Z.; Jiang, J.; Wang, W.; Li, X.; Chen, J.; Liu, K.; Li, C.; et al. Exosomes Derived from Hypoxic Oral Squamous Cell Carcinoma Cells Deliver miR-21 to Normoxic Cells to Elicit a Prometastatic Phenotype. *Cancer Research* **2016**, *76*, 1770–1780, doi:10.1158/0008-5472.CAN-15-1625.
102. Aga, M.; Bentz, G.L.; Raffa, S.; Torrisi, M.R.; Kondo, S.; Wakisaka, N.; Yoshizaki, T.; Pagano, J.S.; Shackelford, J. Exosomal HIF1α Supports Invasive Potential of Nasopharyngeal Carcinoma-Associated LMP1-Positive Exosomes. *Oncogene* **2014**, *33*, 4613–4622, doi:10.1038/onc.2014.66.
103. Huang, Z.; Yang, M.; Li, Y.; Yang, F.; Feng, Y. Exosomes Derived from Hypoxic Colorectal Cancer Cells Transfer Wnt4 to Normoxic Cells to Elicit a Prometastatic Phenotype. *Int J Biol Sci* **2018**, *14*, 2094–2102, doi:10.7150/ijbs.28288.
104. Park, J.E.; Dutta, B.; Tse, S.W.; Gupta, N.; Tan, C.F.; Low, J.K.; Yeoh, K.W.; Kon, O.L.; Tam, J.P.; Sze, S.K. Hypoxia-Induced Tumor Exosomes Promote M2-like Macrophage Polarization of Infiltrating Myeloid Cells and microRNA-Mediated Metabolic Shift. *Oncogene* **2019**, *38*, 5158–5173, doi:10.1038/s41388-019-0782-x.
105. Yu, Y.; Min, Z.; Zhou zhihang; Linhong, M.; Tao, R.; Yan, L.; Song, H. Hypoxia-Induced Exosomes Promote Hepatocellular Carcinoma Proliferation and Metastasis via miR-1273f Transfer. *Experimental Cell Research* **2019**, *385*, 111649, doi:10.1016/j.yexcr.2019.111649.
106. Wang, X.; Luo, G.; Zhang, K.; Cao, J.; Huang, C.; Jiang, T.; Liu, B.; Su, L.; Qiu, Z. Correction: Hypoxic Tumor-Derived Exosomal miR-301a Mediates M2 Macrophage Polarization via PTEN/PI3Kγ to Promote Pancreatic Cancer Metastasis. *Cancer Research* **2020**, *80*, 922–922, doi:10.1158/0008-5472.CAN-19-3872.
107. Cummins, E.P.; Keogh, C.E.; Crean, D.; Taylor, C.T. The Role of HIF in Immunity and Inflammation. *Molecular Aspects of Medicine* **2016**, *47–48*, 24–34, doi:10.1016/j.mam.2015.12.004.
108. Monaci, S.; Aldinucci, C.; Rossi, D.; Giuntini, G.; Filippi, I.; Ulivieri, C.; Marotta, G.; Sozzani, S.; Carraro, F.; Naldini, A. Hypoxia Shapes Autophagy in LPS-Activated Dendritic Cells. *Frontiers in Immunology* **2020**, *11*.
109. Lu, X.; Kang, Y. Hypoxia and Hypoxia-Inducible Factors: Master Regulators of Metastasis. *Clinical Cancer Research* **2010**, *16*, 5928–5935, doi:10.1158/1078-0432.CCR-10-1360.
110. Semenza, G.L. Hypoxia-Inducible Factors in Physiology and Medicine. *Cell* **2012**, *148*, 399–408, doi:10.1016/j.cell.2012.01.021.
111. Semenza, G.L. Life with Oxygen. *Science* **2007**, *318*, 62–64, doi:10.1126/science.1147949.
112. Kaelin, W.G., Jr.; Ratcliffe, P.J. Oxygen Sensing by Metazoans: The Central Role of the HIF Hydroxylase Pathway. *Molecular Cell* **2008**, *30*, 393–402, doi:10.1016/j.molcel.2008.04.009.

113. Smith, T.G.; Robbins, P.A.; Ratcliffe, P.J. The Human Side of Hypoxia-Inducible Factor. *British Journal of Haematology* **2008**, *141*, 325–334, doi:10.1111/j.1365-2141.2008.07029.x.
114. Zhang, W.; Zhou, X.; Yao, Q.; Liu, Y.; Zhang, H.; Dong, Z. HIF-1-Mediated Production of Exosomes during Hypoxia Is Protective in Renal Tubular Cells. *American Journal of Physiology-Renal Physiology* **2017**, *313*, F906–F913, doi:10.1152/ajprenal.00178.2017.
115. Choudhry, H.; Harris, A.L. Advances in Hypoxia-Inducible Factor Biology. *Cell Metabolism* **2018**, *27*, 281–298, doi:10.1016/j.cmet.2017.10.005.
116. Dengler, V.L.; Galbraith, M.D.; Espinosa, J.M. Transcriptional Regulation by Hypoxia Inducible Factors. *Critical Reviews in Biochemistry and Molecular Biology* **2014**, *49*, 1–15, doi:10.3109/10409238.2013.838205.
117. Castillo-Rodríguez, R.A.; Trejo-Solís, C.; Cabrera-Cano, A.; Gómez-Manzo, S.; Dávila-Borja, V.M. Hypoxia as a Modulator of Inflammation and Immune Response in Cancer. *Cancers* **2022**, *14*, doi:10.3390/cancers14092291.
118. Potter, C.P.S.; Harris, A.L. Diagnostic, Prognostic and Therapeutic Implications of Carbonic Anhydrases in Cancer. *British Journal of Cancer* **2003**, *89*, 2–7, doi:10.1038/sj.bjc.6600936.
119. Morgan, P.E.; Pastoreková, S.; Stuart-Tilley, A.K.; Alper, S.L.; Casey, J.R. Interactions of Transmembrane Carbonic Anhydrase, CAIX, with Bicarbonate Transporters. *American Journal of Physiology-Cell Physiology* **2007**, *293*, C738–C748, doi:10.1152/ajpcell.00157.2007.
120. Ng, H.L.; Lu, A.; Lin, G.; Qin, L.; Yang, Z. The Potential of Liposomes with Carbonic Anhydrase IX to Deliver Anticancer Ingredients to Cancer Cells in Vivo. *International Journal of Molecular Sciences* **2015**, *16*, 230–255, doi:10.3390/ijms16010230.
121. Pucciarelli, D.; Lengger, N.; Takacova, M.; Csaderova, L.; Bartosova, M.; Breiteneder, H.; Pastorekova, S.; Hafner, C. Anti-Chondroitin Sulfate Proteoglycan 4-Specific Antibodies Modify the Effects of Vemurafenib on Melanoma Cells Differentially in Normoxia and Hypoxia. *Int J Oncol* **2015**, *47*, 81–90, doi:10.3892/ijo.2015.3010.
122. Saarnio, J.; Parkkila, S.; Parkkila, A.-K.; Haukipuro, K.; Pastoreková, S.; Pastorek, J.; Kairaluoma, M.I.; Karttunen, T.J. Immunohistochemical Study of Colorectal Tumors for Expression of a Novel Transmembrane Carbonic Anhydrase, MN/CA IX, with Potential Value as a Marker of Cell Proliferation. *The American Journal of Pathology* **1998**, *153*, 279–285, doi:10.1016/S0002-9440(10)65569-1.
123. Andreucci, E.; Ruzzolini, J.; Peppicelli, S.; Bianchini, F.; Laurenzana, A.; Carta, F.; Supuran, C.T.; Calorini, L. The Carbonic Anhydrase IX Inhibitor SLC-0111 Sensitises Cancer Cells to Conventional Chemotherapy. *Journal of Enzyme Inhibition and Medicinal Chemistry* **2019**, *34*, 117–123, doi:10.1080/14756366.2018.1532419.
124. Pastorekova, S.; Gillies, R.J. The Role of Carbonic Anhydrase IX in Cancer Development: Links to Hypoxia, Acidosis, and Beyond. *Cancer and Metastasis Reviews* **2019**, *38*, 65–77, doi:10.1007/s10555-019-09799-0.
125. Marks, I.S.; Gardeen, S.S.; Kurdziel, S.J.; Nicolaou, S.T.; Woods, J.E.; Kularatne, S.A.; Low, P.S. Development of a Small Molecule Tubulysin B Conjugate for Treatment of Carbonic Anhydrase IX Receptor Expressing Cancers. *Mol. Pharmaceutics* **2018**, *15*, 2289–2296, doi:10.1021/acs.molpharmaceut.8b00139.
126. Saginala, K.; Barsouk, A.; Aluru, J.S.; Rawla, P.; Barsouk, A. Epidemiology of Melanoma. *Medical Sciences* **2021**, *9*, doi:10.3390/medsci9040063.
127. Teixido, C.; Castillo, P.; Martinez-Vila, C.; Arance, A.; Alos, L. Molecular Markers and Targets in Melanoma. *Cells* **2021**, *10*, doi:10.3390/cells10092320.
128. Davis, L.E.; Shalin, S.C.; Tackett, A.J. Current State of Melanoma Diagnosis and Treatment. *Cancer Biology & Therapy* **2019**, *20*, 1366–1379, doi:10.1080/15384047.2019.1640032.
129. Ziani, L.; Buart, S.; Chouaib, S.; Thiery, J. Hypoxia Increases Melanoma-Associated Fibroblasts Immunosuppressive Potential and Inhibitory Effect on T Cell-Mediated Cytotoxicity. *OncoImmunology* **2021**, *10*, 1950953, doi:10.1080/2162402X.2021.1950953.

130. Bedogni, B.; Powell, M.B. Hypoxia, Melanocytes and Melanoma – Survival and Tumor Development in the Permissive Microenvironment of the Skin. *Pigment Cell & Melanoma Research* **2009**, *22*, 166–174, doi:10.1111/j.1755-148X.2009.00553.x.
131. Lartigau, E.; Randrianarivelo, H.; Avril, M.-F.; Margulis, A.; Spatz, A.; Eschwége, F.; Guichard, M. Intratumoral Oxygen Tension in Metastatic Melanoma. *Melanoma Research* **1997**, *7*.
132. Dratkiewicz, E.; Simiczyjew, A.; Mazurkiewicz, J.; Ziętek, M.; Matkowski, R.; Nowak, D. Hypoxia and Extracellular Acidification as Drivers of Melanoma Progression and Drug Resistance. *Cells* **2021**, *10*, doi:10.3390/cells10040862.
133. Malekan, M.; Ebrahimzadeh, M.A.; Sheida, F. The Role of Hypoxia-Inducible Factor-1alpha and Its Signaling in Melanoma. *Biomedicine & Pharmacotherapy* **2021**, *141*, 111873, doi:10.1016/j.biopha.2021.111873.
134. Li, L.; Ren, F.; Qi, C.; Xu, L.; Fang, Y.; Liang, M.; Feng, J.; Chen, B.; Ning, W.; Cao, J. Intermittent Hypoxia Promotes Melanoma Lung Metastasis via Oxidative Stress and Inflammation Responses in a Mouse Model of Obstructive Sleep Apnea. *Respiratory Research* **2018**, *19*, 28, doi:10.1186/s12931-018-0727-x.
135. Wen, J.; Yang, T.; Mallouk, N.; Zhang, Y.; Li, H.; Lambert, C.; Li, G. Urinary Exosomal CA9 mRNA as a Novel Liquid Biopsy for Molecular Diagnosis of Bladder Cancer. *International Journal of Nanomedicine* **2021**, *Volume 16*, 4805–4811, doi:10.2147/IJN.S312322.
136. Takacova, M.; Barathova, M.; Zatovicova, M.; Golias, T.; Kajanova, I.; Jelenska, L.; Sedlakova, O.; Svastova, E.; Kopacek, J.; Pastorekova, S. Carbonic Anhydrase IX—Mouse versus Human. *International Journal of Molecular Sciences* **2020**, *21*, doi:10.3390/ijms21010246.
137. Himbert, D.; Zeuschner, P.; Ayoubian, H.; Heinzelmann, J.; Stöckle, M.; Junker, K. Characterization of CD147, CA9, and CD70 as Tumor-Specific Markers on Extracellular Vesicles in Clear Cell Renal Cell Carcinoma. *Diagnostics* **2020**, *10*, doi:10.3390/diagnostics10121034.
138. Allelein, S.; Medina-Perez, P.; Lopes, A.L.H.; Rau, S.; Hause, G.; Kölsch, A.; Kuhlmeier, D. Potential and Challenges of Specifically Isolating Extracellular Vesicles from Heterogeneous Populations. *Scientific Reports* **2021**, *11*, 11585, doi:10.1038/s41598-021-91129-y.
139. Venturella, M.; Falsini, A.; Coppola, F.; Giuntini, G.; Carraro, F.; Zocco, D.; Chiesi, A.; Naldini, A. CA-IX-Expressing Small Extracellular Vesicles (sEVs) Are Released by Melanoma Cells under Hypoxia and in the Blood of Advanced Melanoma Patients. *International Journal of Molecular Sciences* **2023**, *24*, doi:10.3390/ijms24076122.
140. Kciuk, M.; Gielecińska, A.; Mujwar, S.; Mojzych, M.; Marciniak, B.; Drozda, R.; Kontek, R. Targeting Carbonic Anhydrase IX and XII Isoforms with Small Molecule Inhibitors and Monoclonal Antibodies. *Journal of Enzyme Inhibition and Medicinal Chemistry* **2022**, *37*, 1278–1298, doi:10.1080/14756366.2022.2052868.
141. Závada J, Závadová Z, Zat'ovicová M, Hyrsl L, Kawaciuk I. Soluble Form of Carbonic Anhydrase IX (CA IX) in the Serum and Urine of Renal Carcinoma Patients. Br J Cancer. 2003 Sep 15;89(6):1067-71. Doi: 10.1038/Sj.Bjc.6601264. PMID: 12966427; PMCID: PMC2376963.
142. Eckert, A.W.; Horter, S.; Bethmann, D.; Kotrba, J.; Kaune, T.; Rot, S.; Bache, M.; Bilkenroth, U.; Reich, W.; Greither, T.; et al. Investigation of the Prognostic Role of Carbonic Anhydrase 9 (CAIX) of the Cellular mRNA/Protein Level or Soluble CAIX Protein in Patients with Oral Squamous Cell Carcinoma. *International Journal of Molecular Sciences* **2019**, *20*, doi:10.3390/ijms20020375.
143. Schütze, D.; Milde-Langosch, K.; Witzel, I.; Rody, A.; Karn, T.; Schmidt, M.; Choschzick, M.; Jänicke, F.; Müller, V. Relevance of Cellular and Serum Carbonic Anhydrase IX in Primary Breast Cancer. *Journal of Cancer Research and Clinical Oncology* **2013**, *139*, 747–754, doi:10.1007/s00432-013-1378-4.
144. Woelber, L.; Kress, K.; Kersten, J.F.; Choschzick, M.; Kilic, E.; Herwig, U.; Lindner, C.; Schwarz, J.; Jaenicke, F.; Mahner, S.; et al. Carbonic Anhydrase IX in Tumor Tissue and Sera of Patients with Primary Cervical Cancer. *BMC Cancer* **2011**, *11*, 12, doi:10.1186/1471-2407-11-12.
145. Rossi, S.; Cordella, M.; Tabolacci, C.; Nassa, G.; D'Arcangelo, D.; Senatore, C.; Pagnotto, P.; Magliozzi, R.; Salvati, A.; Weisz, A.; et al. TNF-Alpha and Metalloproteases as Key Players in

Melanoma Cells Aggressiveness. *Journal of Experimental & Clinical Cancer Research* **2018**, *37*, 326, doi:10.1186/s13046-018-0982-1.
146. Giuntini, G.; Monaci, S.; Cau, Y.; Mori, M.; Naldini, A.; Carraro, F. Inhibition of Melanoma Cell Migration and Invasion Targeting the Hypoxic Tumor Associated CAXII. *Cancers* **2020**, *12*, doi:10.3390/cancers12103018.
147. Liang, Y.; Lehrich, B.M.; Zheng, S.; Lu, M. Emerging Methods in Biomarker Identification for Extracellular Vesicle-Based Liquid Biopsy. *Journal of Extracellular Vesicles* **2021**, *10*, e12090, doi:10.1002/jev2.12090.
148. Wan, Y.; Liu, B.; Lei, H.; Zhang, B.; Wang, Y.; Huang, H.; Chen, S.; Feng, Y.; Zhu, L.; Gu, Y.; et al. Nanoscale Extracellular Vesicle-Derived DNA Is Superior to Circulating Cell-Free DNA for Mutation Detection in Early-Stage Non-Small-Cell Lung Cancer. *Annals of Oncology* **2018**, *29*, 2379–2383, doi:10.1093/annonc/mdy458.
149. Logozzi, M.; Mizzoni, D.; Capasso, C.; Del Prete, S.; Di Raimo, R.; Falchi, M.; Angelini, D.F.; Sciarra, A.; Maggi, M.; Supuran, C.T.; et al. Plasmatic Exosomes from Prostate Cancer Patients Show Increased Carbonic Anhydrase IX Expression and Activity and Low pH. *Journal of Enzyme Inhibition and Medicinal Chemistry* **2020**, *35*, 280–288, doi:10.1080/14756366.2019.1697249.
150. Logozzi, M.; Capasso, C.; Di Raimo, R.; Del Prete, S.; Mizzoni, D.; Falchi, M.; Supuran, C.T.; Fais, S. Prostate Cancer Cells and Exosomes in Acidic Condition Show Increased Carbonic Anhydrase IX Expression and Activity. *Journal of Enzyme Inhibition and Medicinal Chemistry* **2019**, *34*, 272–278, doi:10.1080/14756366.2018.1538980.
151. Horie, K.; Kawakami, K.; Fujita, Y.; Sugaya, M.; Kameyama, K.; Mizutani, K.; Deguchi, T.; Ito, M. Exosomes Expressing Carbonic Anhydrase 9 Promote Angiogenesis. *Biochemical and Biophysical Research Communications* **2017**, *492*, 356–361, doi:10.1016/j.bbrc.2017.08.107.
152. Ha, D.H.; Kim, H.; Lee, J.; Kwon, H.H.; Park, G.-H.; Yang, S.H.; Jung, J.Y.; Choi, H.; Lee, J.H.; Sung, S.; et al. Mesenchymal Stem/Stromal Cell-Derived Exosomes for Immunomodulatory Therapeutics and Skin Regeneration. *Cells* **2020**, *9*, doi:10.3390/cells9051157.
153. Han, C.; Sun, X.; Liu, L.; Jiang, H.; Shen, Y.; Xu, X.; Li, J.; Zhang, G.; Huang, J.; Lin, Z.; et al. Exosomes and Their Therapeutic Potentials of Stem Cells. *Stem Cells International* **2015**, *2016*, 7653489, doi:10.1155/2016/7653489.
154. Borakati, A.; Mafi, R.; Mafi, P.; Khan, S.W. A Systematic Review And Meta-Analysis of Clinical Trials of Mesenchymal Stem Cell Therapy for Cartilage Repair. *Current Stem Cell Research & Therapy* **2018**, *13*, 215–225, doi:10.2174/1574888X12666170915120620.
155. Jeong, H.; Yim, H.W.; Park, H.-J.; Cho, Y.; Hong, H.; Kim, N.J.; Oh, I.-H. Mesenchymal Stem Cell Therapy for Ischemic Heart Disease: Systematic Review and Meta-Analysis. *IJSC* **2018**, *11*, 1–12, doi:10.15283/ijsc17061.
156. Lalu, M.M.; Mazzarello, S.; Zlepnig, J.; Dong, Y.Y. (Ryan); Montroy, J.; McIntyre, L.; Devereaux, P.J.; Stewart, D.J.; David Mazer, C.; Barron, C.C.; et al. Safety and Efficacy of Adult Stem Cell Therapy for Acute Myocardial Infarction and Ischemic Heart Failure (SafeCell Heart): A Systematic Review and Meta-Analysis. *Stem Cells Translational Medicine* **2018**, *7*, 857–866, doi:10.1002/sctm.18-0120.
157. Yim, H.; Jeong, H.; Cho, Y.; Jeong, S.; Oh, I. Safety of Mesenchymal Stem Cell Therapy: A Systematic Review and Meta-Analysis. *Cytotherapy* **2016**, *18*, S132, doi:10.1016/j.jcyt.2016.03.258.
158. Andrzejewska, A.; Lukomska, B.; Janowski, M. Concise Review: Mesenchymal Stem Cells: From Roots to Boost. *Stem Cells* **2019**, *37*, 855–864, doi:10.1002/stem.3016.
159. Harrell, C.R.; Fellabaum, C.; Jovicic, N.; Djonov, V.; Arsenijevic, N.; Volarevic, V. Molecular Mechanisms Responsible for Therapeutic Potential of Mesenchymal Stem Cell-Derived Secretome. *Cells* **2019**, *8*, doi:10.3390/cells8050467.
160. Dominici, M.; Le Blanc, K.; Mueller, I.; Slaper-Cortenbach, I.; Marini, F.C.; Krause, D.S.; Deans, R.J.; Keating, A.; Prockop, D.J.; Horwitz, E.M. Minimal Criteria for Defining Multipotent Mesenchymal Stromal Cells. The International Society for Cellular Therapy Position Statement. *Cytotherapy* **2006**, *8*, 315–317, doi:10.1080/14653240600855905.

161. Lai, R.C.; Arslan, F.; Lee, M.M.; Sze, N.S.K.; Choo, A.; Chen, T.S.; Salto-Tellez, M.; Timmers, L.; Lee, C.N.; El Oakley, R.M.; et al. Exosome Secreted by MSC Reduces Myocardial Ischemia/Reperfusion Injury. *Stem Cell Research* **2010**, *4*, 214–222, doi:10.1016/j.scr.2009.12.003.
162. Keshtkar, S.; Azarpira, N.; Ghahremani, M.H. Mesenchymal Stem Cell-Derived Extracellular Vesicles: Novel Frontiers in Regenerative Medicine. *Stem Cell Research & Therapy* **2018**, *9*, 63, doi:10.1186/s13287-018-0791-7.
163. Witwer, K.W.; Van Balkom, B.W.M.; Bruno, S.; Choo, A.; Dominici, M.; Gimona, M.; Hill, A.F.; De Kleijn, D.; Koh, M.; Lai, R.C.; et al. Defining Mesenchymal Stromal Cell (MSC)-Derived Small Extracellular Vesicles for Therapeutic Applications. *Journal of Extracellular Vesicles* **2019**, *8*, 1609206, doi:10.1080/20013078.2019.1609206.
164. Lener, T.; Gimona, M.; Aigner, L.; Börger, V.; Buzas, E.; Camussi, G.; Chaput, N.; Chatterjee, D.; Court, F.A.; del Portillo, H.A.; et al. Applying Extracellular Vesicles Based Therapeutics in Clinical Trials – an ISEV Position Paper. *Journal of Extracellular Vesicles* **2015**, *4*, 30087, doi:10.3402/jev.v4.30087.
165. Watson, D.C.; Bayik, D.; Srivatsan, A.; Bergamaschi, C.; Valentin, A.; Niu, G.; Bear, J.; Monninger, M.; Sun, M.; Morales-Kastresana, A.; et al. Efficient Production and Enhanced Tumor Delivery of Engineered Extracellular Vesicles. *Biomaterials* **2016**, *105*, 195–205, doi:10.1016/j.biomaterials.2016.07.003.
166. Markov, A.; Thangavelu, L.; Aravindhan, S.; Zekiy, A.O.; Jarahian, M.; Chartrand, M.S.; Pathak, Y.; Marofi, F.; Shamlou, S.; Hassanzadeh, A. Mesenchymal Stem/Stromal Cells as a Valuable Source for the Treatment of Immune-Mediated Disorders. *Stem Cell Research & Therapy* **2021**, *12*, 192, doi:10.1186/s13287-021-02265-1.
167. Lou, G.; Chen, Z.; Zheng, M.; Liu, Y. Mesenchymal Stem Cell-Derived Exosomes as a New Therapeutic Strategy for Liver Diseases. *Experimental & Molecular Medicine* **2017**, *49*, e346–e346, doi:10.1038/emm.2017.63.
168. Bian, S.; Zhang, L.; Duan, L.; Wang, X.; Min, Y.; Yu, H. Extracellular Vesicles Derived from Human Bone Marrow Mesenchymal Stem Cells Promote Angiogenesis in a Rat Myocardial Infarction Model. *Journal of Molecular Medicine* **2014**, *92*, 387–397, doi:10.1007/s00109-013-1110-5.
169. Phinney, D.G.; Pittenger, M.F. Concise Review: MSC-Derived Exosomes for Cell-Free Therapy. *Stem Cells* **2017**, *35*, 851–858, doi:10.1002/stem.2575.
170. Cho, B.S.; Kim, J.O.; Ha, D.H.; Yi, Y.W. Exosomes Derived from Human Adipose Tissue-Derived Mesenchymal Stem Cells Alleviate Atopic Dermatitis. *Stem Cell Research & Therapy* **2018**, *9*, 187, doi:10.1186/s13287-018-0939-5.
171. Vrijsen, K.R.; Maring, J.A.; Chamuleau, S.A.J.; Verhage, V.; Mol, E.A.; Deddens, J.C.; Metz, C.H.G.; Lodder, K.; van Eeuwijk, E.C.M.; van Dommelen, S.M.; et al. Exosomes from Cardiomyocyte Progenitor Cells and Mesenchymal Stem Cells Stimulate Angiogenesis Via EMMPRIN. *Advanced Healthcare Materials* **2016**, *5*, 2555–2565, doi:10.1002/adhm.201600308.
172. Vader, P.; Mol, E.A.; Pasterkamp, G.; Schiffelers, R.M. Extracellular Vesicles for Drug Delivery. *Advanced Drug Delivery Reviews* **2016**, *106*, 148–156, doi:10.1016/j.addr.2016.02.006.
173. Gao, W.; He, R.; Ren, J.; Zhang, W.; Wang, K.; Zhu, L.; Liang, T. Exosomal HMGB1 Derived from Hypoxia-Conditioned Bone Marrow Mesenchymal Stem Cells Increases Angiogenesis via the JNK/HIF-1α Pathway. *FEBS Open Bio* **2021**, *11*, 1364–1373, doi:10.1002/2211-5463.13142.
174. Zhang, B.; Tian, X.; Qu, Z.; Hao, J.; Zhang, W. Hypoxia-Preconditioned Extracellular Vesicles from Mesenchymal Stem Cells Improve Cartilage Repair in Osteoarthritis. *Membranes* **2022**, *12*, doi:10.3390/membranes12020225.
175. Nekanti, U.; Dastidar, S.; Venugopal, P.; Totey, S.; Ta, M. Increased Proliferation and Analysis of Differential Gene Expression in Human Wharton's Jelly-Derived Mesenchymal Stromal Cells under Hypoxia. *Int J Biol Sci* **2010**, *6*, 499–512, doi:10.7150/ijbs.6.499.
176. Xue, C.; Shen, Y.; Li, X.; Li, B.; Zhao, S.; Gu, J.; Chen, Y.; Ma, B.; Wei, J.; Han, Q.; et al. Exosomes Derived from Hypoxia-Treated Human Adipose Mesenchymal Stem Cells Enhance Angiogenesis

Through the PKA Signaling Pathway. *Stem Cells and Development* **2018**, *27*, 456–465, doi:10.1089/scd.2017.0296.
177. Almeria, C.; Weiss, R.; Roy, M.; Tripisciano, C.; Kasper, C.; Weber, V.; Egger, D. Hypoxia Conditioned Mesenchymal Stem Cell-Derived Extracellular Vesicles Induce Increased Vascular Tube Formation in Vitro. *Frontiers in Bioengineering and Biotechnology* **2019**, *7*.
178. Zhu, J.; Lu, K.; Zhang, N.; Zhao, Y.; Ma, Q.; Shen, J.; Lin, Y.; Xiang, P.; Tang, Y.; Hu, X.; et al. Myocardial Reparative Functions of Exosomes from Mesenchymal Stem Cells Are Enhanced by Hypoxia Treatment of the Cells via Transferring microRNA-210 in an nSMase2-Dependent Way. *Artificial Cells, Nanomedicine, and Biotechnology* **2018**, *46*, 1659–1670, doi:10.1080/21691401.2017.1388249.
179. Webber, J.; Clayton, A. How Pure Are Your Vesicles? *Journal of Extracellular Vesicles* **2013**, *2*, 19861, doi:10.3402/jev.v2i0.19861.
180. Cox, J.; Mann, M. MaxQuant Enables High Peptide Identification Rates, Individualized p.p.b.-Range Mass Accuracies and Proteome-Wide Protein Quantification. *Nature Biotechnology* **2008**, *26*, 1367–1372, doi:10.1038/nbt.1511.
181. Cox, J.; Neuhauser, N.; Michalski, A.; Scheltema, R.A.; Olsen, J.V.; Mann, M. Andromeda: A Peptide Search Engine Integrated into the MaxQuant Environment. *J. Proteome Res.* **2011**, *10*, 1794–1805, doi:10.1021/pr101065j.
182. Tyanova, S.; Temu, T.; Sinitcyn, P.; Carlson, A.; Hein, M.Y.; Geiger, T.; Mann, M.; Cox, J. The Perseus Computational Platform for Comprehensive Analysis of (Prote)Omics Data. *Nature Methods* **2016**, *13*, 731–740, doi:10.1038/nmeth.3901.
183. Anders, S.; Huber, W. Differential Expression Analysis for Sequence Count Data. *Genome Biology* **2010**, *11*, R106, doi:10.1186/gb-2010-11-10-r106.
184. Aparicio-Puerta, E.; Hirsch, P.; Schmartz, G.P.; Kern, F.; Fehlmann, T.; Keller, A. miEAA 2023: Updates, New Functional microRNA Sets and Improved Enrichment Visualizations. *Nucleic Acids Research* **2023**, *51*, W319–W325, doi:10.1093/nar/gkad392.
185. Carpentier, G.; Berndt, S.; Ferratge, S.; Rasband, W.; Cuendet, M.; Uzan, G.; Albanese, P. Angiogenesis Analyzer for ImageJ — A Comparative Morphometric Analysis of "Endothelial Tube Formation Assay" and "Fibrin Bead Assay." *Scientific Reports* **2020**, *10*, doi:10.1038/s41598-020-67289-8.
186. Love, M.I.; Huber, W.; Anders, S. Moderated Estimation of Fold Change and Dispersion for RNA-Seq Data with DESeq2. *Genome Biology* **2014**, *15*, 550, doi:10.1186/s13059-014-0550-8.
187. Benjamini, Y.; Hochberg, Y. Controlling the False Discovery Rate: A Practical and Powerful Approach to Multiple Testing. *Journal of the Royal Statistical Society: Series B (Methodological)* **1995**, *57*, 289–300, doi:10.1111/j.2517-6161.1995.tb02031.x.
188. Samaeekia, R.; Rabiee, B.; Putra, I.; Shen, X.; Park, Y.J.; Hematti, P.; Eslani, M.; Djalilian, A.R. Effect of Human Corneal Mesenchymal Stromal Cell-Derived Exosomes on Corneal Epithelial Wound Healing. *Investigative Ophthalmology & Visual Science* **2018**, *59*, 5194–5200, doi:10.1167/iovs.18-24803.
189. Zhang, J.; Liu, X.; Li, H.; Chen, C.; Hu, B.; Niu, X.; Li, Q.; Zhao, B.; Xie, Z.; Wang, Y. Exosomes/Tricalcium Phosphate Combination Scaffolds Can Enhance Bone Regeneration by Activating the PI3K/Akt Signaling Pathway. *Stem Cell Research & Therapy* **2016**, *7*, 136, doi:10.1186/s13287-016-0391-3.
190. Liang, B.; Liang, J.-M.; Ding, J.-N.; Xu, J.; Xu, J.-G.; Chai, Y.-M. Dimethyloxaloylglycine-Stimulated Human Bone Marrow Mesenchymal Stem Cell-Derived Exosomes Enhance Bone Regeneration through Angiogenesis by Targeting the AKT/mTOR Pathway. *Stem Cell Research & Therapy* **2019**, *10*, 335, doi:10.1186/s13287-019-1410-y.
191. Zhang, L.; Jiao, G.; Ren, S.; Zhang, X.; Li, C.; Wu, W.; Wang, H.; Liu, H.; Zhou, H.; Chen, Y. Exosomes from Bone Marrow Mesenchymal Stem Cells Enhance Fracture Healing through the Promotion of Osteogenesis and Angiogenesis in a Rat Model of Nonunion. *Stem Cell Research & Therapy* **2020**, *11*, 38, doi:10.1186/s13287-020-1562-9.

192. Nguyen, V.V.T.; Witwer, K.W.; Verhaar, M.C.; Strunk, D.; van Balkom, B.W.M. Functional Assays to Assess the Therapeutic Potential of Extracellular Vesicles. *Journal of Extracellular Vesicles* **2020**, *10*, e12033, doi:10.1002/jev2.12033.
193. Crabtree, B.; Subramanian, V. Behavior of Endothelial Cells on Matrigel and Development of a Method for a Rapid and Reproducible in Vitro Angiogenesis Assay. *In Vitro Cellular & Developmental Biology - Animal* **2007**, *43*, 87–94, doi:10.1007/s11626-007-9012-x.
194. Ferratge, S.; Ha, G.; Carpentier, G.; Arouche, N.; Bascetin, R.; Muller, L.; Germain, S.; Uzan, G. Initial Clonogenic Potential of Human Endothelial Progenitor Cells Is Predictive of Their Further Properties and Establishes a Functional Hierarchy Related to Immaturity. *Stem Cell Research* **2017**, *21*, 148–159, doi:10.1016/j.scr.2017.04.009.
195. Khoo, C.P.; Micklem, K.; Watt, S.M. A Comparison of Methods for Quantifying Angiogenesis in the Matrigel Assay In Vitro. *Tissue Engineering Part C: Methods* **2011**, *17*, 895–906, doi:10.1089/ten.tec.2011.0150.
196. Gong, M.; Yu, B.; Wang, J.; Wang, Y.; Liu, M.; Paul, C.; Millard, R.W.; Xiao, D.-S.; Ashraf, M.; Xu, M. Mesenchymal Stem Cells Release Exosomes That Transfer miRNAs to Endothelial Cells and Promote Angiogenesis. *Oncotarget; Vol 8, No 28* **2017**.